FINITE DIFFERENCE ANALYSIS OF A CYLINDRICAL TWO CONDUCTOR MICROSTRIP TRANSMISSION LINE WITH TRUNCATED DIELECTRICS

Technical Report

Prepared by

Atef Elsherbeni, Ying Yuan and Charles Smith.

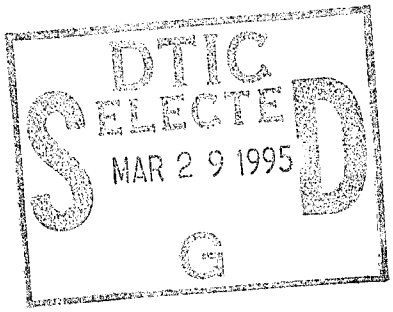

January, 1995

U. S. Army Research Office
Research agreement No.
DAAH04-94-G-0355

Technical Report No. 95-1
Department of Electrical Engineering
The University of Mississippi

MASTER COPY KEEP THIS COPY FOR REPRODUCTION PURPOSES

REPORT DOCUMENTATION PAGE

Form Approved
OMB No. 0704-0188

1. AGENCY USE ONLY (Leave blank)	2. REPORT DATE	3. REPORT TYPE AND DATES COVERED
	Jan. 27, 1995	Technical Report, Sept. 1 - Dec. 31, 1994

4. TITLE AND SUBTITLE

Finite Difference Analysis of a Cylindrical Two Conductor Microstrip Transmission Line with Truncated Dielectrics

5. FUNDING NUMBERS

DAAH04-94-G-0355

6. AUTHOR(S)

A. Z. Elsherbeni, Y. Ying, C. E. Smith

7. PERFORMING ORGANIZATION NAME(S) AND ADDRESS(ES)

Department of Electrical Engineering
University of Misssissippi
University, MS 38677

8. PERFORMING ORGANIZATION REPORT NUMBER

95-1

9. SPONSORING / MONITORING AGENCY NAME(S) AND ADDRESS(ES)

U.S. Army Research Office
P. O. Box 12211
Research Triangle Park, NC 27709-2211

10. SPONSORING / MONITORING AGENCY REPORT NUMBER

ARO 33869.1-EL-DPS

11. SUPPLEMENTARY NOTES

The views, opinions and/or findings contained in this report are those of the author(s) and should not be construed as an official Department of the Army position, policy, or decision, unless so designated by other documentation.

12a. DISTRIBUTION / AVAILABILITY STATEMENT

Approved for public release; distribution unlimited.

12b. DISTRIBUTION CODE

13. ABSTRACT *(Maximum 200 words)*

The characteristics of the quasi-static TEM mode of a cylindrical microstrip transmission line are investigated using the finite difference technique. The transmission line consists of two perfectly conducting strips located between two different layers of dielectric materials, and a dielectric notch embedded in the substrate between two strips. The dielectric overlay and substrate are truncated for practical purposes. The formulation of the problem is based on the solution of Laplace's equation subject to appropriate boundary conditions and the use of Taylor's expansion to approximate the first and the second order derivatives in Laplace's equation. To truncate the finite difference mesh, three different kinds of artificial boundaries have been considered. It has been found that an efficient solution is obtained when the artificial boundary is separated from the conducting core at a distance of the order of the height of the substrate. The goal of this research is to study the effects of the parameters of the multi-layered cylindrical transmission line on the odd and even mode phase velocities, and on the electrical coupling. Another objective of this study is to present several techniques to minimize the coupling between the two conductors. Once the odd and even mode phase velocities are equalized, the design of a distortionless line is achievable. The line capacitances are found to vary linearly with the dielectric constants of the overlay and the substrate.

14. SUBJECT TERMS

Crosstalk, Transmission Line Coupling, Conformed Microstrip Lines.

15. NUMBER OF PAGES

16. PRICE CODE

17. SECURITY CLASSIFICATION OF REPORT	18. SECURITY CLASSIFICATION OF THIS PAGE	19. SECURITY CLASSIFICATION OF ABSTRACT	20. LIMITATION OF ABSTRACT
UNCLASSIFIED	UNCLASSIFIED	UNCLASSIFIED	UL

ABSTRACT

The characteristics of the quasi-static TEM mode of a cylindrical microstrip transmission line are investigated using the finite difference technique. The transmission line consists of two perfectly conducting strips located between two different layers of dielectric materials, and a dielectric notch embedded in the substrate between two strips. The dielectric overlay and substrate are truncated for practical purposes. The formulation of the problem is based on the solution of Laplace's equation subject to appropriate boundary conditions and the use of Taylor's expansion to approximate the first and the second order derivatives in Laplace's equation. To truncate the finite difference mesh, three different kinds of artificial boundaries have been considered. It has been found that an efficient solution is obtained when the artificial boundary is separated from the conducting core at a distance of the order of the height of the substrate. The goal of this research is to study the effects of the parameters of the multi-layered cylindrical transmission line on the odd and even mode phase velocities, and on the electrical coupling. Another objective of this study is to present several techniques to minimize the coupling between the two conductors. Once the odd and even mode phase velocities are equalized, the design of a distortionless line is achievable. The line capacitances are found to vary linearly with the dielectric constants of the overlay and the substrate.

ACKNOWLEDGMENT

This work was supported in part by the Army Research Office under grant number DAAH04-94-G-0355, and The University of Mississippi through a Faculty Research Award.

The authors would like to express their appreciation to Mr. Vicente Rodriguez-Pereyra for helping in the preparation of this document.

TABLE OF CONTENTS

Chapter

LIST OF FIGURES

Figure Page

Figure Page

Figure Page

Figure Page

Figure Page

Figure Page

Figure Page

Figure Page

Figure Page

LIST OF SYMBOLS

α_o	Angle between x-axis and edge of overlay	(Degrees)
α_s	Angle between x-axis and edge of substrate	(Degrees)
c	Speed of light	(m/s)
C_{ii}	Self capacitance	(pF/m)
C_{ij}	Mutual capacitance	(pF/m)
$\bar{D}$	Displacement vector	(C/m^2)
$\bar{E}$	Electric field	(V/m)
h	Thickness of different dielectric layers	(m)
k_e	Coupling coefficient of the transmission line	(dB)
g	Length of the transmission line in the z-direction	(m)
L	Contour surrounding a conductor	(m)
$\hat{n}$	Normal vector direction	(Dimensionless)
Q^i	Total charge on the i^{th} conductor	(pC/m)
s	Surface	(m^2)
V_i	Scaler potential at grid point i	(V)
v_e	Even-mode phase velocity of the transmission line.	(m/s)
v_o	Odd-mode phase velocity of the transmission line	(m/s)
ρ	Radius in cylindrical coordinate system	(m)
ϕ	Angle in cylindrical coordinate system	(Degrees)

δ_w	Angular width of strips	(Degrees)
δ_s	Angular spacing between strips	(Degrees)
δ	Angular width of overlay/substrate	(Degrees)
t	Normalized thickness of strips	(Dimensionless)
Z_o	Characteristic impedance of the transmission line	(Ω/m)
Z_{oe}	Even-mode characteristic impedance of the transmission line	(Ω/m)
Z_{oo}	Odd-mode characteristic impedance of the transmission line	(Ω/m)
ϵ_{re}	Relative even-mode effective permittivity	(Dimensionless)
ϵ_{ro}	Relative odd-mode effective permittivity	(Dimensionless)

I. INTRODUCTION

Cylindrical microstrip transmission lines with multilayer dielectrics operating in the quasi-TEM mode have recently received much attention in the microwave literature [1-5]. Using flexible dielectrics, it is possible to construct non-planar transmission lines that can be placed around conducting cylindrical surfaces. With the application of smaller and denser circuit dimensions, the coupling between circuit connections limits the performance of the cylindrical microstrip transmission lines (CMSTL). It is very important to find practical methods to accurately analyze and control the coupling between transmission lines.

In this project, attention is focused on the problem of reducing coupling between two conducting microstrip transmission lines. One possible technique is by employing a dielectric notch embedded between the two conducting lines as shown in Fig.1. The reduction of coupling can be approached by proper selecting the size of the notch and the relative permittivities of the overlay, substrate and notch regions.

The CMSTL geometry shown in Fig.1 is treated as quasi-TEM mode problem. Laplace's equation is solved for the potential distribution $V(\rho,\phi)$ in the various dielectric regions by applying the proper boundary conditions. The finite difference method (FD) is used to approximate the derivatives involved in Laplace's equation. Then, the integral form of Gauss's law is used to derive an expression for the scalar potential on the interfaces between different dielectric regions and to compute the total charge on the strips. Two approximate (asymptotic) boundary conditions (ABC) at the outer artificial boundary are developed to truncate the finite difference mesh. The solution of Laplace's equation in cylindrical coordinate system has been described by R.F. Harrington and Pontoppidan [6]. A method for the solution of the problem

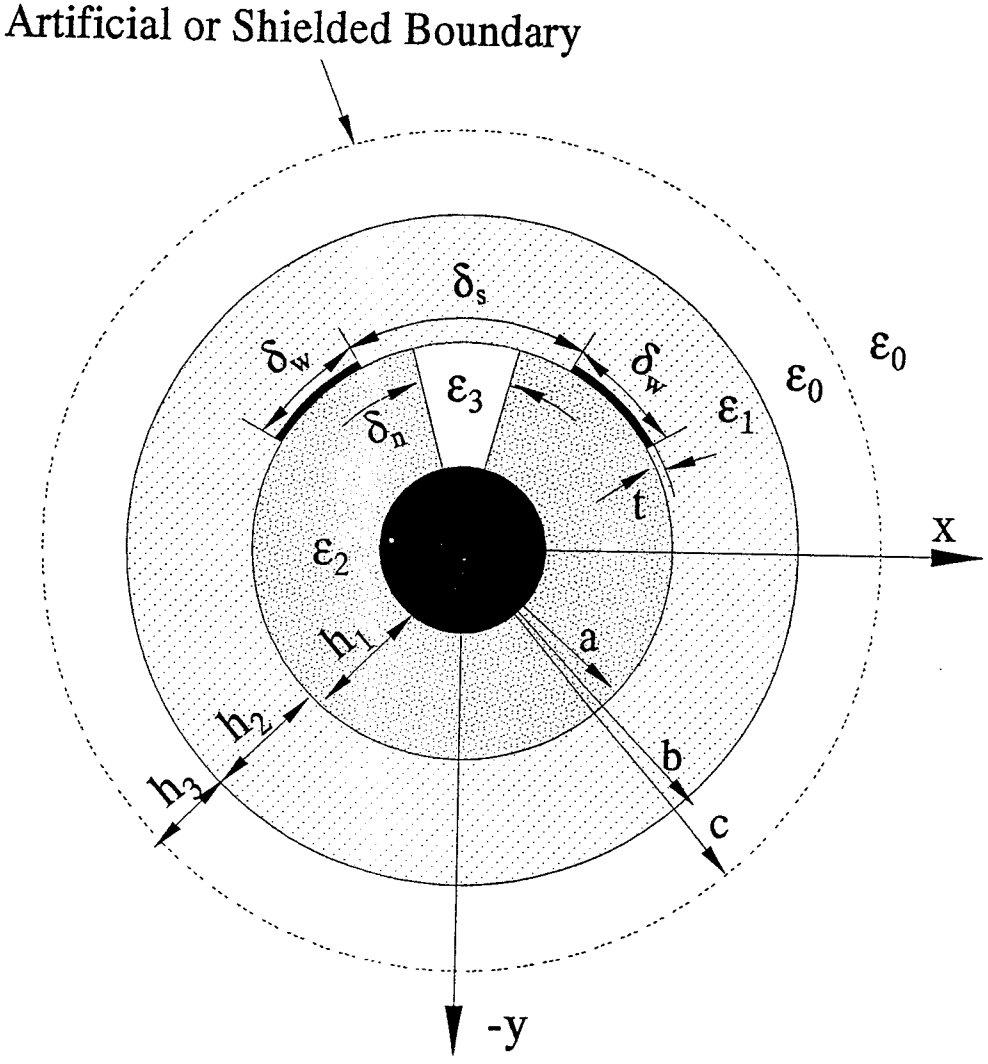

Fig.1 The geometry of a coupled cylindrical microstrip transmission line

of cylindrical transmission line in one homogeneous dielectric medium is discussed by Joshi [7]. The theory of quasi-TEM modes on coupled transmission lines in terms of voltage and current eigenvectors is developed by Kajfez [8, 9]. It has been shown that the even and odd modes are possible only when the coupled transmission lines are of symmetric shape.

The purpose of this study is to present a FD solution to analyze and to control the coupling between the conducting lines through the use of dielectric notch and truncated dielectric substrate and superstrate. Here, an ideal model is considered, where the conductors are assumed to be perfectly conducting, the dielectric materials are lossless, isotopic and homogeneous. The thickness of each conductor is not necessary assumed to be zero.

With a program written in FORTRAN language, the characteristic parameters of the CMSLTs shown in Figs.1 and 2, such as the self and mutual capacitances (C_{11}, C_{21}), coupling coefficient (k_e), even and odd modes characteristic impedances (Z_e, Z_o), normalized phase velocities (v_e, v_o), and the effective permittivities (ϵ_{eff}) are studied through a set of numerical examples presented in this report.

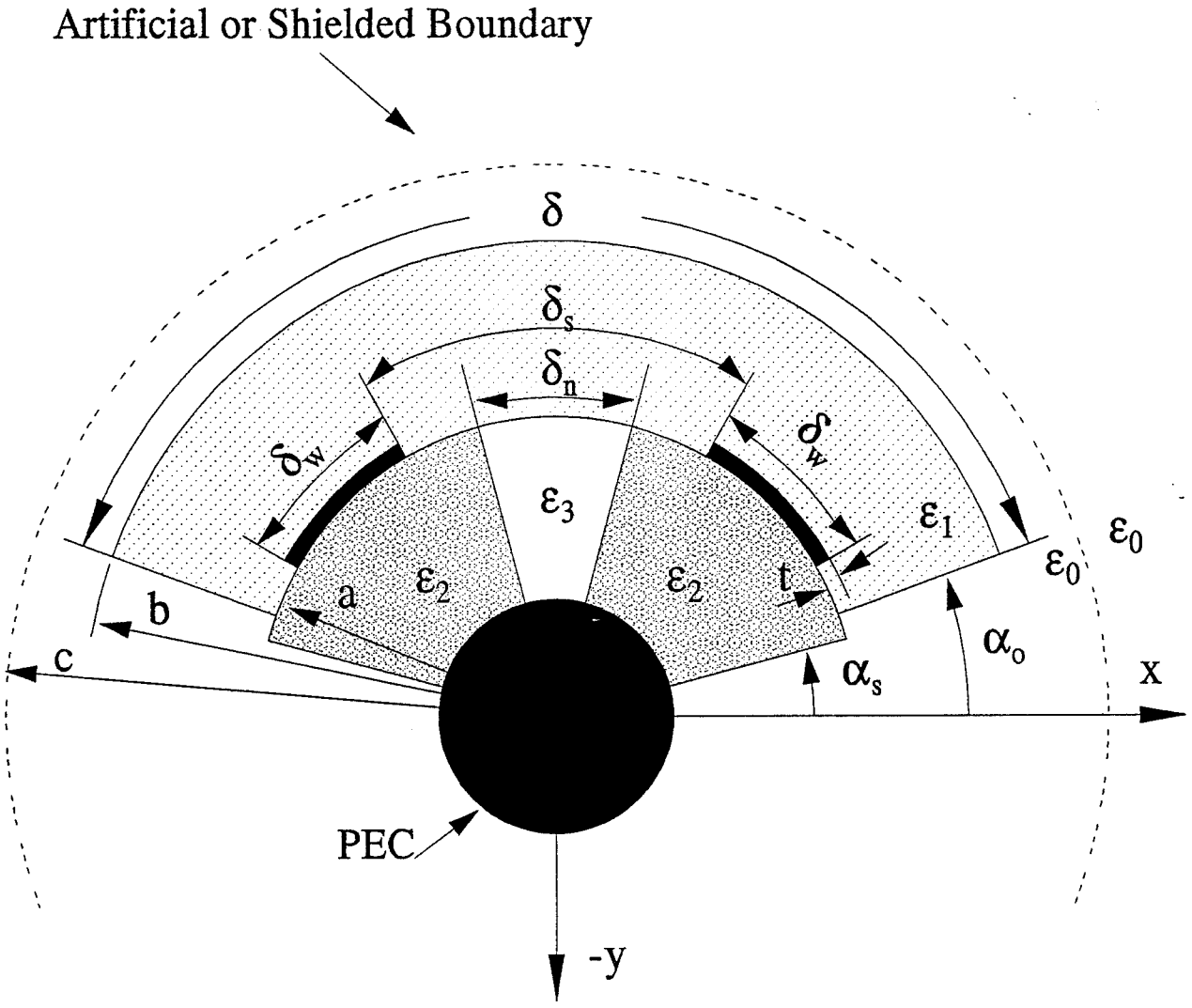

Fig.2 Truncation of the substrate and superstrate of a cylindrical transmission line

II. FORMULATION

2-1. Finite Difference Approximations

Through the years, many numerical methods have been developed for the analysis of the characteristics of microstrip transmission lines [6]. Among those is the widely known finite difference technique. For the quasi-static 2-D problems shown in Fig.1, the potential, V, everywhere can be described using Laplace's equation in the cylindrical coordinates as:

$$\frac{\partial^2 V}{\partial \rho^2} + \frac{1}{\rho}\frac{\partial V}{\partial \rho} + \frac{1}{\rho^2}\frac{\partial^2 V}{\partial \phi^2} = 0 \tag{1}$$

The finite difference technique is used to approximate the derivatives involved in Laplace's equation. This numerical approximation is based upon calculating the potential at a certain node as a function of neighboring grid points, or nodes. In general, assuming that we have three consecutive nodes ℓ, c, r, as shown in Fig.3, if Taylor's expansion is applied at node r and ℓ in the ϕ direction, this resulting equation can be expressed as:

$$V_r = V_c - (\phi_c - \phi_r)\frac{\partial V_c}{\partial \phi} + \frac{1}{2}(\phi_c - \phi_r)^2 \frac{\partial^2 V_c}{\partial \phi^2} \tag{2}$$

$$V_\ell = V_c + (\phi_\ell - \phi_c)\frac{\partial V_c}{\partial \phi} + \frac{1}{2}(\phi_\ell - \phi_c)^2 \frac{\partial^2 V_c}{\partial \phi^2} \tag{3}$$

where V_r, V_c, V_ℓ represent the potential at node r, c and ℓ respectively. Equations (2) and (3) can be rearranged to solve for the first and second derivatives with respect to ϕ as:

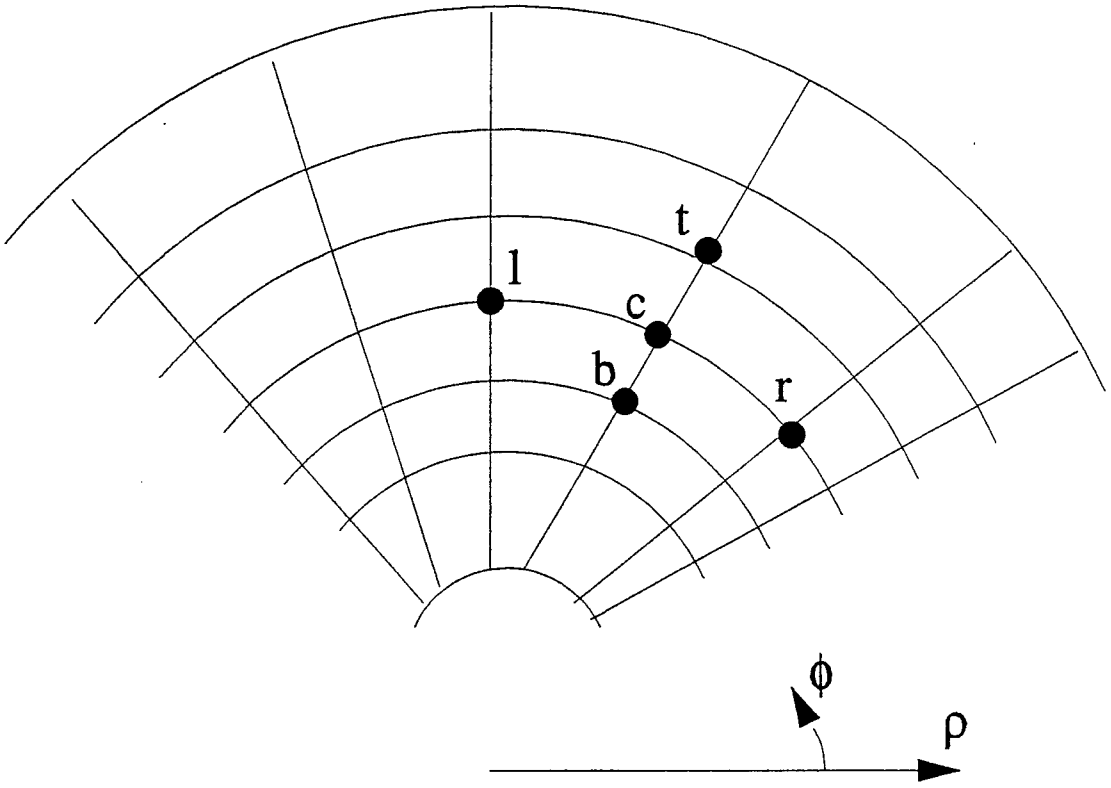

Fig.3 Finite difference mesh

$$\frac{\partial V_c}{\partial \phi} = V_c \frac{(\phi_r + \phi_\ell - 2\phi_c)}{(\phi_\ell - \phi_r)(\phi_\ell - \phi_c)} + V_\ell \frac{(\phi_c - \phi_r)}{(\phi_\ell - \phi_r)(\phi_\ell - \phi_c)} - V_r \frac{(\phi_\ell - \phi_c)}{(\phi_\ell - \phi_r)(\phi_c - \phi_r)} \tag{4}$$

$$\frac{\partial^2 V_c}{\partial \phi^2} = V_r \frac{2}{(\phi_c - \phi_r)(\phi_\ell - \phi_r)} + V_\ell \frac{2}{(\phi_\ell - \phi_c)(\phi_\ell - \phi_r)} - V_c \frac{2}{(\phi_\ell - \phi_c)(\phi_c - \phi_r)} \tag{5}$$

Similar expressions for the first and the second derivatives with respect to ρ can be obtained by applying Taylor's expansion at nodes t and b in the ρ direction as shown in Fig.3, which are expressed as:

$$\frac{\partial V_c}{\partial \rho} = V_c \frac{(\rho_t + \rho_b - 2\rho_c)}{(\rho_t - \rho_c)(\rho_c - \rho_b)} + V_t \frac{(\rho_c - \rho_b)}{(\rho_c - \rho_b)(\rho_t - \rho_c)} - V_b \frac{(\rho_t - \rho_c)}{(\rho_t - \rho_b)(\rho_c - \rho_b)} \tag{6}$$

and

$$\frac{\partial^2 V_c}{\partial \rho^2} = V_t \frac{2}{(\rho_t - \rho_c)(\rho_t - \rho_b)} + V_b \frac{2}{(\rho_c - \rho_b)(\rho_t - \rho_b)} - V_c \frac{2}{(\rho_t - \rho_c)(\rho_c - \rho_b)} \tag{7}$$

where V_t and V_b are potentials at nodes t and b, respectively.

Figure 4 shows how the grid points are distributed in different regions. It also shows a node point c and its four immediate neighbors in a homogeneous medium and on an interface between two dielectric regions. For example, the grid point c in a homogeneous region is adjacent to four nodes; t and b in ρ direction, and ℓ and r in ϕ direction. Applying Laplace's equation (1), to a point c in a homogeneous region yields

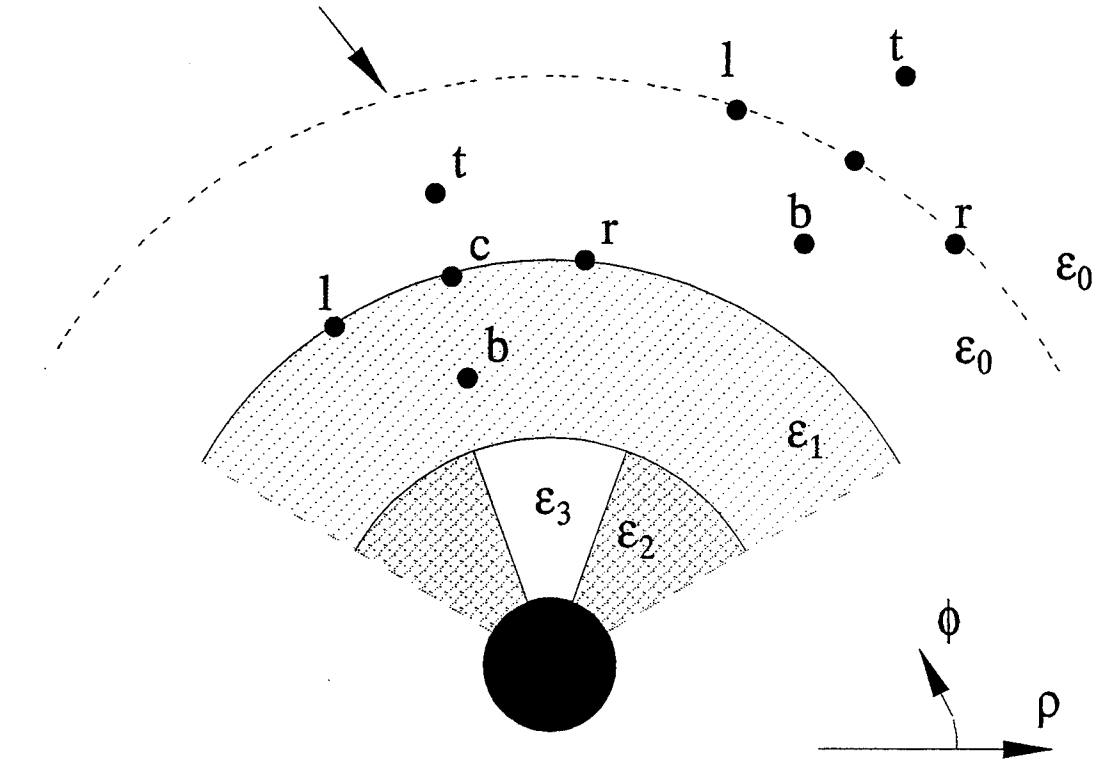

Fig.4 Grid points at an interface between different resions or at the outer boundary

$$V_c\left\{\frac{2\rho_c^2}{(\rho_t-\rho_c)(\rho_c-\rho_b)}+\frac{2}{(\phi_t-\phi_c)(\phi_c-\phi_r)}-\frac{\rho_c(\rho_t+\rho_b-2\rho_c)}{(\rho_t-\rho_c)(\rho_c-\rho_b)}\right\}$$

$$-V_t\left\{\frac{2\rho_c^2}{(\rho_t-\rho_c)(\rho_t-\rho_b)}+\frac{\rho_c(\rho_c-\rho_b)}{(\rho_t-\rho_c)(\rho_t-\rho_b)}\right\}-V_b\left\{\frac{2\rho_c^2}{(\rho_c-\rho_b)(\rho_t-\rho_b)}-\frac{\rho_c(\rho_t-\rho_c)}{(\rho_c-\rho_b)(\rho_t-\rho_b)}\right\} \tag{8}$$

$$-V_l\left\{\frac{2}{(\phi_l-\phi_c)(\phi_l-\phi_r)}\right\}-V_r\left\{\frac{2}{(\phi_c-\phi_r)(\phi_l-\phi_r)}\right\}=0$$

It is important to note, at this point, that this type of analysis applies to uniform as well as to nonuniform meshes. In fact, equation (8) could be easily specified for a uniform mesh where the potential at node point *c* reduces to

$$V_c = \frac{1}{4}[V_l + V_r + V_t + V_b] \; . \tag{9}$$

Equation (9) is known as the five-point equal arm difference equation.

The boundary conditions for the CMSTL shown in Figs.1 and 2 are:

$V = v_1$ on strip 1

$V = v_2$ on strip 2

$V = 0$ on the surface of the circular core

$\int \mathbf{D}\cdot d\mathbf{s} = 0$ on any closed surface containing a dielectric interface

On a dielectric interface separating two regions, the normal component of displacement vector *D* must be continuous and hence:

$$D_{1n} = D_{2n} \tag{10}$$

This condition is based on Gauss's law for the electric field, which can be described as

$$\oint_s \boldsymbol{D}\cdot d\boldsymbol{s} = \oint_s \epsilon \boldsymbol{E}\cdot d\boldsymbol{s} = Q_{enc} = 0 \tag{11}$$

Where Q_{enc} is set to zero since no free charges exist on the dielectric boundary or in dielectric regions. Since there is no dependence of z, the integral along z-axis is a constant, thus, substituting $\boldsymbol{E} = -\nabla V$ in equation (11) yields

$$\oint_s \epsilon \nabla V\cdot d\boldsymbol{s} = g \oint_L \epsilon \nabla V\cdot \boldsymbol{n} d\ell = g \oint_L \epsilon \frac{\partial V}{\partial n} d\ell = 0 \tag{12}$$

where $\partial V/\partial n$ denotes the derivative of V normal to the contour L, and g is the length of the line along the z-axis. The surface integration on left hand side of equation (12) has been replaced by a contour integration, because the microstrip transmission lines considered are two-dimensional structures, and the solution of the potential is independent of z.

For the geometry shown in Fig.1, a general expression for a node point which is surrounded by different dielectric regions can be obtained. Figure 5 is an expanded view of a special node point which is surrounded by four dielectric regions. Based on Gauss's law, equation (12) can be written for a point c at the intersection of four different regions (as shown in Fig.5) as:

$$\oint_L \epsilon \left(\frac{\partial V}{\partial \rho} \rho d\phi + \frac{\partial V}{\rho \partial \phi} d\rho\right) = 0 \tag{13}$$

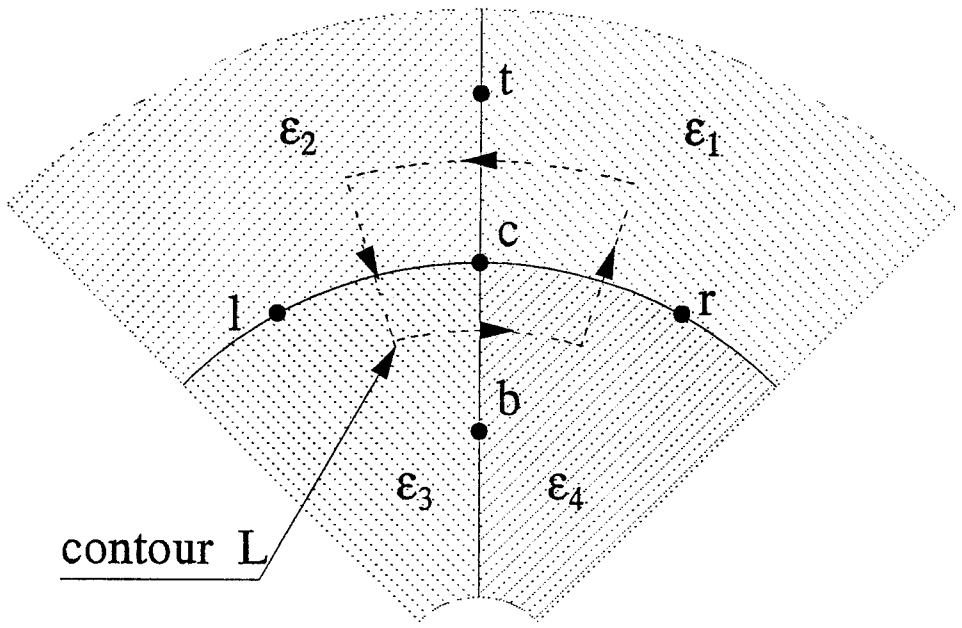

Fig.5 Grid point c at the intersection of four different dielectric regions

Applying the left hand side of equation (13) to the contour normal to the interface between regions 1 and 2, as shown in Fig.5, gives

$$\int \epsilon \frac{\partial V}{\partial \rho} \rho d\phi = \epsilon_1 \frac{(\rho_t+\rho_c)(\phi_c-\phi_r)}{4(\rho_t-\rho_c)}(V_t-V_c) + \epsilon_2 \frac{(\rho_t+\rho_c)(\phi_t-\phi_c)}{4(\rho_t-\rho_c)}(V_t-V_c) \tag{14}$$

At the interface between regions 2 and 3,

$$\int \epsilon \frac{\partial V}{\rho \partial \phi} d\rho = \epsilon_2 \frac{(\rho_t-\rho_c)}{2\rho(\phi_t-\phi_c)}(V_t-V_c) + \epsilon_3 \frac{(\rho_c-\rho_b)}{2\rho(\phi_t-\phi_c)}(V_t-V_c) \tag{15}$$

At the interface between regions 3 and 4,

$$-\int \epsilon \frac{\partial V}{\partial \rho} \rho d\phi = -\epsilon_3 \frac{(\rho_c+\rho_b)(\phi_t-\phi_c)}{4(\rho_c-\rho_b)}(V_c-V_b) - \epsilon_4 \frac{(\rho_c+\rho_b)(\phi_c-\phi_r)}{4(\rho_c-\rho_b)}(V_c-V_b) \tag{16}$$

Finally, at the interface between regions 4 and 1,

$$-\int \epsilon \frac{\partial V}{\rho \partial \phi} d\rho = -\epsilon_4 \frac{(\rho_c-\rho_b)}{2\rho_c(\phi_c-\phi_r)}(V_c-V_r) - \epsilon_1 \frac{(\rho_t-\rho_c)}{2\rho_c(\phi_c-\phi_r)}(V_c-V_r) \tag{17}$$

After arranging these terms we obtain a general expression for the node equation at point *c* as:

$$
\begin{aligned}
&V_c\left\{\begin{array}{l}\dfrac{(\rho_t+\rho_c)}{4(\rho_t-\rho_c)}[\epsilon_1(\phi_c-\phi_r)+\epsilon_2(\phi_t-\phi_c)]+\dfrac{1}{2\rho_c(\phi_t-\phi_c)}[\epsilon_2(\rho_t-\rho_c)+\epsilon_3(\rho_c-\rho_b)]\\ +\dfrac{(\rho_c+\rho_b)}{4(\rho_c-\rho_b)}[\epsilon_3(\phi_t-\phi_c)+\epsilon_4(\phi_c-\phi_r)]+\dfrac{1}{2\rho_c(\phi_c-\phi_r)}[\epsilon_4(\rho_c-\rho_b)+\epsilon_1(\rho_t-\rho_c)]\end{array}\right\}\\
&-V_t\left\{\frac{(\rho_t+\rho_c)}{4(\rho_t-\rho_c)}[\epsilon_1(\phi_c-\phi_r)+\epsilon_2(\phi_t-\phi_c)]\right\}-V_t\left\{\frac{1}{2\rho_c(\phi_t-\phi_c)}[\epsilon_2(\rho_t-\rho_c)+\epsilon_3(\rho_c-\rho_b)]\right\}\\
&-V_b\left\{\frac{(\rho_c+\rho_b)}{4(\rho_c-\rho_b)}[\epsilon_3(\phi_t-\phi_c)+\epsilon_4(\phi_c-\phi_r)]\right\}-V_r\left\{\frac{1}{2\rho_c(\phi_c-\phi_r)}[\epsilon_4(\rho_c-\rho_b)+\epsilon_1(\rho_t-\rho_c)]\right\}=0
\end{aligned}
\tag{18}
$$

Special cases can be obtained from this general expression for a node at the corner of three different dielectric regions as shown in Fig.6.

2-2. First Order Approximate Boundary Condition (ABC1)

For the transmission lines shown in Figs.1 and 2, the outer artificial boundary can be shielded using a perfect electric conductor (PEC), and hence, the potential at the boundary is set to zero. However, when the transmission line is not shielded by a PEC, an approximate boundary condition should be applied at an artificial boundary in order to truncate the FD mesh so that numerical analysis can be carried out. The first order boundary condition used is proposed by A.Khebir, et.al.[10]. The series expansion for the electric potential is defined as

$$
V(\rho,\phi) = C_0 + A_0(\phi)\ln\rho + \sum_{n=1}^{\infty}\frac{A_n(\phi)}{\rho^n} \tag{19}
$$

The constant term, C_0, is dropped because the potential at infinity is zero. The second term in equation (19) is also dropped because of the charge free enclosed by the mesh bounded by the

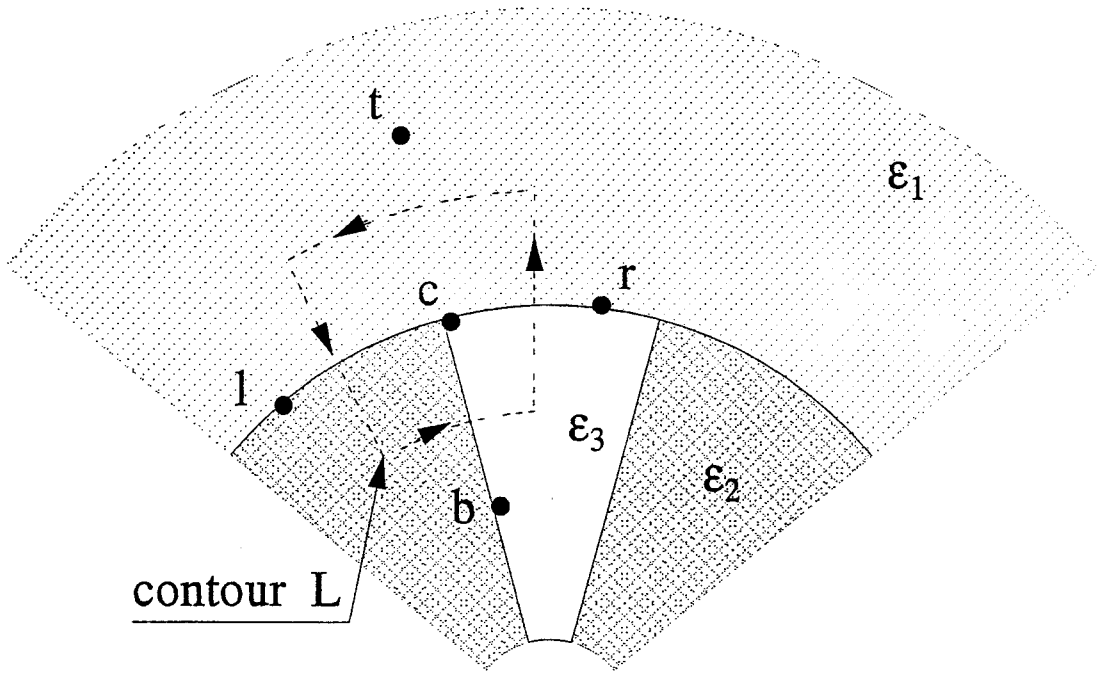

Fig.6 Grid point c at a corner of dielectric notch

artificial boundary. Therefore, equation (19) reduces to

$$V(\rho,\phi) = \frac{A_1(\phi)}{\rho} + \frac{A_2(\phi)}{\rho^2} + \frac{A_3(\phi)}{\rho^3} + \ldots \tag{20}$$

Differentiating equation (20) with respect to ρ gives

$$\frac{\partial V(\rho,\phi)}{\partial \rho} = -\frac{A_1(\phi)}{\rho^2} - \frac{2A_2(\phi)}{\rho^3} - \frac{3A_3(\phi)}{\rho^4} - \ldots \tag{21}$$

Then, equation (20) is multiplied by $1/\rho$ and then added to equation (21), we get:

$$\frac{V}{\rho} + \frac{\partial V}{\partial \rho} = -\frac{A_2}{\rho^3} - \frac{2A_3}{\rho^4} - \frac{3A_4}{\rho^5} - \ldots \tag{22}$$

As an approximation to equation (22), the right hand side will be assumed to be zero. The amount of error caused by this truncation in the analysis will be reduced as the value of ρ at the outer boundary increases, which means that the error is getting smaller and smaller as the outer boundary is moved away from the strips. This approximation leads to:

$$\frac{V}{\rho} + \frac{\partial V}{\partial \rho} = 0 \tag{23}$$

Equation (23) will be implemented along the outer boundary of the mesh. The grid point system on the outer boundary of the mesh is shown in Fig.4. The grid point *c* resides on the outer boundary and *t* is a point outside the outer boundary. Because point *t* lies outside the mesh, it is not possible to enforce Laplace's equation (8) at node point *c* in the usual manner. Instead, equation (23) is applied first to determine the potential at point *t*, in terms of V_t, V_c, V_r and V_b. Once the V_t is known then equation (8) can be enforced. At the point *c*, if equation (6) is

substituted equation (23), it can be arranged to obtain the expression:

$$V_t = -V_c\left\{\frac{(\rho_t+\rho_b-2\rho_c)(\rho_t-\rho_b)}{(\rho_c-\rho_b)^2}+\frac{(\rho_t-\rho_c)(\rho_t-\rho_b)}{\rho_c(\rho_c-\rho_b)}\right\}+V_b\frac{(\rho_t-\rho_c)^2}{(\rho_c-\rho_b)^2} \tag{24}$$

Further substitution of (24) into the Laplace's equation (8), one obtains:

$$\begin{aligned} &V_c\left\{\frac{2}{(\rho_t-\rho_c)(\rho_c-\rho_b)}+\frac{2}{\rho_c^2(\phi_t-\phi_c)(\phi_c-\phi_r)}-\frac{(\rho_t+\rho_b-2\rho_c)}{\rho_c(\rho_t-\rho_c)(\rho_c-\rho_b)}\right.\\ &\qquad\left.+\frac{(3\rho_c-\rho_b)(\rho_t+\rho_b-2\rho_c)}{\rho_c(\rho_t-\rho_c)(\rho_c-\rho_b)^2}+\frac{(3\rho_c-\rho_b)}{\rho_c^2(\rho_c-\rho_b)}\right\}\\ &-V_b\left\{\frac{(3\rho_c-\rho_t)}{\rho_c(\rho_c-\rho_b)(\rho_t-\rho_b)}+\frac{(3\rho_c-\rho_b)(\rho_t-\rho_c)}{\rho_c(\rho_t-\rho_b)(\rho_c-\rho_b)^2}\right\}\\ &-V_t\left\{\frac{2}{\rho_c^2(\phi_t-\phi_c)(\phi_t-\phi_r)}\right\}-V_r\left\{\frac{2}{\rho_c^2(\phi_c-\phi_r)(\phi_t-\phi_r)}\right\}=0 \end{aligned} \tag{25}$$

Alternatively, one can substitute (24) into (18) to obtain:

$$
\begin{aligned}
V_c \Bigg\{ & \frac{(\rho_t+\rho_c)(\rho_t+\rho_b-2\rho_c)(\rho_t-\rho_b)}{4(\rho_t-\rho_c)(\rho_c-\rho_b)^2}[\epsilon_1(\phi_c-\phi_r)+\epsilon_2(\phi_\ell-\phi_c)] \\
& + \frac{(\rho_t+\rho_c)(\rho_t-\rho_b)}{4\rho_c(\rho_c-\rho_b)}[\epsilon_1(\phi_c-\phi_r)+\epsilon_2(\phi_\ell-\phi_c)] \\
& + \frac{(\rho_t+\rho_c)}{4(\rho_t-\rho_c)}[\epsilon_1(\phi_c-\phi_r)+\epsilon_2(\phi_\ell-\phi_c)] + \frac{1}{2\rho_c(\phi_\ell-\phi_c)}[\epsilon_2(\rho_t-\rho_c)+\epsilon_3(\rho_c-\rho_b)] \\
& + \frac{(\rho_c+\rho_b)}{4(\rho_c-\rho_b)}[\epsilon_3(\phi_\ell-\phi_c)+\epsilon_4(\phi_c-\phi_r)] + \frac{1}{2\rho_c(\phi_c-\phi_r)}[\epsilon_4(\rho_c-\rho_b)+\epsilon_1(\rho_t-\rho_c)] \Bigg\} \\
-V_b & \left\{ \frac{(\rho_t+\rho_c)(\rho_t-\rho_c)}{4(\rho_c-\rho_b)^2}[\epsilon_1(\phi_c-\phi_r)+\epsilon_2(\phi_\ell-\phi_c)] + \frac{(\rho_c+\rho_b)}{4(\rho_c-\rho_b)}[\epsilon_3(\phi_\ell-\phi_c)+\epsilon_4(\phi_c-\phi_r)] \right\} \\
-V_\ell & \left\{ \frac{1}{2\rho_c(\phi_\ell-\phi_c)}[\epsilon_2(\rho_t-\rho_c)+\epsilon_3(\rho_c-\rho_b)] \right\} \\
-V_r & \left\{ \frac{1}{2\rho_c(\phi_c-\phi_r)}[\epsilon_4(\rho_c-\rho_b)+\epsilon_1(\rho_t-\rho_c)] \right\} = 0
\end{aligned}
\tag{26}
$$

2-3. Second Order Approximate Boundary Condition (ABC2)

In this section, a higher order approximate boundary condition will be developed. This higher order A.B.C. includes more terms than the lower order ABC1, and should thus be more accurate when the outer artificial boundary is relatively close to the strips. In order to develop a general expression for ABC2, we first define:

$$U = \frac{\partial V}{\partial \rho} + \frac{V}{\rho} \tag{27}$$

Then, the right hand side of equation (22) is replaced with U to obtain:

$$U = -\frac{A_2}{\rho^3} - \frac{2A_3}{\rho^4} - \frac{3A_4}{\rho^5} \cdots \tag{28}$$

Equation (28) can be differentiated with respect to ρ to obtain:

$$\frac{\partial U}{\partial \rho} = \frac{3A_2}{\rho^4} + \frac{8A_3}{\rho^5} + \frac{15A_4}{\rho^6} + \cdots \tag{29}$$

Now, multiply (28) by $3/\rho$ and then add it to (29) to obtain:

$$\frac{3}{\rho}U + \frac{\partial U}{\partial \rho} = -\frac{3A_2}{\rho^4} - \frac{6A_3}{\rho^5} - \frac{9A_4}{\rho^6} - \cdots + \frac{3A_2}{\rho^4} + \frac{8A_3}{\rho^5} + \frac{15A_4}{\rho^6} + \cdots \tag{30}$$

which can be rewritten as:

$$\frac{\partial U}{\partial \rho} + \frac{3}{\rho}U = \frac{2A_3}{\rho^5} + \frac{6A_4}{\rho^6} + \frac{12A_5}{\rho^7} + \cdots \tag{31}$$

if the definition of U is used and the right hand side of the equation is set equal to zero, one obtains:

$$\left(\frac{\partial}{\partial \rho} + \frac{3}{\rho}\right)\left(\frac{\partial}{\partial \rho} + \frac{1}{\rho}\right)V = 0 \tag{32}$$

which is equivalent to:

$$\frac{\partial^2 V_c}{\partial \rho^2} + \frac{4}{\rho_c^2}\frac{\partial V_c}{\partial \rho} + \frac{2}{\rho_c^2}V_c = 0 \tag{33}$$

This expression can be used to obtain the voltage at point t for the grid point system on the outer boundary of the mesh as shown in Fig.4. The grid point c resides on the outer boundary and t is a point outside the outer boundary. To obtain V_t in terms of V_c and V_b, substituting equations

(6) and (7) into (33) to obtain V_t in terms of V_ℓ, V_c, V_r and V_b, which can be written as:

$$V_t = V_c\left\{\frac{(\rho_t-\rho_b)}{\rho_c(\rho_c-\rho_b)(3\rho_c-2\rho_b)}-\frac{2(\rho_t-\rho_b)(\rho_t+\rho_b-2\rho_c)}{\rho_c^{\,2}(\rho_c-\rho_b)(3\rho_c-2\rho_b)}-\frac{(\rho_t-\rho_c)(\rho_c-\rho_b)}{\rho_c^{\,3}(3\rho_c-2\rho_b)}\right\} \\ -V_b\left\{\frac{(\rho_t-\rho_c)}{\rho_c(\rho_c-\rho_b)(3\rho_c-2\rho_b)}-\frac{2(\rho_t-\rho_c)^2}{\rho_c^{\,2}(\rho_c-\rho_b)(3\rho_c-2\rho_b)}\right\} \tag{34}$$

Equation (34) can then be substituted into the Laplace's equation (8) to obtain:

$$V_c\left\{\begin{array}{l}\dfrac{2}{(\rho_t-\rho_c)(\rho_c-\rho_b)}+\dfrac{2}{\rho_c^{\,2}(\phi_\ell-\phi_c)(\phi_c-\phi_r)}-\dfrac{(\rho_t+\rho_b-2\rho_c)}{\rho_c(\rho_t-\rho_c)(\rho_c-\rho_b)} \\ -\dfrac{(3\rho_c-\rho_b)}{(\rho_t-\rho_c)(\rho_c-\rho_b)(3\rho_c-2\rho_b)}+\dfrac{(3\rho_c-\rho_b)}{\rho_c^{\,2}(3\rho_c-2\rho_b)}+\dfrac{2(3\rho_c-\rho_b)(\rho_t+\rho_b-2\rho_c)}{\rho_c(\rho_t-\rho_c)(\rho_c-\rho_b)(3\rho_c-2\rho_b)}\end{array}\right\} \\ -V_b\left\{\frac{(3\rho_c-\rho_t)}{\rho_c(\rho_c-\rho_b)(\rho_t-\rho_b)}-\frac{(3\rho_c-\rho_b)}{(\rho_t-\rho_b)(\rho_c-\rho_b)(3\rho_c-2\rho_b)}+\frac{2(\rho_t-\rho_c)(3\rho_c-\rho_b)}{\rho_c(\rho_t-\rho_b)(\rho_c-\rho_b)(3\rho_c-2\rho_b)}\right\} \\ -V_\ell\left\{\frac{2}{\rho_c^{\,2}(\phi_\ell-\phi_c)(\phi_\ell-\phi_r)}\right\}-V_r\left\{\frac{2}{\rho_c^{\,2}(\phi_c-\phi_r)(\phi_\ell-\phi_r)}\right\} = 0 \tag{35}$$

However, when substituting (34) into (18), one obtains a general expression for grid points at the artificial boundary, as:

$$
\begin{aligned}
V_b & \left\{ \left(\frac{(\rho_t+\rho_c)(\rho_t-\rho_c)}{2(\rho_c-\rho_b)(3\rho_c-2\rho_b)} - \frac{\rho_c(\rho_t+\rho_c)}{4(\rho_c-\rho_b)(3\rho_c-2\rho_b)} \right)(\epsilon_1(\phi_c-\phi_r)+\epsilon_2(\phi_\ell-\phi_c)) \right. \\
& \left. + \frac{(\rho_c+\rho_b)}{4(\rho_c-\rho_b)}(\epsilon_3(\phi_\ell-\phi_c)+\epsilon_4(\phi_c-\phi_r)) \right\} \\
+V_\ell & \left\{ \frac{1}{2\rho_c(\phi_\ell-\phi_c)}[\epsilon_2(\rho_t-\rho_c)+\epsilon_3(\rho_c-\rho_b) \right\} + V_r \left\{ \frac{1}{2\rho_c(\phi_c-\phi_r)}(\epsilon_4(\rho_c-\rho_b)+\epsilon_1(\rho_t-\rho_c)) \right\} \\
-V_c & \left\{ \begin{array}{l}
\dfrac{(\rho_t+\rho_c)}{4(\rho_t-\rho_c)}(\epsilon_1(\phi_c-\phi_r)+\epsilon_2(\phi_\ell-\phi_c)) + \dfrac{1}{2\rho_c(\phi_\ell-\phi_c)}(\epsilon_2(\rho_t-\rho_c)+\epsilon_3(\rho_c-\rho_b)) \\
+\dfrac{(\rho_c+\rho_b)}{4(\rho_c-\rho_b)}(\epsilon_3(\phi_\ell-\phi_c)+\epsilon_4(\phi_c-\phi_r)) + \dfrac{1}{(2\rho_c(\phi_c-\phi_r)}(\epsilon_4(\rho_c-\rho_b)+\epsilon_1(\rho_t-\rho_c)) \\
+\left(\dfrac{(\rho_t+\rho_c)(\rho_t-\rho_b)(\rho_t+\rho_b-2\rho_c)}{2(\rho_t-\rho_c)(\rho_c-\rho_b)(3\rho_c-2\rho_b)} + \dfrac{(\rho_t+\rho_c)(\rho_t-\rho_b)}{4\rho_c(3\rho_c-2\rho_b)} \right. \\
\left. - \dfrac{\rho_c(\rho_t+\rho_c)(\rho_t-\rho_b)}{4(\rho_t-\rho_c)(\rho_c-\rho_b)(3\rho_c-2\rho_b)} \right)(\epsilon_1(\phi_c-\phi_r)+\epsilon_2(\phi_\ell-\phi_c))
\end{array} \right\} = 0
\end{aligned}
\tag{36}
$$

2-4. Banded Matrix Solution

From the equations describing the potential at the grid points, it is noted that the potential V at each node is related only to its four immediate neighbor nodes. Therefore, application of any of those equations to all grid points in the solution mesh leads to a set of simultaneous equations of the form

$$[A][X] = [B]$$

where matrix [*A*] is a sparse matrix, i.e. it contains many zero elements, [*X*] is a column matrix containing all unknown potentials, *V*, for node points, and [*B*] is a column matrix which contains

the known potential at some fixed nodes. Matrix [*A*] is banded in which its non-zero elements are clustered near the main diagonal. Matrix [*X*], can be obtained from

$$[X] = [A]^{-1}[B]$$

Where the Linpack [11] subroutines SGBCO and SGBSL are used to invert and factorize the banded matrix [*A*]. Once the solution of the unknown matrix [*X*] is obtained, the characteristic parameters of the CMSTL can be determined as described in the next section.

III. COMPUTATION OF THE CYLINDRICAL TRANSMISSION LINE CHARACTERISTIC PARAMETERS

3-1. The Charges on the Strip Lines

The computation of the characteristic impedance and the phase velocity for cylindrical transmission line with an inhomogeneous medium requires calculating the capacitances of the structure, with and without the dielectric material. Since the capacitance per unit length is directly related to the charges per unit length on the strips, the problem is reduced to finding the total charge per unit length on the strips. The microstrip transmission lines shown in Figs. 1 and 2 have two conductors which are placed between the two different dielectrics, superstrate and substrate. It is assumed throughout the analysis of the problem that the conductors are perfectly conducting strips and the dielectric materials are lossless, isotopic, and homogeneous. Let Q^i denote the total charge on the i^{th} conductor. If Gauss's law is applied to a closed path L enclosing the i^{th} conductor, the total charge on that conductor is then expressed as:

$$\oint_s \boldsymbol{D}\cdot d\boldsymbol{s} = \oint_s \epsilon \boldsymbol{E}\cdot d\boldsymbol{s} = Q^i_{enc} \tag{37}$$

where $\boldsymbol{D}$ is the displacement vector and $\boldsymbol{ds}$ is the element area. Substituting for $\boldsymbol{E} = -\nabla V$ in equation (37) yields:

$$-\oint_s \epsilon \nabla V \cdot \boldsymbol{n}\, ds = -\oint_L \int_0^g \epsilon \frac{\partial V}{\partial n} dz \cdot d\ell = Q^i_{enc} \tag{38}$$

where g is the length of the line along the z-axis and L is the contour surrounds the i^{th} conductor.

The integrand in equation (38) is independent of z, and hence the integral along the z-axis is a constant. The total charge per unit length is then given from equation (38) as

$$\frac{Q^i_{enc}}{g} = -\oint_L \epsilon \frac{\partial V}{\partial n} d\ell \tag{39}$$

Equation (39) can be explicitly prescribed on the four sides surrounding the conductor, as

$$\begin{aligned}\frac{Q^i_{enc}}{g} = -\oint_L \epsilon \frac{\partial V}{\partial n} d\ell &= \int_{rs} \epsilon(\rho) \frac{\partial V}{\rho \partial \phi} d\rho + \int_{ts} \epsilon(\phi) \frac{\partial V}{\partial \phi} \rho d\phi \\ &+ \int_{\ell s} \epsilon(\rho) \frac{\partial V}{\rho \partial \phi} d\rho + \int_{bs} \epsilon(\phi) \frac{\partial V}{\partial \rho} \rho d\phi\end{aligned} \tag{40}$$

where the notation *rs*, *ℓs*, *ts* and *bs* stand for the right, left, top and bottom sides respectively. To further illustrate how equation (40) is applied, consider the grid points shown in Fig.7a. Applying (38) on the right and left sides yields an approximate result of

$$\begin{aligned}Q^i_{rs} &= \frac{\epsilon_2}{2}\left[\frac{V_1 - V_3}{\rho_2(\phi_1 - \phi_3)} + \frac{V_4 - V_6}{\rho_5(\phi_4 - \phi_6)}\right](\rho_5 - \rho_2) \\ &+ \frac{\epsilon_1}{2}\left[\frac{V_4 - V_6}{\rho_5(\phi_4 - \phi_6)} + \frac{V_7 - V_9}{\rho_8(\phi_7 - \phi_9)}\right](\rho_8 - \rho_5)\end{aligned} \tag{41}$$

Further partial contribution to charge from right side integral, the left side contribution is:

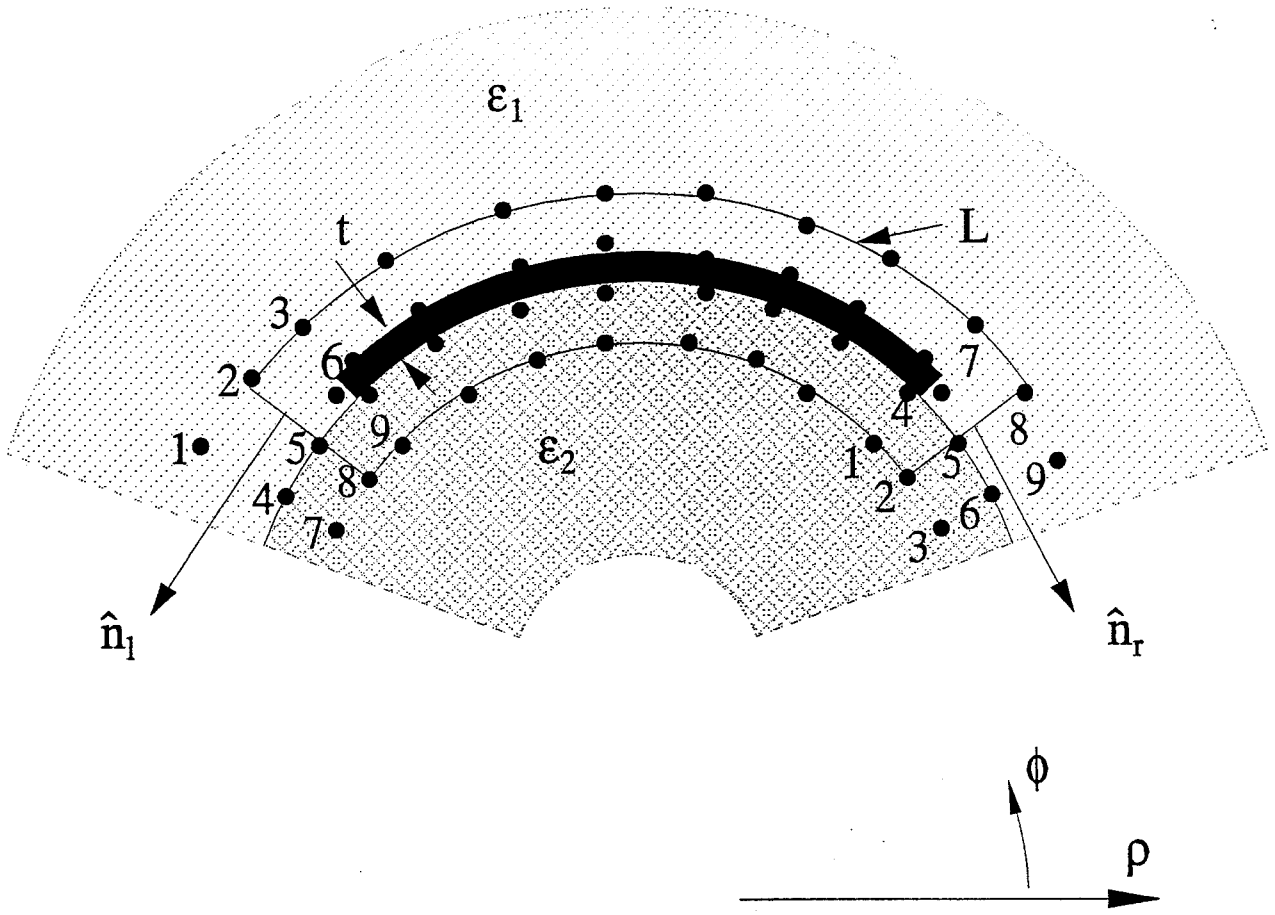

Fig.7a Charge computation on the right and left sides

$$Q_{ts}^{i} = \frac{\epsilon_1}{2}\left[\frac{V_1-V_3}{\rho_2(\phi_1-\phi_3)}+\frac{V_4-V_6}{\rho_5(\phi_4-\phi_6)}\right](\rho_2-\rho_5) + \frac{\epsilon_2}{2}\left[\frac{V_4-V_6}{\rho_5(\phi_4-\phi_6)}+\frac{V_7-V_9}{\rho_8(\phi_7-\phi_9)}\right](\rho_5-\rho_8) \tag{42}$$

For simplicity, the charge along the top and bottom sides can be expanded by assuming that there are only a few grid points on the closed contour as shown in Fig.7b. Applying (38) on the top and bottom sides yields the approximate result:

$$Q_{bs}^{i} = -\frac{\epsilon_2}{2}\left[\frac{V_1-V_3}{\rho_1-\rho_3}+\frac{V_4-V_6}{\rho_4-\rho_6}\right](\phi_2-\phi_5)\rho_2 \; -\frac{\epsilon_2}{2}\left[\frac{V_4-V_6}{\rho_4-\rho_6}+\frac{V_7-V_9}{\rho_7-\rho_9}\right](\phi_5-\phi_8)\rho_5 - \frac{\epsilon_2}{2}\left[\frac{V_7-V_9}{\rho_7-\rho_9}+\frac{V_{10}-V_{12}}{\rho_{10}-\rho_{12}}\right](\phi_8-\phi_{11})\rho_8 \; -\frac{\epsilon_2}{2}\left[\frac{V_{10}-V_{12}}{\rho_{10}-\rho_{12}}+\frac{V_{13}-V_{15}}{\rho_{13}-\rho_{15}}\right](\phi_{11}-\phi_{14})\rho_{11} \tag{43}$$

and

$$Q_{ts}^{i} = -\frac{\epsilon_1}{2}\left[\frac{V_3-V_1}{\rho_3-\rho_1}+\frac{V_6-V_4}{\rho_6-\rho_4}\right](\phi_5-\phi_2)\rho_2 \; -\frac{\epsilon_1}{2}\left[\frac{V_6-V_4}{\rho_6-\rho_4}+\frac{V_9-V_7}{\rho_9-\rho_7}\right](\phi_8-\phi_5)\rho_5 - \frac{\epsilon_1}{2}\left[\frac{V_9-V_7}{\rho_9-\rho_7}+\frac{V_{12}-V_{10}}{\rho_{12}-\rho_{10}}\right](\phi_{11}-\phi_8)\rho_8 \; -\frac{\epsilon_1}{2}\left[\frac{V_{12}-V_{10}}{\rho_{12}-\rho_{10}}+\frac{V_{15}-V_{13}}{\rho_{15}-\rho_{13}}\right](\phi_{14}-\phi_{11})\rho_{11} \tag{44}$$

Where the total charge per unit length on the i^{th} conductor is then described as the sum of the partial charge contributions:

$$\frac{Q_{enc}^{i}}{g} = -[Q_{rs}^{i} + Q_{ts}^{i} + Q_{ts}^{i} + Q_{bs}^{i}], \qquad i=1,2 \tag{45}$$

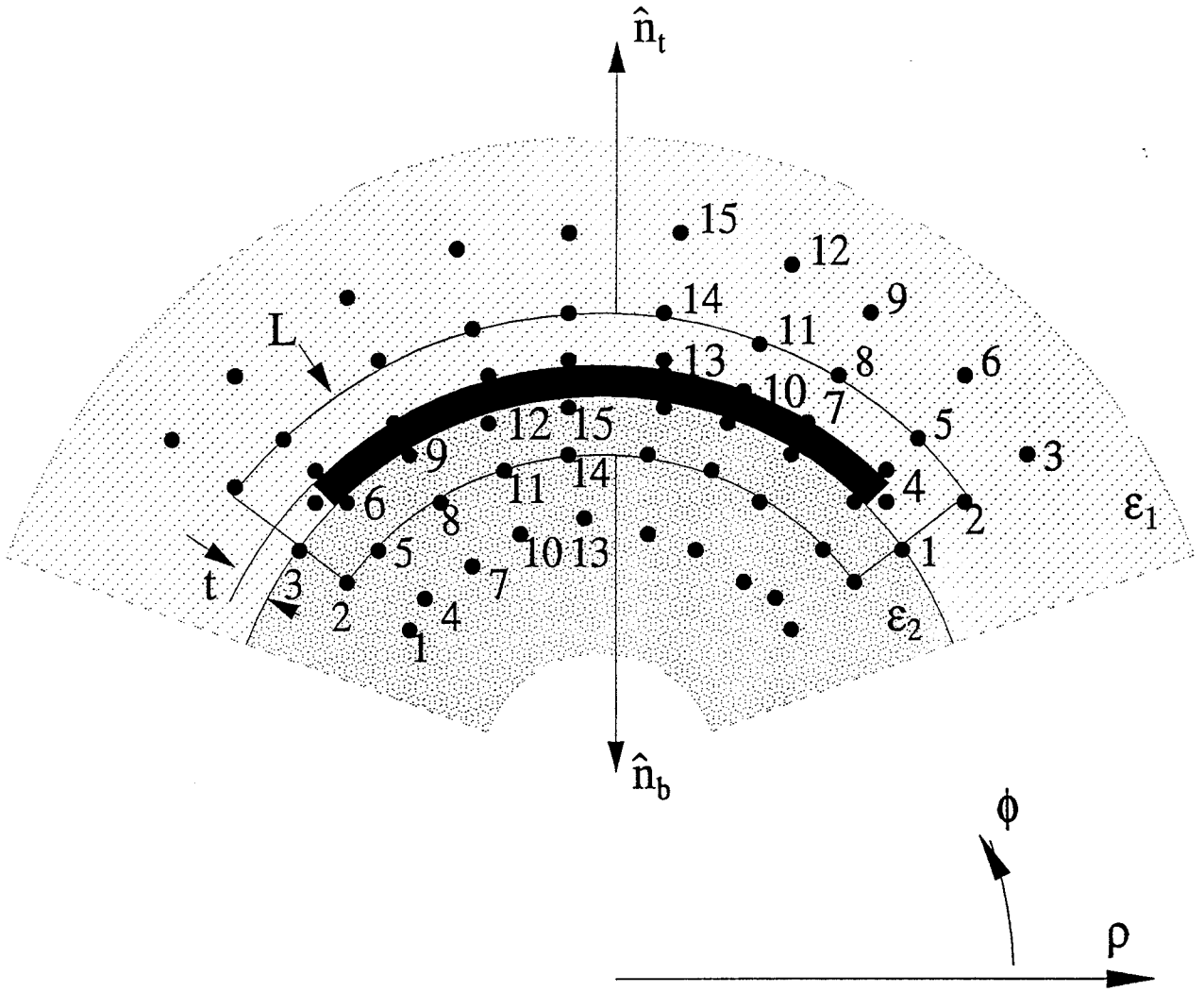

Fig.7b Charge computation on the top and bottom sides

3-2. Computation of Mutual and Self Capacitances

The theory of multi-conductor transmission lines has been widely discussed. In general the equations relating voltages and charges to capacitances are given by

$$Q_1 = C_{11}v_1+C_{12}(v_1-v_2) \quad , \quad Q_2 = C_{21}(v_2-v_1)+C_{22}v_2 \tag{46}$$

where the coefficients C_{ii} are called self capacitances, and C_{ij} are mutual capacitances. For the odd mode of excitation, $v_1=-v_2=1$ V and hence the charges on strips 1 and 2 are denoted by Q_{1o}, Q_{2o}, respectively. Whereas, when $v_1=v_2=1$ V, the charges on strips 1 and 2 are denoted by Q_{1e}, Q_{2e}, respectively. Applying these two types of excitations on the cylindrical microstrip line, and using equation (46), one gets

$$C_{11} = Q_{1e}, \quad C_{12} = \frac{Q_{1o}-Q_{1e}}{2}, \quad C_{21} = \frac{-Q_{2o}-Q_{2e}}{2}, \quad C_{22} = Q_{2e} \tag{47}$$

3-3. Impedance, Phase Velocity and Effective Permittivity

For a symmetric transmission line, the total charge per unit length on the conductors will be of equal magnitude and sign for even mode, i.e.,

$$Q_1 = Q_2 = Q_e \tag{48}$$

while for odd mode, the charges will be equal in magnitude but opposite in sign, i.e.,

$$Q_1 = -Q_2 = Q_o \tag{49}$$

In such a case, the capacitances can be related to the odd and even total charges as:

$$C_{11} = C_{22} = Q_e \tag{50}$$

$$C_{12} = C_{21} = \frac{Q_o - Q_e}{2} \tag{51}$$

The effective permittivity of the line for the even and odd modes are then defined, respectively by:

$$\epsilon_{re} = \frac{Q_e}{Q_{ae}}, \quad \epsilon_{ro} = \frac{Q_o}{Q_{ao}} \tag{52}$$

where the subscript a stands for the charge with the dielectric material replaced by free space. With known effective permittivities, the even and odd mode velocities of propagation (v_e and v_o) are given by:

$$v_e = \frac{c}{\sqrt{\epsilon_{re}}} = c\sqrt{\frac{Q_{ae}}{Q_e}}, \quad v_o = \frac{c}{\sqrt{\epsilon_{ro}}} = c\sqrt{\frac{Q_{ao}}{Q_o}} \tag{53}$$

where the velocity of light, $c \approx 2.998 \times 10^8$ m/s. Once the capacitance and velocities of propagation, are determined, the impedances Z_{oe} and Z_{oo} are obtained from:

$$Z_{oe} = \frac{1}{v_e Q_e}, \quad Z_{oo} = \frac{1}{v_o Q_o} \tag{54}$$

and in terms of the charges only, Z_{oe} and Z_{oo} can be written as:

$$Z_{oe} = \frac{1}{c\sqrt{Q_e Q_{ae}}}, \quad Z_{oo} = \frac{1}{c\sqrt{Q_o Q_{ao}}} \tag{55}$$

When this coupled transmission line is used as a coupling device, its characteristic impedance is usually given by

$$Z_o=\sqrt{Z_{oe}\,Z_{oo}} \tag{56}$$

3-4 Coupling Coefficient

Another important parameter that describes the electrical coupling factor between strip 1 and strip 2 is defined as $k_e=V^2/V^1$, where V^2 is the voltage induced on strip 2 due to V^1 applied on strip 1 [12]. Hence, from the open circuit voltage for a symmetric CMSTL, k_e reduces to

$$k_e = 20\log_{10}\left[\frac{C_{12}}{C_{11}+C_{12}}\right] \tag{57}$$

IV. NUMERICAL RESULTS

In all the numerical examples presented here, it is necessary to point out that all radial distances are normalized to the radius of the conducting core, r, and h_1, h_2, and h_3, are defined as $(a\text{-}r)/r$, $(b\text{-}a)/r$ and $(c\text{-}b)/r$, respectively; t is defined as normalized thickness of strips, as shown in the Figs.1 and 2. The truncation of the dielectric substrate and the overlay, as shown in Fig.2, can be specified by changing α_s and α_o, non-truncated geometry is defined as $\delta=360°$, and N_w, N_1, N_2, N_3, and N_4 represent the number of the FD nodes on each strip, and the number of nodes along the radial direction along the substrate, strip, overlay, and air-layer, respectively. It is always assumed that the geometry of the CMSTL is symmetric around the y axis.

4.1 Microstrip Transmission Line with a Dielectric Notch

4.1.1 Verification of Computed Data

In order to verify the numerical results generated by our computer program, a special case is selected to compare its results with the published data in [3]. The configuration parameters for this case are such that $h_2=0.2$, $h_3=0.5$, $t=0.001$, $\delta=360°$, $\delta_s=\delta_w=2.0(a\text{-}r)/a$, $\epsilon_{r1}=1.0$, $\epsilon_{r2}=\epsilon_{r3}=9.6$. The ratio of r/a, is then varied from 0.5 to 0.9. Figs.8a and 8b show the odd and even modes characteristic impedances and effective permittivities versus r/a. As shown in the figures, the results obtained in this study and those in Figs.3 and 4 in [3] indicate good agreement with a maximum difference of 2.2%.

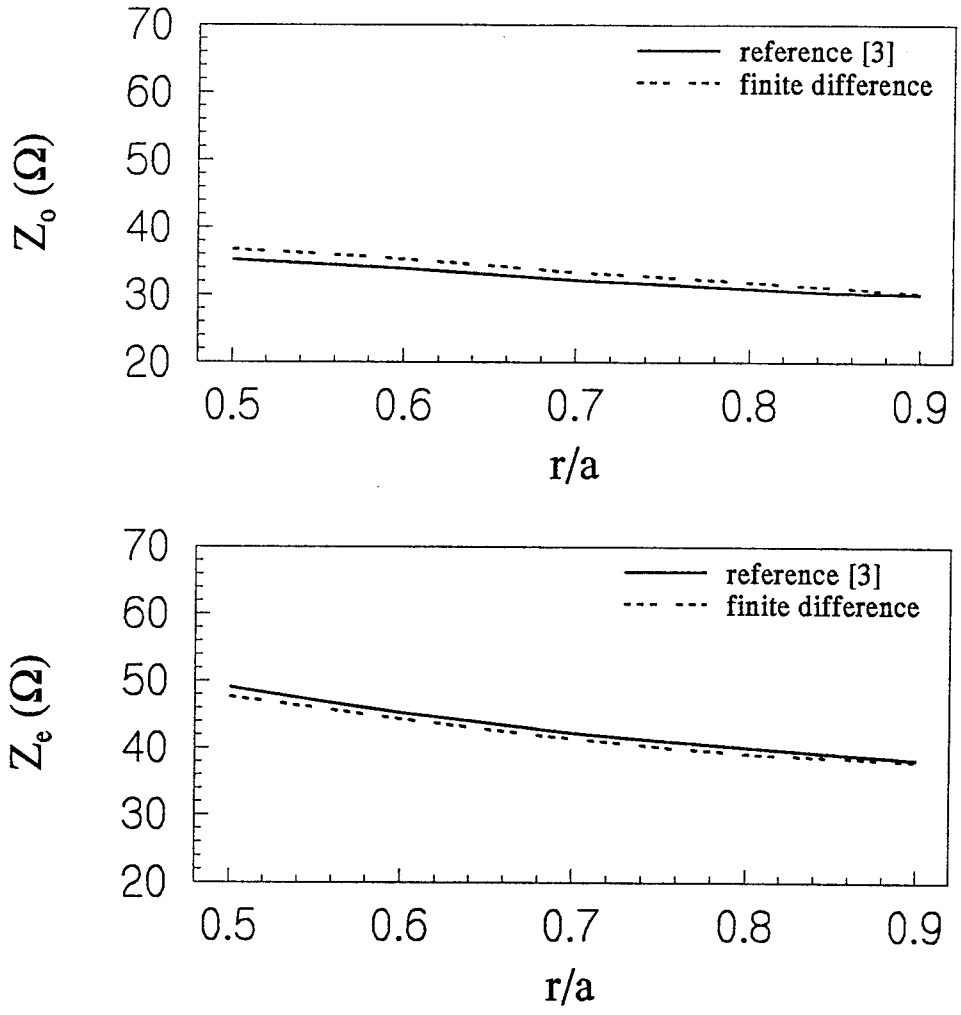

Fig.8a Odd and even modes characteristic impedance

(h_2=0.2, h_3=0.5, t=0.001, $\delta_w=\delta_s$=2.0 (a-r)/a, ε_{r1}=1.0, $\varepsilon_{r2}=\varepsilon_{r3}$=9.6, δ=360°, N_2=1, N_3=4, N_4=5)

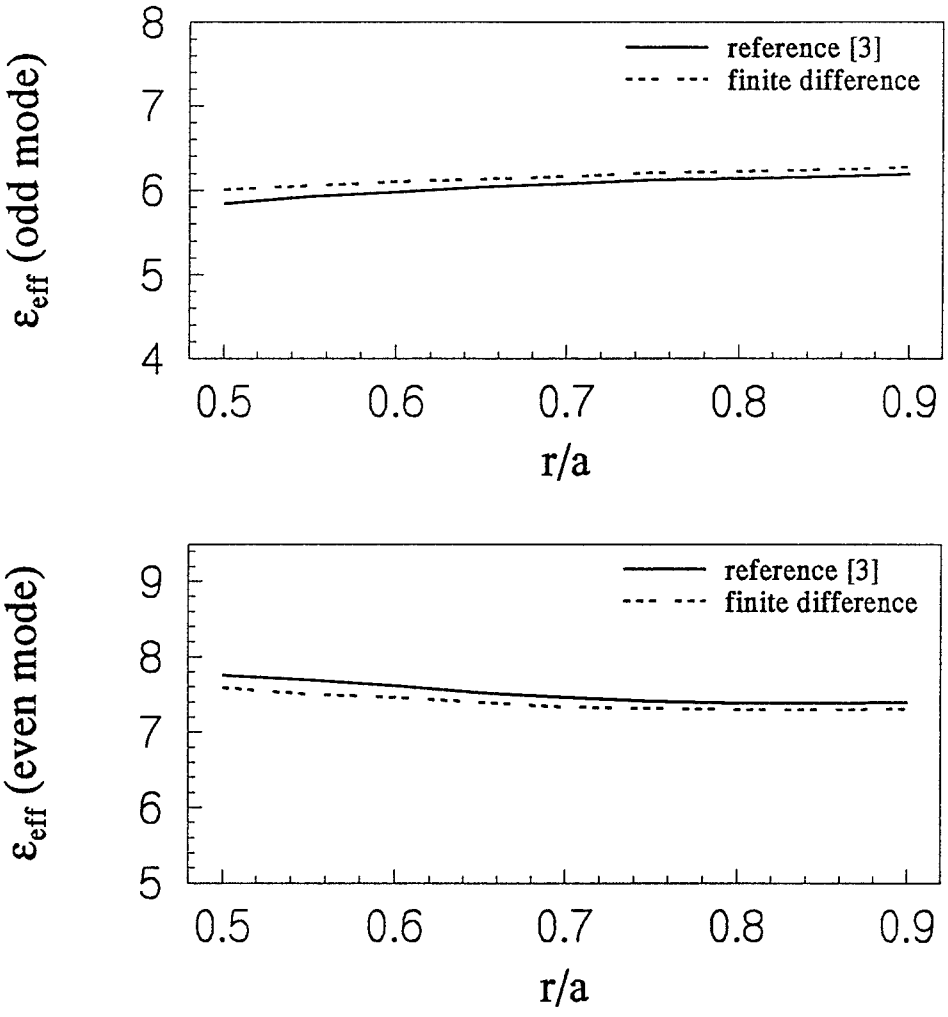

Fig.8b Odd and even modes effective permittivities

(h_2=0.2, h_3=0.5, t=0.001, δ_w=δ_s=2.0 (a-r)/a,
ε_{r1}=1.0, ε_{r2}=ε_{r3}=9.6, δ=360°, N_2=1, N_3=4,
N_4=5)

4.1.2. Effect of Artificial Boundary

It is very important to place the artificial boundary for the finite difference analysis at the proper position in order to obtain accurate results for the characteristics of the transmission line. It is also always desirable to place the artificial boundary as close to the strips as possible and yet, not affect the accuracy of the numerical results. The closer the distance between the artificial boundary and the strips, the smaller the FD mesh size will be, and consequently, the order of the resulting matrix equations is reduced and faster numerical solution is achievable. In order to study the effects of position of the artificial boundary on the characteristics of the transmission line, a geometry, as shown in Fig.1, is selected for this analysis, where, the distance h_3 is varied from 0.1 to 1.7. Other parameters selected are such that h_1=0.2, h_2=0.1, t=0.001, δ_w=10°, δ_s=10°, δ_n=6°, and ϵ_{r1}, ϵ_{r2}, and ϵ_{r3} are set to 2.2, 4.7 and 9.6, respectively. Figures.9a to 9d show the capacitances, coupling coefficient, and characteristic impedances, normalized phase velocities and effective permittivities for even and odd modes versus h_3. It can be easily seen that, in this group of results, using ABC2, the artificial boundary can be placed at a closer position to the strips than using the ABC1 or the PEC boundaries. This is because there are no significant changes in the CMSTL characteristics using ABC2 when the distance h_3 becomes greater than 0.5. The numerical results based on ABC1 and ABC2 are almost identical when h_3 is larger than 1 as expected. This behavior is clearly observed for the CMSTL with full or truncated dielectric material and with thin or thick strips. Similar results are obtained for truncated CMSTL in Fig.2, although the results are not shown here. The second order approximate boundary condition, ABC2, with h_3=0.5, is then applied in all subsequent numerical results presented here.

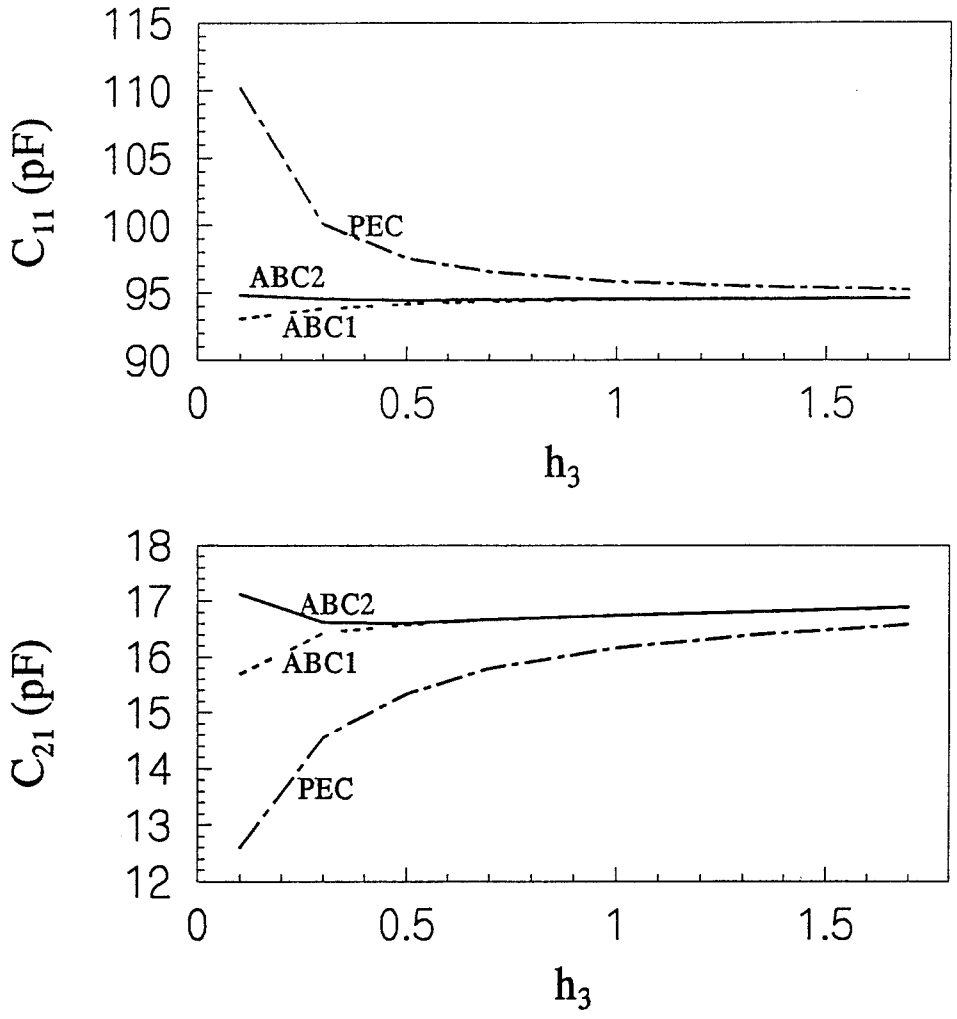

Fig.9a Effect of artificial boundary on capacitances for non-truncated CMSTL

(h_1=0.2, h_2=0.1, t=0.001, δ=360°, δ_w=10°, δ_s=10°, δ_n=6°, ε_{r1}=2.2, ε_{r2}=4.7, ε_{r3}=9.6, N_w=10, N_1=4, N_2=1, N_3=3, N_4=3 - 8)

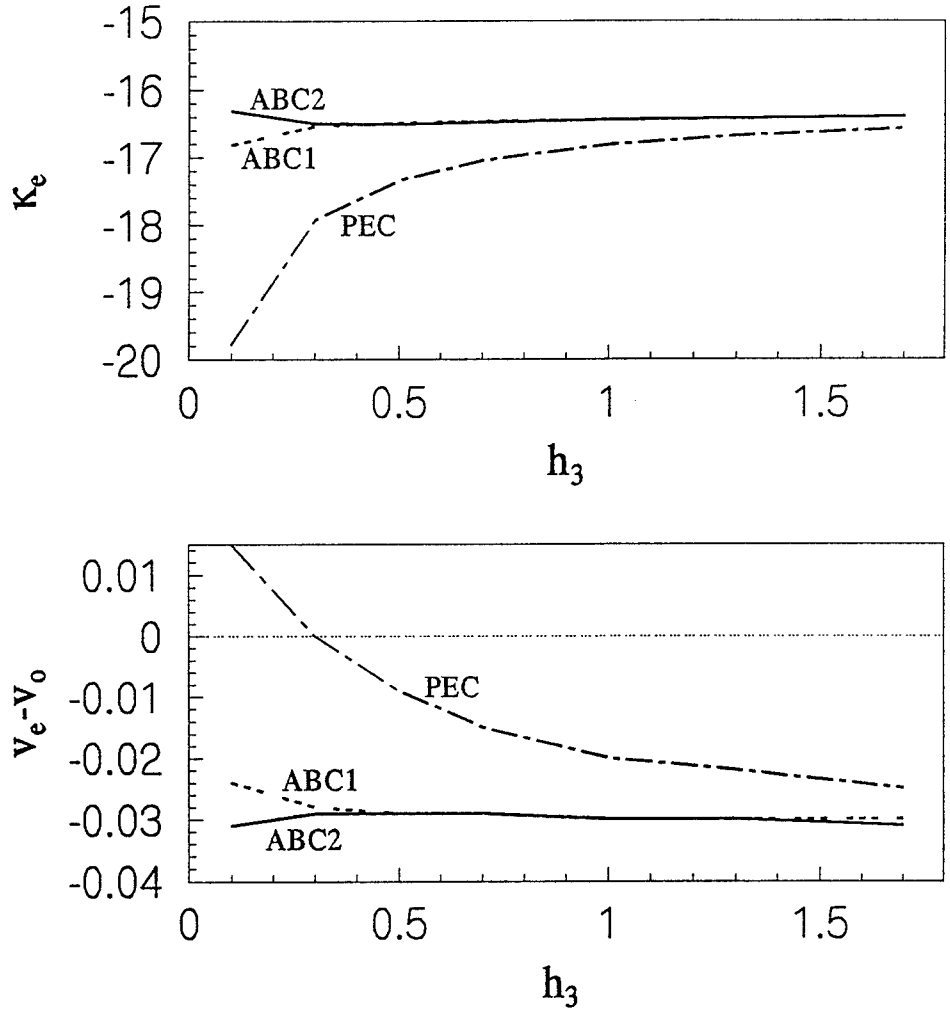

Fig.9b Effect of artificial boundary on coupling and phase velocities for non-truncated CMSTL

(h_1=0.2, h_2=0.1, t=0.001, δ=360°, δ_w=10°, δ_s=10°, δ_n=6°, ε_{r1}=2.2, ε_{r2}=4.7, ε_{r3}=9.6, N_w=10, N_1=4, N_2=1, N_3=3, N_4= 3 - 8)

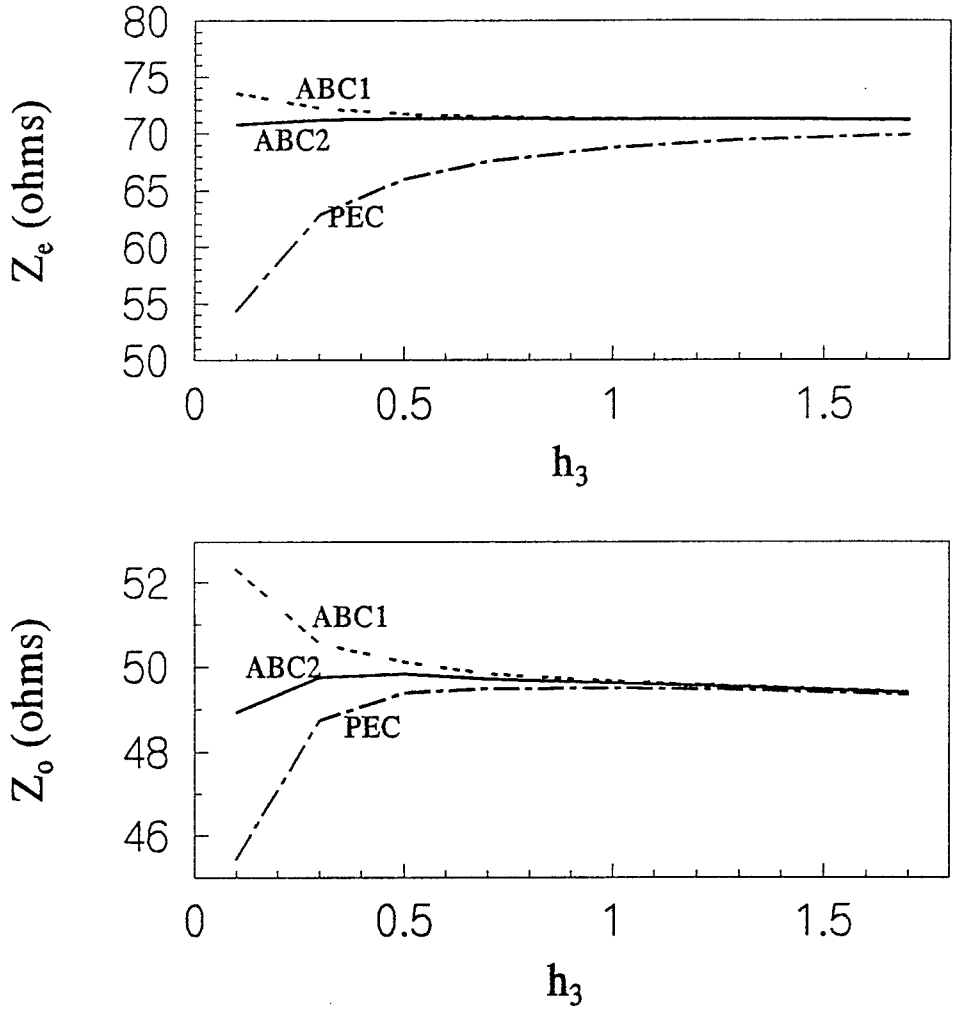

Fig.9c Effect of artificial boundary on impedances for non-truncated CMSTL

(h_1=0.2, h_2=0.1, t=0.001, δ=360°, δ_w=10°, δ_s=10°, δ_n=6°, ε_{r1}=2.2, ε_{r2}=4.7, ε_{r3}=9.6, N_w=10, N_1=4, N_2=1, N_3=3, N_4=3 - 8)

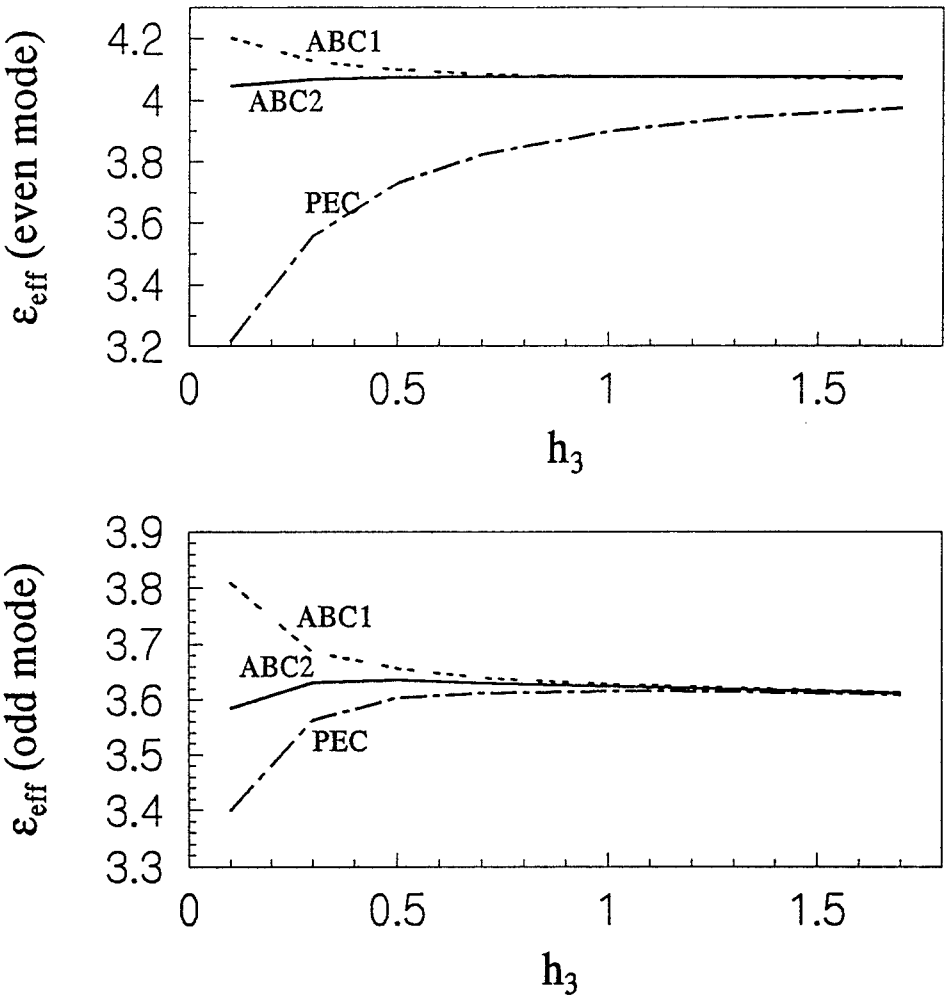

Fig.9d Effect of artificial boundary on effective dielectric constant for non-truncated CMSTL

(h_1=0.2, h_2=0.1, t=0.001, δ=360°, δ_w=10°, δ_s=10°, δ_n=6°, ε_{r1}=2.2, ε_{r2}=4.7, ε_{r3}=9.6, N_w=10, N_1=4, N_2=3, N_3=3, N_4=3 - 8)

4.1.3. Convergence of Numerical Results

The convergence of our numerical solution can be observed in Figs.10a and 10b for non-truncated and truncated CMSTLs, respectively. In the figures the even and odd mode characteristic impedances, Z_e and Z_o, versus N which is the order of the matrix [X], are shown. For the results shown in Figs.10a and 10b, h_1=0.2, h_2=0.1, and h_3 is set to 0.5, t=0.001, δ_w=10°, δ_s=10°, δ_n=6°, ϵ_{r1}=2.2, ϵ_{r2}=4.7 and ϵ_{r3}=9.6. With fixed h_3, increasing N improves the accuracy of the numerical results, however, it is clearly seen from the figures that convergence is achievable when N is in the order of 2000.

4.1.4a Effect of the Dielectric Material of the Overlay (Superstrate)

The effects of the dielectric material of the superstrate is studied with the configuration defined by h_1=0.2, h_2=0.1, h_3=0.5, t=0.001, δ_w=10°, δ_s=10°, δ_n=6°, ϵ_{r2}=4.7 and ϵ_{r3} is set to 1.0 and 9.6, respectively. The dielectric constant, ϵ_{r1}, is then varied from 1 to 16. The influences of various ϵ_{r1} and different ϵ_{r3} on the characteristic parameters of the transmission line are tested for both truncated and non-truncated geometries as shown in Figs.1 and 2. The size of the truncated geometry, α_s and α_o, in this case, are set to 72°, which means, the edges of the substrate and the overlay are at 3° away from the conductor strips. Fig.11a shows the influences of ϵ_{r1} and ϵ_{r3} on the self and mutual capacitances for non-truncated geometry, while Fig.12a shows those influences for truncated geometry. As can be seen, the mutual capacitances are directly proportional to the ϵ_{r1}, while ϵ_{r3}=1.0 and 9.6. It is noted that self capacitance obtained by placing dielectric material into the notch exhibits a marked deviation from the result obtained by removing dielectric material from the notch. In this case, using dielectric material in the

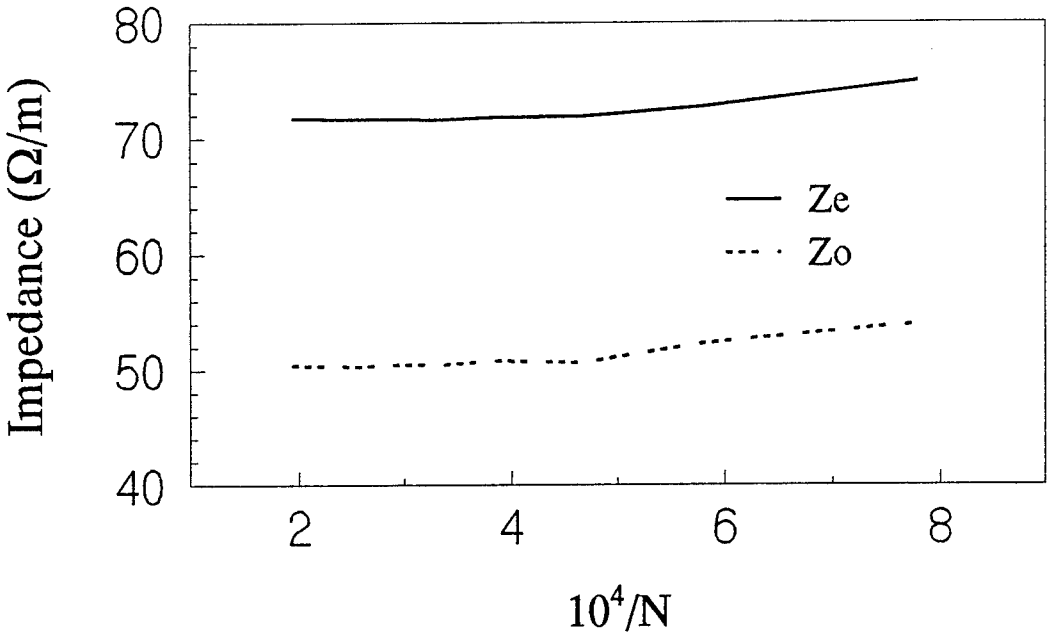

Fig.10a Convergence of numerical results for non-truncated CMSTL

(h_1=0.2, h_2=0.1, h_3=0.5, t=0.001, δ=360°, δ_w=10°, δ_s=10°, δ_n=6°, ε_{r1}=2.2, ε_{r2}=4.7, ε_{r3}=9.6, N_w=4 - 12, N_1=4, N_2=1, N_3=3, N_4=4)

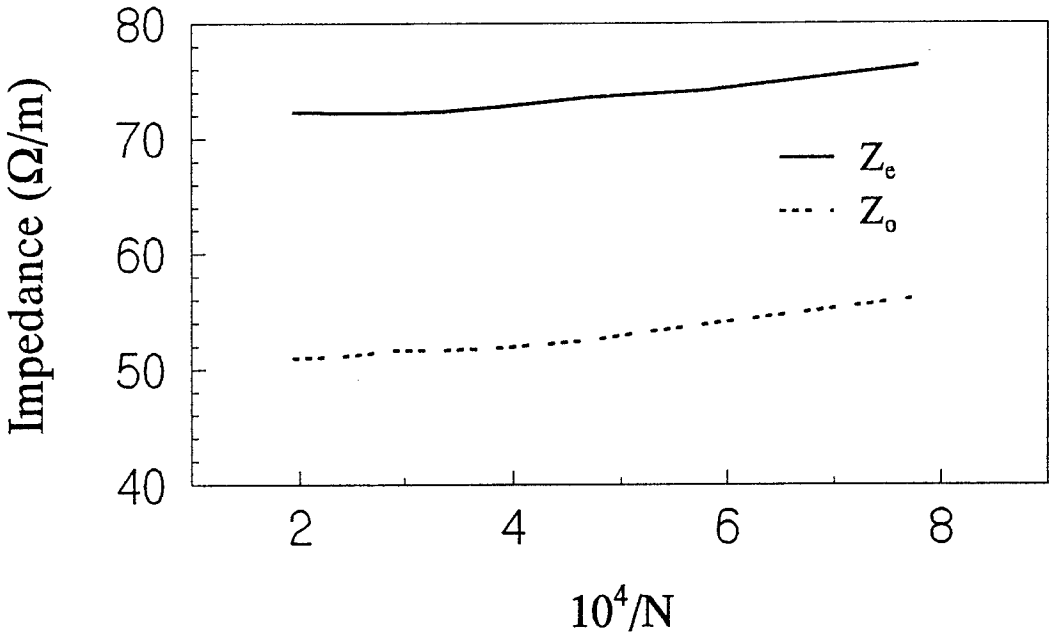

Fig.10b Convergence of numerical results for truncated CMSTL

(h_1=0.2, h_2=0.1, h_3=0.5, t=0.001, δ_w=10°, δ_s=10°, δ_n=6°, ε_{r1}=2.2, ε_{r2}=4.7, ε_{r3}=9.6, α_s=α_o=72°, N_w=4 - 12, N_1=4, N_2=1, N_3=3, N_4=4)

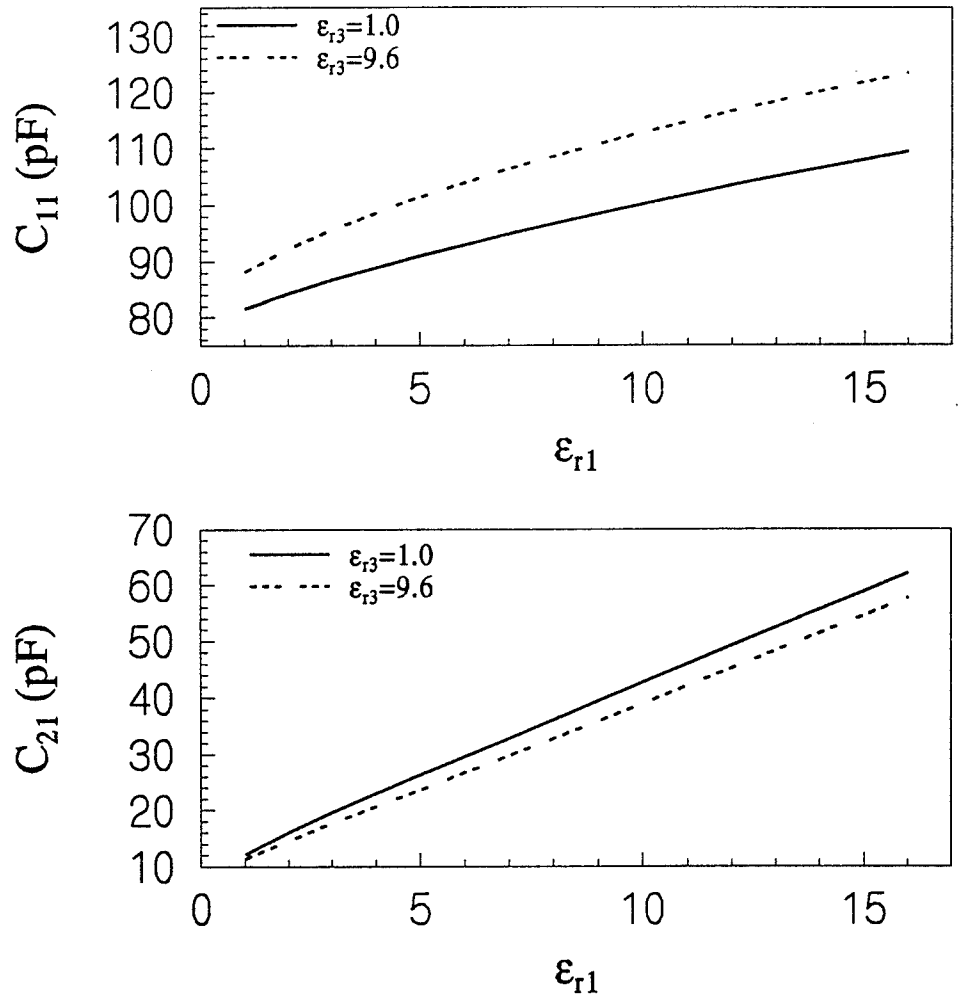

Fig.11a Effect of dielectric overlay on capacitances for non-truncated CMSTL

(h_1=0.2, h_2=0.1, h_3=0.5, t=0.001, δ_w=10°, δ_s=10°, δ_n=6°, δ=360°, ε_{r2}=4.7, N_w=8, N_1=4, N_2=1, N_3=3, N_4=4)

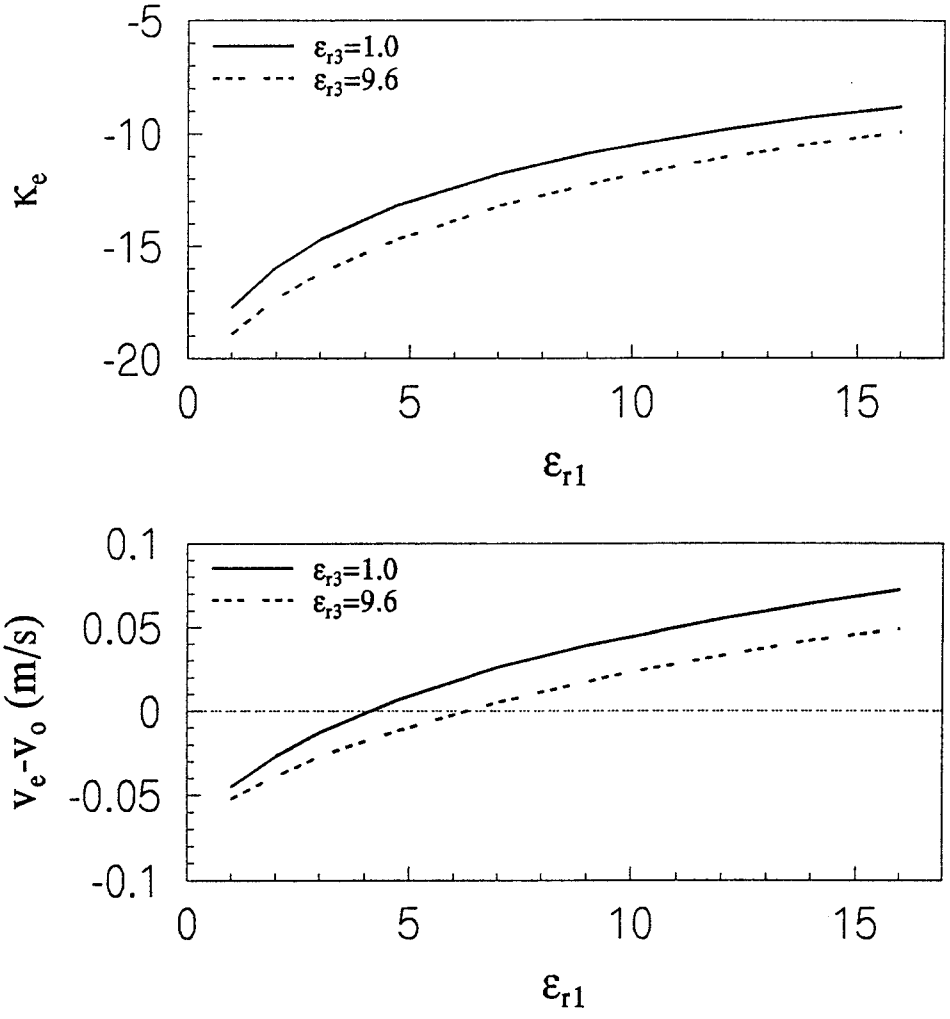

Fig.11b Effect of dielectric overlay on coupling and phase velocities for non-truncated CMSTL

(h_1=0.2, h_2=0.1, h_3=0.5, t=0.001, δ_w=10°, δ_s=10°, δ_n=6°, δ=360°, ε_{r2}=4.7, N_W=8, N_1=4, N_2=1, N_3=3, N_4=4)

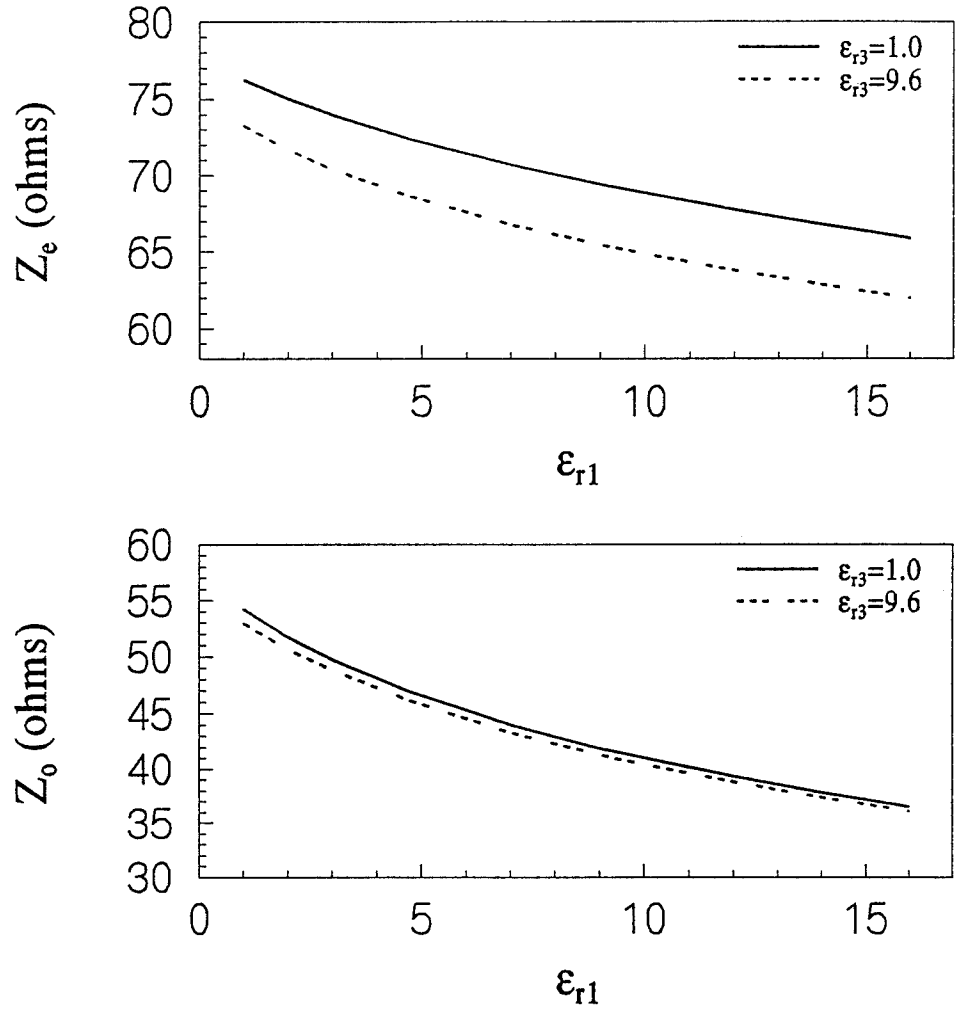

Fig.11c Effect of dielectric overlay on impedances for non-truncated CMSTL

(h_1=0.2, h_2=0.1, h_3=0.5, t=0.001, δ_w=10°, δ_s=10°, δ_n=6°, δ=360°, ε_{r2}=4.7, N_w=8, N_1=4, N_2=1, N_3=3, N_4=4)

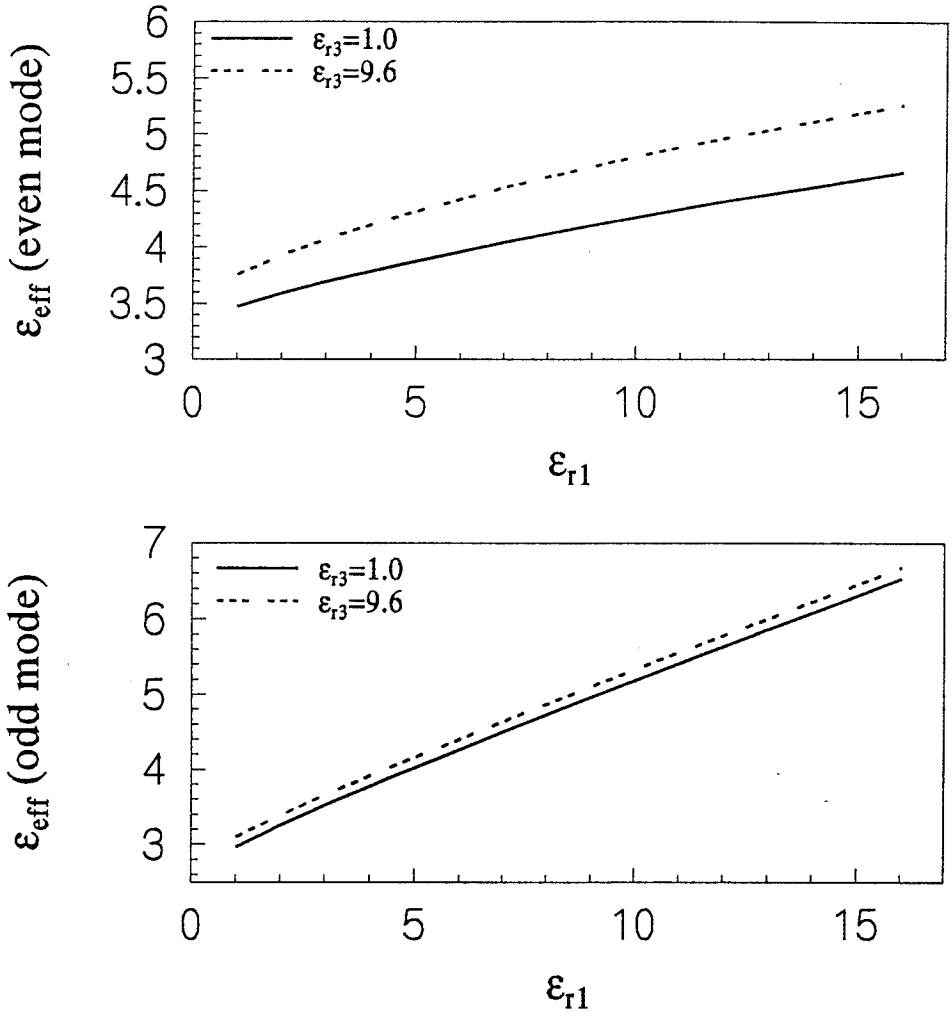

Fig.11d Effect of dielectric overlay on effective dielectric constants for non-truncated CMSTL

(h_1=0.2, h_2=0.1, h_3=0.5, t=0.001, δ_w=10°, δ_s=10°, δ_n=6°, δ=360°, ε_{r2}=4.7, N_w=8, N_1=4, N_2=1, N_3=3, N_4=4)

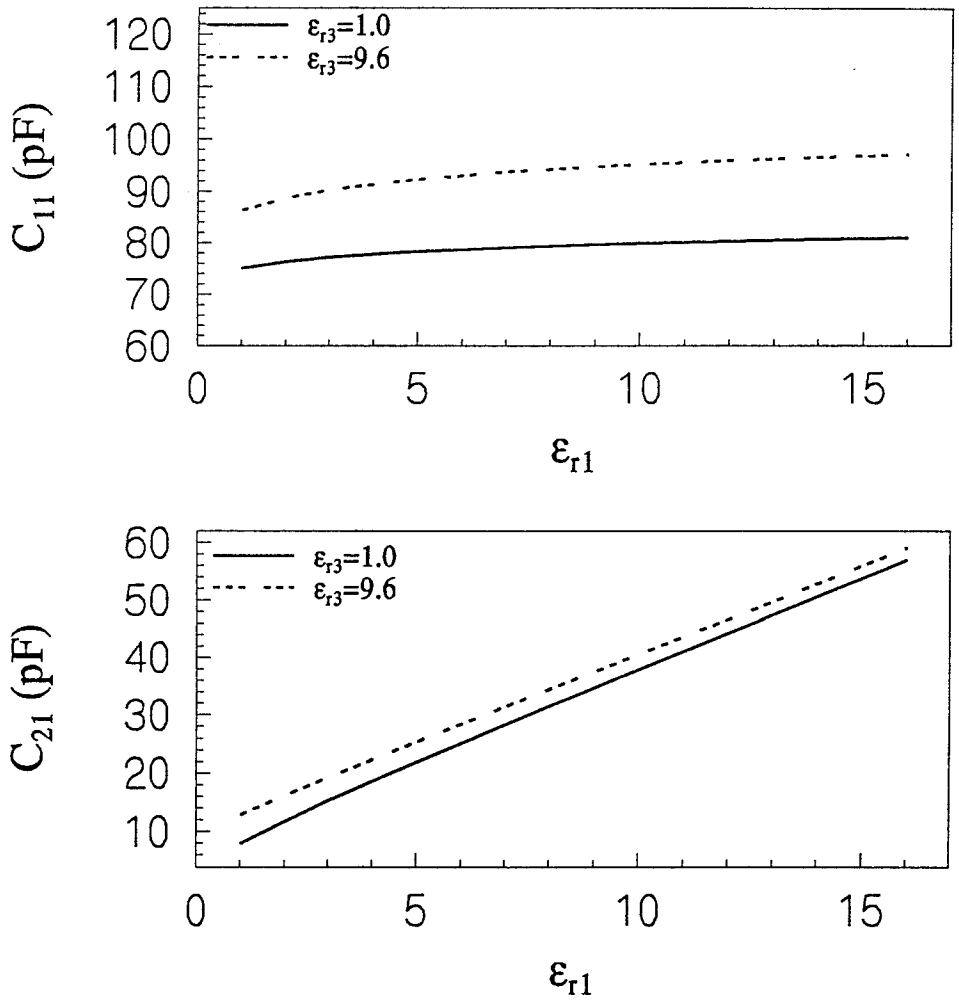

Fig.12a Effect of dielectric overlay on capacitances for truncated CMSTL

(h_1=0.2, h_2=0.1, h_3=0.5, t=0.001, δ_w=10°, δ_s=10°, δ_n=6°, ε_{r2}=4.7, α_s=α_o=72°, N_w=10, N_1=4, N_2=1, N_3=3, N_4=4)

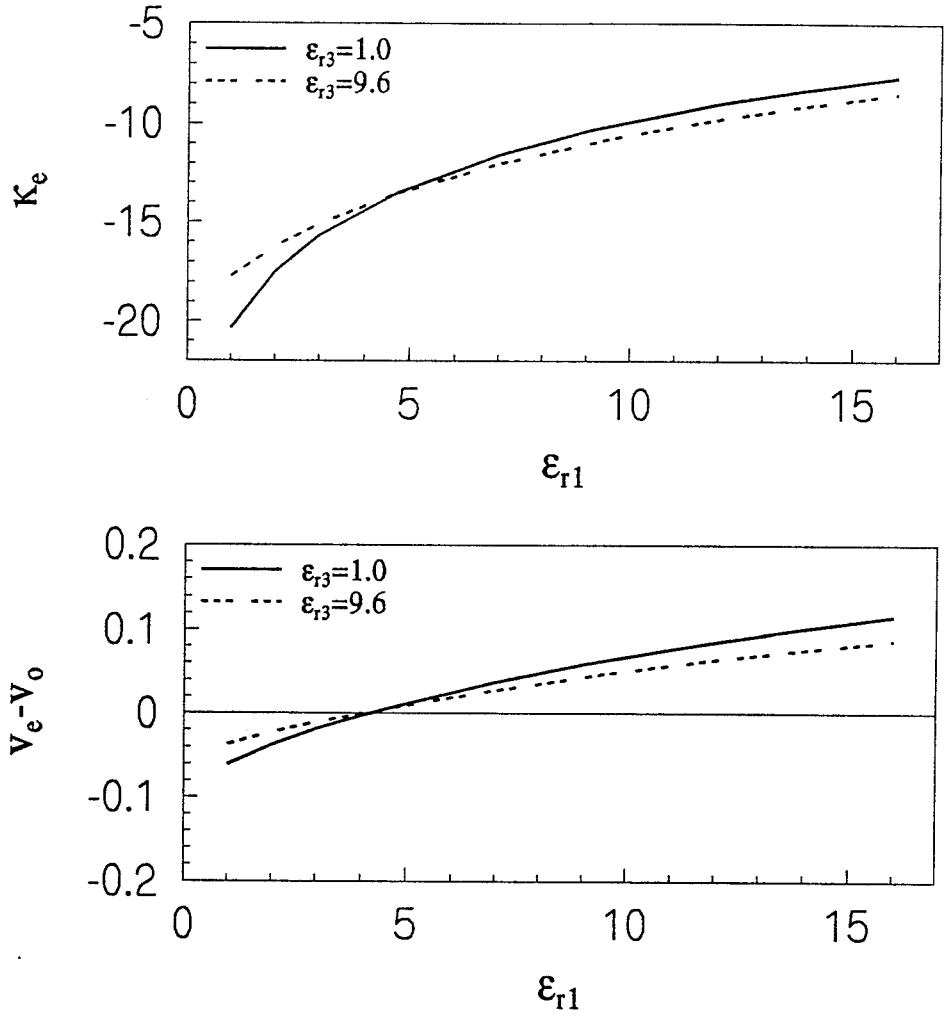

Fig.12b Effect of dielectric overlay on coupling and phase velocities for truncated CMSTL
(h_1=0.2, h_2=0.1, h_3=0.5, t=0.001, δ_w=10°, δ_s=10°, δ_n=6°, ε_{r2}=4.7, α_s=α_o=72°, N_w=10, N_1=4, N_2=1, N_3=3, N_4=4)

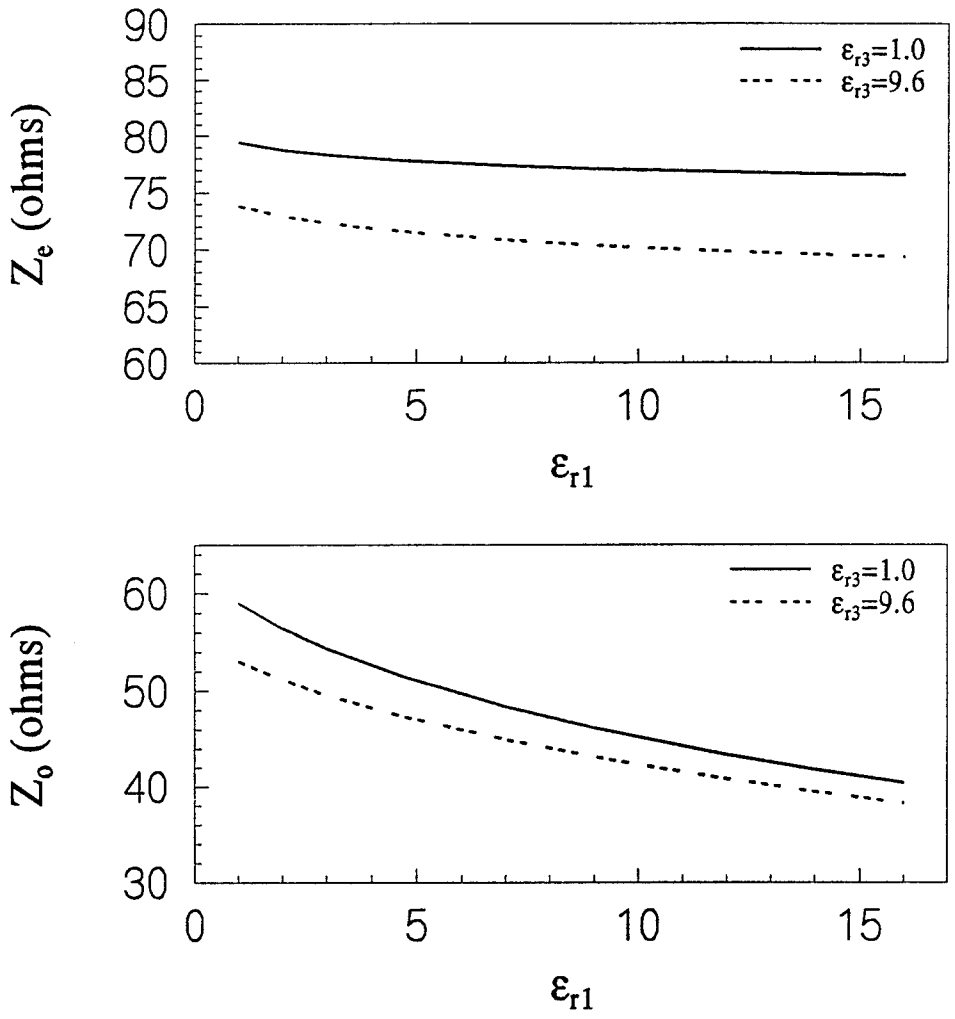

Fig.12c Effect of dielectric overlay on impedances for truncated CMSTL

(h_1=0.2, h_2=0.1, h_3=0.5, t=0.001, δ_w=10°, δ_s=10°, δ_n=6°, ε_{r2}=4.7, α_s=α_o=72°, N_w=10, N_1=4, N_2=1, N_3=3, N_4=4)

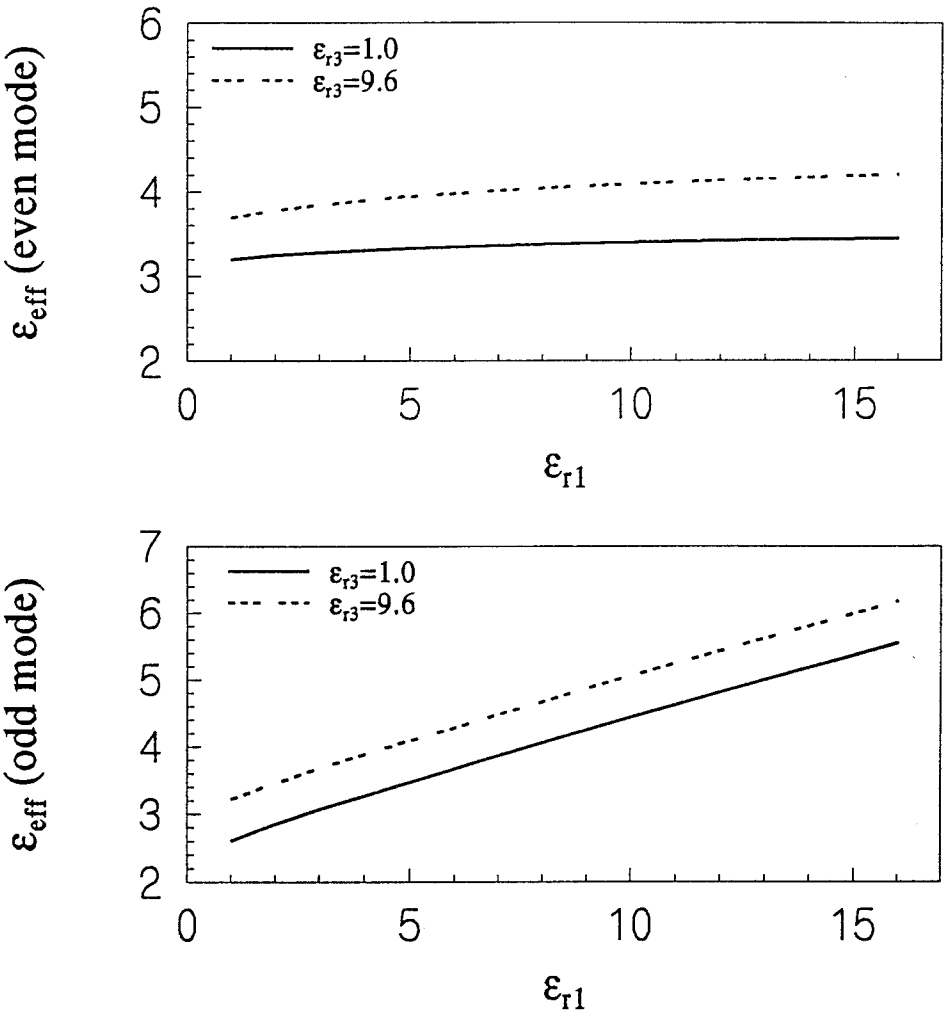

Fig.12d Effect of dielectric overlay on effective dielectric constants for truncated CMSTL
(h_1=0.2, h_2=0.1, h_3=0.5, t=0.001, δ_w=10°, δ_s=10°, δ_n=6°, ε_{r2}=4.7, α_s=α_o=72°, N_w=10, N_1=4, N_2=1, N_3=3, N_4=4)

notch reduces the mutual capacitances, but not significantly, as shown in the Fig.11a and Fig.12a. Figures 11b and 12b show that the coupling coefficient increases with ϵ_{r1}. It is found that, for this geometry, using a dielectric notch between strips did not show significant decoupling between lines. Furthermore, the influences on the characteristic impedances, effective permittivities and normalized phase velocities are studied for even and odd modes of the transmission line with truncated and non-truncated geometries, respectively. Figs.11c and 11d show characteristic impedances Z_e, Z_o, and effective permittivities ϵ_{eff} versus ϵ_{r1} with different ϵ_{r3}, for non-truncated geometry. The Z_e, Z_o and ϵ_{eff} versus ϵ_{r1} with different ϵ_{r3}, for truncated geometry are depicted in Figs.12c and 12d, respectively. It is noted from Fig.11b that the even and odd normalized phase velocities, v_e and v_o, are equalized at approximately $\epsilon_{r1}=4$ and $\epsilon_{r1}=6.5$, as $\epsilon_{r3}=1.0$ and $\epsilon_{r3}=9.6$ respectively, which means, for this specific case (non-truncated geometry), the line distortion is eliminated. Similar behavior for truncated geometry can be observed in the Fig.12b, v_e and v_o are equalized at almost the same point, where $\epsilon_{r1}=4.2$, for $\epsilon_{r3}=1.0$ and $\epsilon_{r3}=9.6$. These properties show that the use of truncated and non-truncated CMSTL with different dielectric material in the notch allow for a distortionless line at different values of the dielectric constant of the overlay.

4.1.4b Effect of the Substrate Dielectric Material

The effect of the dielectric constant in the substrate is investigated. The configuration selected was such that $h_1=0.2$, $h_2=0.2$, $h_3=0.5$, $t=0.001$, $\delta_w=10°$, $\delta_s=10°$, and $\delta_n=6°$. The dielectric constant of superstrate, ϵ_{r1}, is set to 2.2, and the dielectric constant of the notch, ϵ_{r3}, is set to 9.6, the angles, α_s and α_o, are set to 72°. The dielectric constant of the substrate, ϵ_{r2},

is then varied from 1 to 16. The same test is made for the truncated geometry with the same parameters. Figs.13a to 13d show the capacitances, coupling coefficient, normalized phase velocity and the even and odd mode impedances as a function of ϵ_{r2}. As can be seen in Fig.13a, the self and mutual capacitances are both directly proportional to the dielectric constant of substrate, ϵ_{r2}, for both truncated and non-truncated geometry. Figure.13b shows that the coupling coefficient, k_e, decreases as ϵ_{r2} increases. Figures.13c and 13d show the characteristic impedances (Z_e,Z_o) and relative effective permittivities (ϵ_{eff}) for even and odd modes versus ϵ_{r2}. As it can be seen, from these figures, all these parameters do not show significant differences, in relative percentages, between the results for use of the truncated and the non-truncated geometry. It should be noted that the even and odd normalized phase velocities, v_e and v_o, as shown in Fig.13b, are equal to each other at approximately $\epsilon_{r2}=1.5$ for non-truncated and $\epsilon_{r2}=2.5$ for truncated geometry, which means, that the distortionless propagation on the line is achievable using a dielectric notch in the substrate between strips for truncated or non-truncated geometries. A special case is created to study the effect of removing the dielectric material from the notch. The same configuration and parameters are used in this case as those in above one, but ϵ_{r3} is now set to 1, which represents an air-dielectric notch. The ϵ_{r2} is then varied from 1 to 16. The influences of ϵ_{r2} on the self and mutual capacitances between these two strips are shown in Fig.14a. It is noted that the influences of ϵ_{r2} on the self capacitance of two strips do not show much differences, compared with the above case in which a dielectric notch was used in the substrate and placed between two strips. However, the influences of ϵ_{r2} on the mutual capacitance C_{12} (or C_{21}) for the use of truncated geometry is very different from the previous case. As can be seen in Fig.14a, the mutual capacitance (using truncated geometry) does not

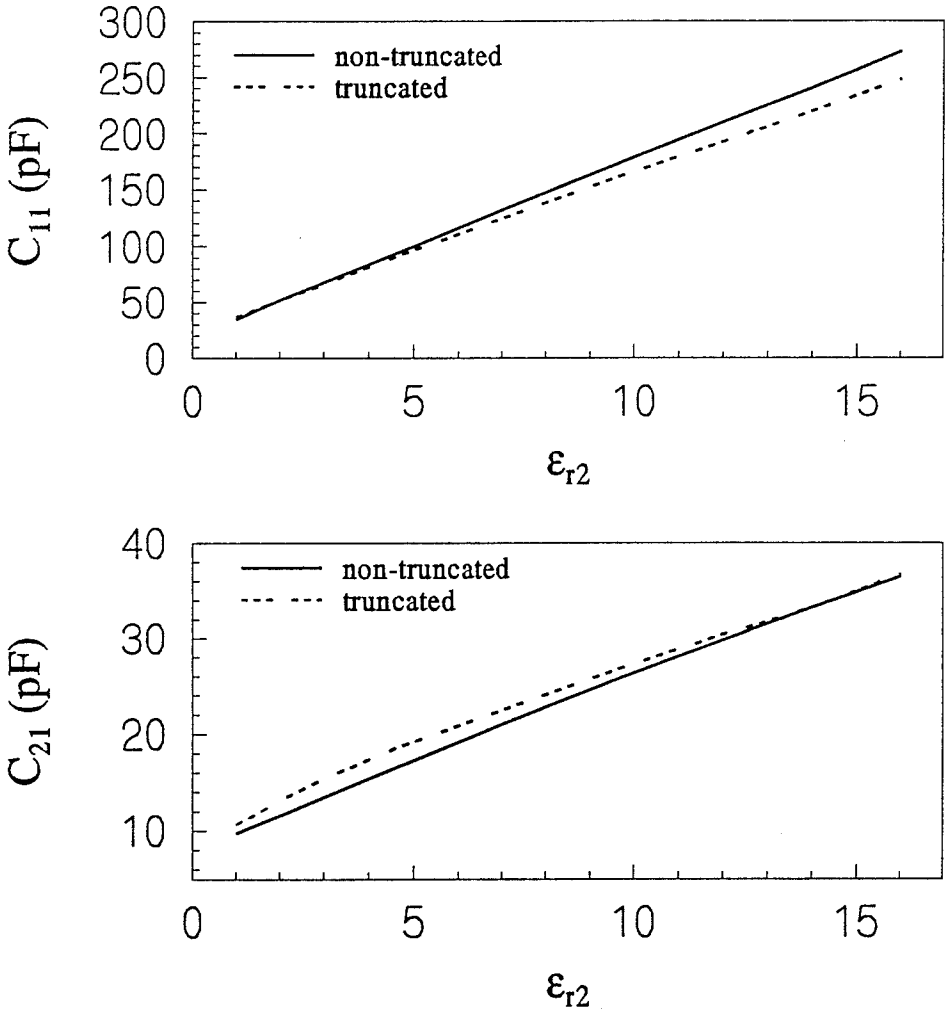

Fig.13a Effect of dielectric substrate on capacitances

(h_1=0.2, h_2=0.2, h_3=0.5, t=0.001, δ_w=10°, δ_s=10°, δ_n=6°, ε_{r1}=2.2, ε_{r3}=9.6, α_s=α_o=72°, N_w=10, N_1=4, N_2=1, N_3=3, N_4=4)

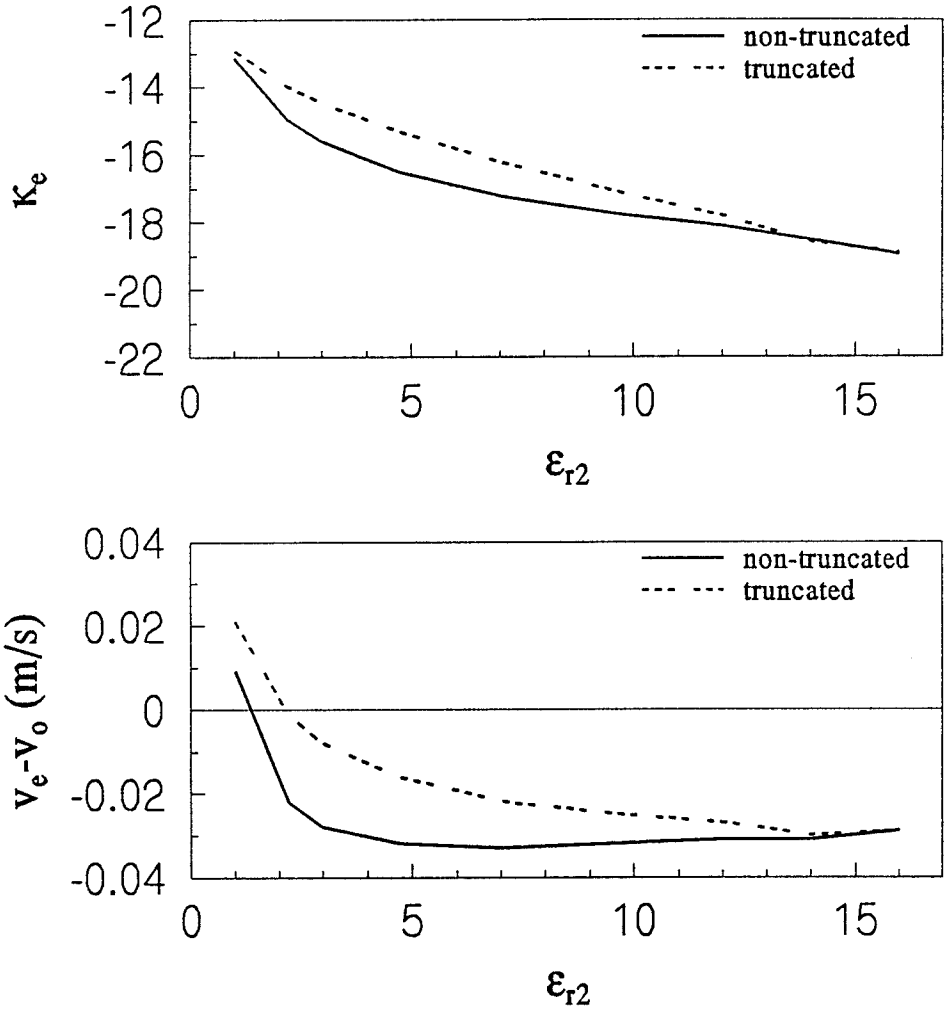

Fig.13b Effect of dielectric substrate on coupling and phase velocities

(h_1=0.2, h_2=0.2, h_3=0.5, t=0.001, δ_w=10°, δ_s=10°, δ_n=6°, ε_{r1}=2.2, ε_{r3}=9.6, α_s=α_o=72°, N_w=10, N_1=4, N_2=1, N_3=3, N_4=4)

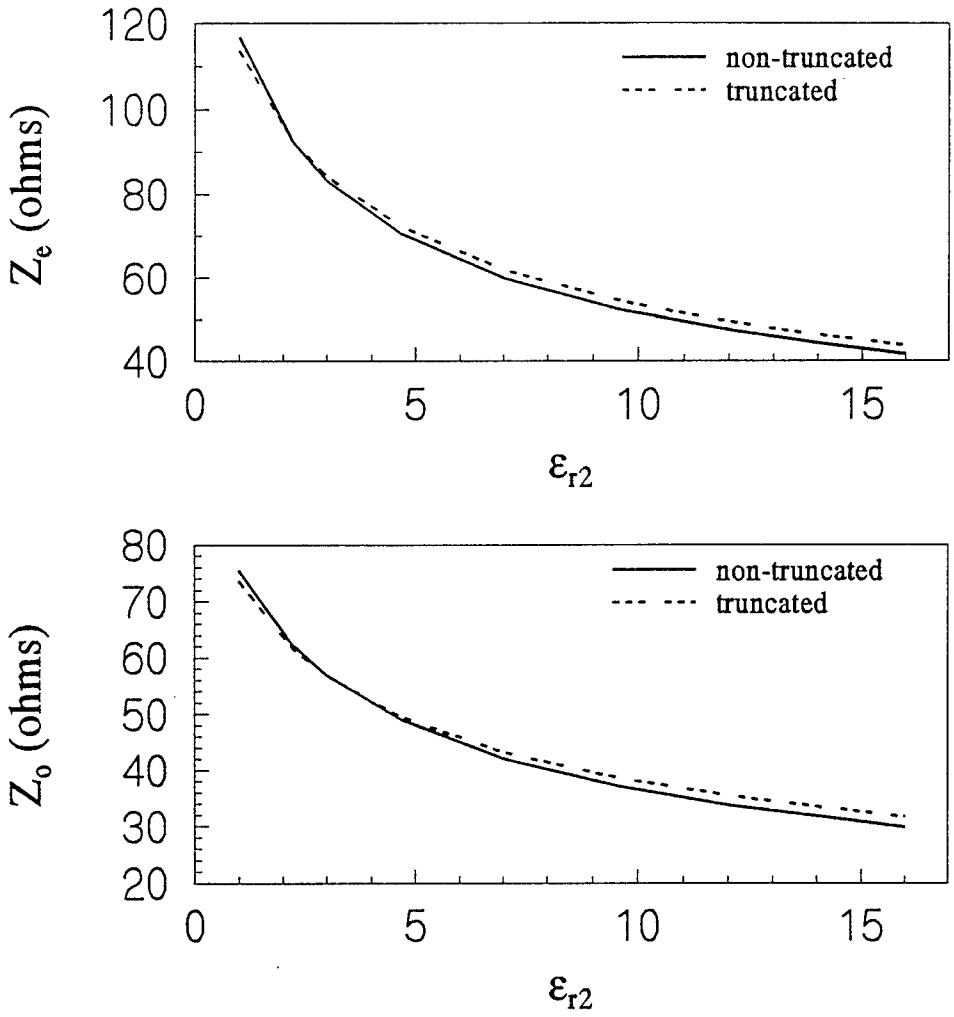

Fig.13c Effect of dielectric substrate on impedances

(h_1=0.2, h_2=0.2, h_3=0.5, t=0.001, δ_w=10°, δ_s=10°, δ_n=6°, ε_{r1}=2.2, ε_{r3}=9.6, α_s=α_o=72°, N_w=10, N_1=4, N_2=1, N_3=3, N_4=4)

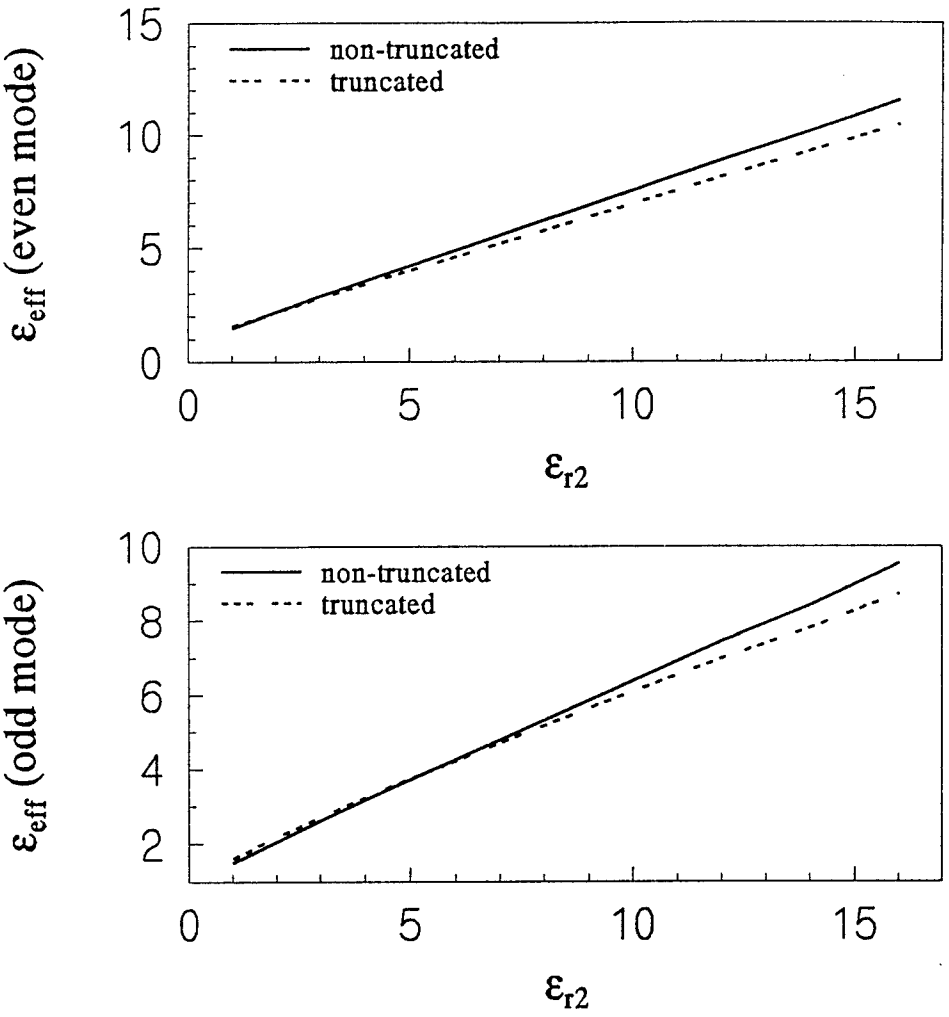

Fig.13d Effect of dielectric substrate on effective dielectric constants

(h_1=0.2, h_2=0.2, h_3=0.5, t=0.001, δ_w=10°, δ_s=10°, δ_n=6°, ε_{r1}=2.2, ε_{r3}=9.6, α_s=α_o=72°, N_w=10, N_1=4, N_2=1, N_3=3, N_4=4)

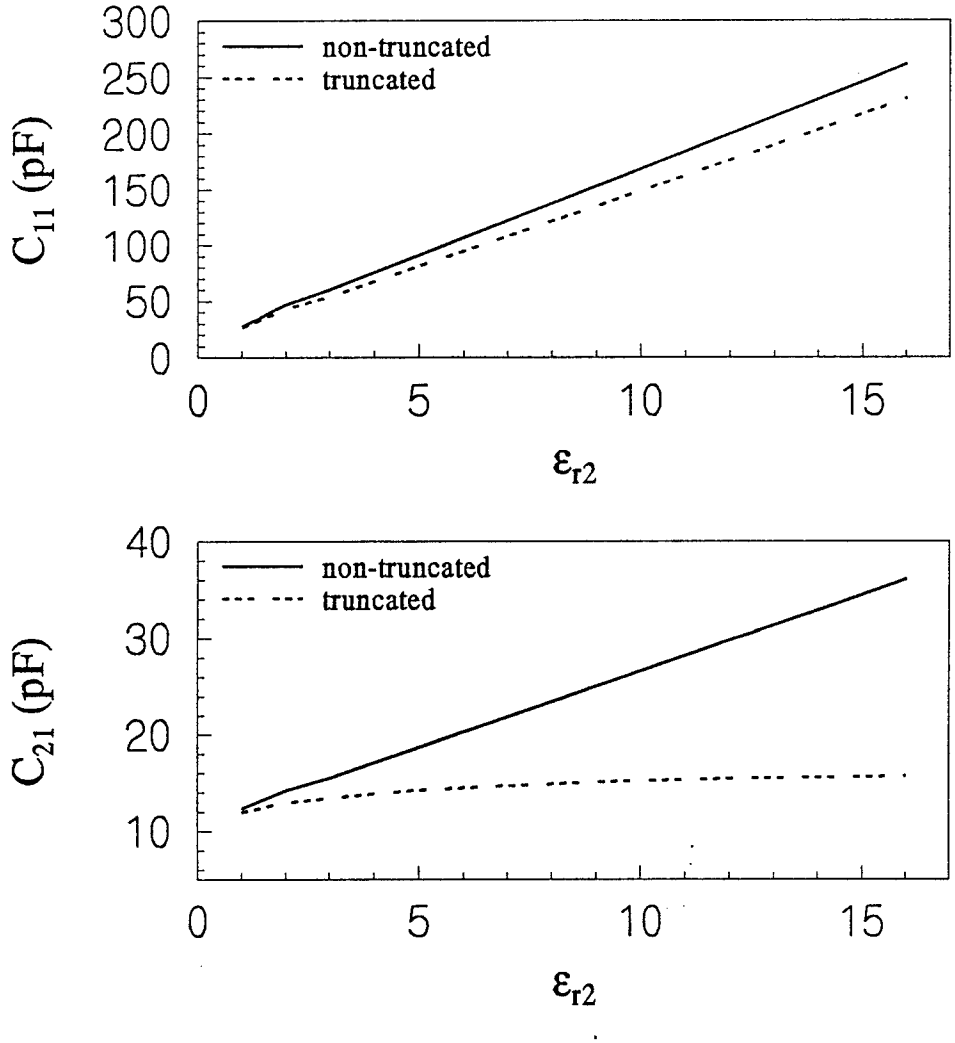

Fig.14a Effect of dielectric substrate on capacitances

(h_1=0.2, h_2=0.2, h_3=0.5, t=0.001, δ_w=10°, δ_s=10°, δ_n=6°, ε_{r1}=2.2, ε_{r3}=1.0, α_s=α_o=72°, N_w=10, N_1=4, N_2=1, N_3=3, N_4=4)

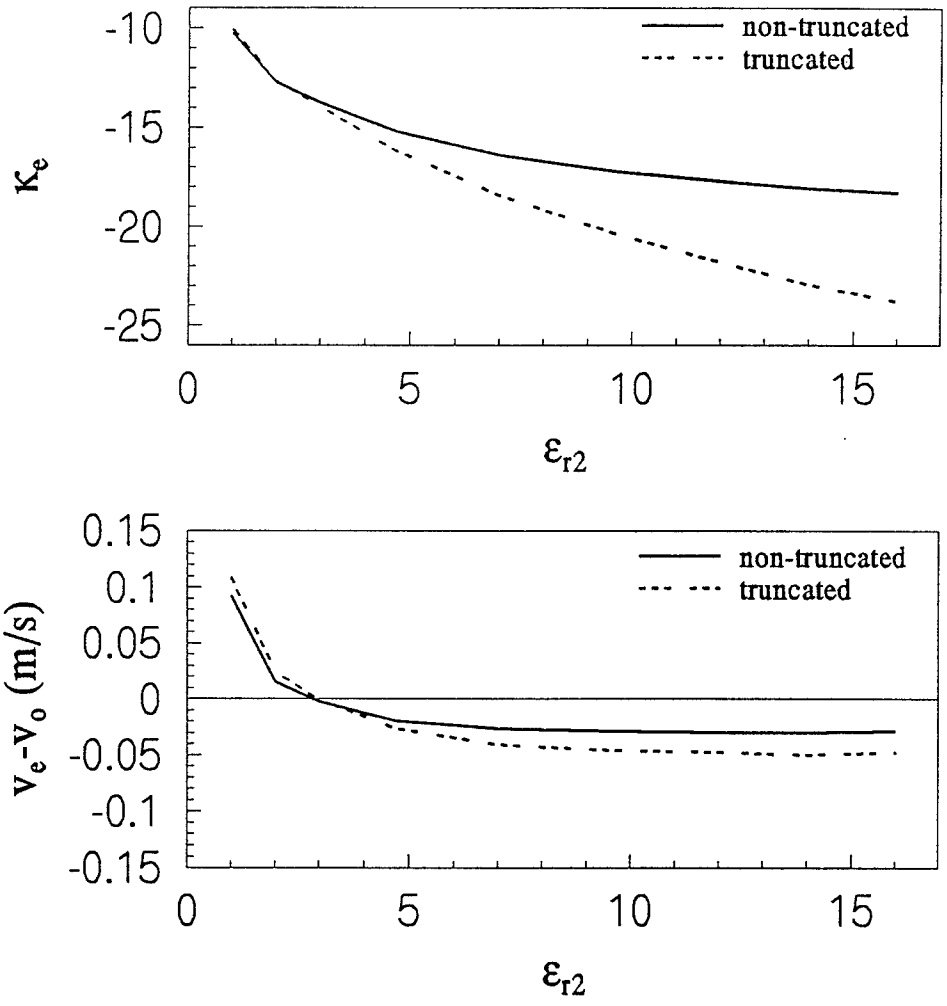

Fig.14b Effect of dielectric substrate on coupling and phase velocities

(h_1=0.2, h_2=0.2, h_3=0.5, t=0.001, δ_w=10°, δ_s=10°, δ_n=6°, ε_{r1}=2.2, ε_{r3}=1.0, α_s=α_o=72°, N_w=10, N_1=4, N_2=1, N_3=3, N_4=4)

show significant percentage variations as ϵ_{r2} increases. Fig.14b shows that the coupling coefficient decreases as ϵ_{r2} increases. It is also noted that the use of truncated geometry with an air-dielectric notch exhibits a better decoupling between lines, compared with the results obtained by using a dielectric notch. Fig.14b also shows that the even and odd modes phase velocities, v_e and v_o, are equalized at approximately $\epsilon_{r2}=3$. These properties show that a possible method for reducing mutual coupling between the transmission lines is by using a truncated geometry with an air-dielectric notch in the substrate and for a distortionless line by selecting proper value of the dielectric constant of the substrate.

4.1.4c Effect of the Notch Dielectric Material

Another case is selected to study the effect of the dielectric constant of the notch. The configuration selected is such that $h_1=0.2$, $h_2=0.2$, $h_3=0.5$, $t=0.001$, $\delta_w=10°$, $\delta_s=10°$ and $\delta_n=6°$. The size of truncation, $\alpha_s=\alpha_o=72°$, and the dielectric constants, ϵ_{r1} and ϵ_{r2}, are set to 2.2 and 4.7, respectively. The dielectric constant of notch, ϵ_{r3}, is then varied from 1 to 16. Figs.15a~15d show the characteristic parameters of transmission line as a function of ϵ_{r3}. Fig.14a shows the linear behavior of the self capacitance as the ϵ_{r3} increases. It is noted that the coupling between strip lines increases when ϵ_{r3} has a small value, and then decreases after $\epsilon_{r3}=6$, for this specific case. This particular property shows the influences of the dielectric constants of substrate and overlay on the mutual capacitance and the coupling coefficient, as it will be tested in the following case.

In order to investigate the influences of the dielectric constant of substrate on the characteristic parameters of the transmission line while ϵ_{r3} is varying, the dielectric constant, ϵ_{r2},

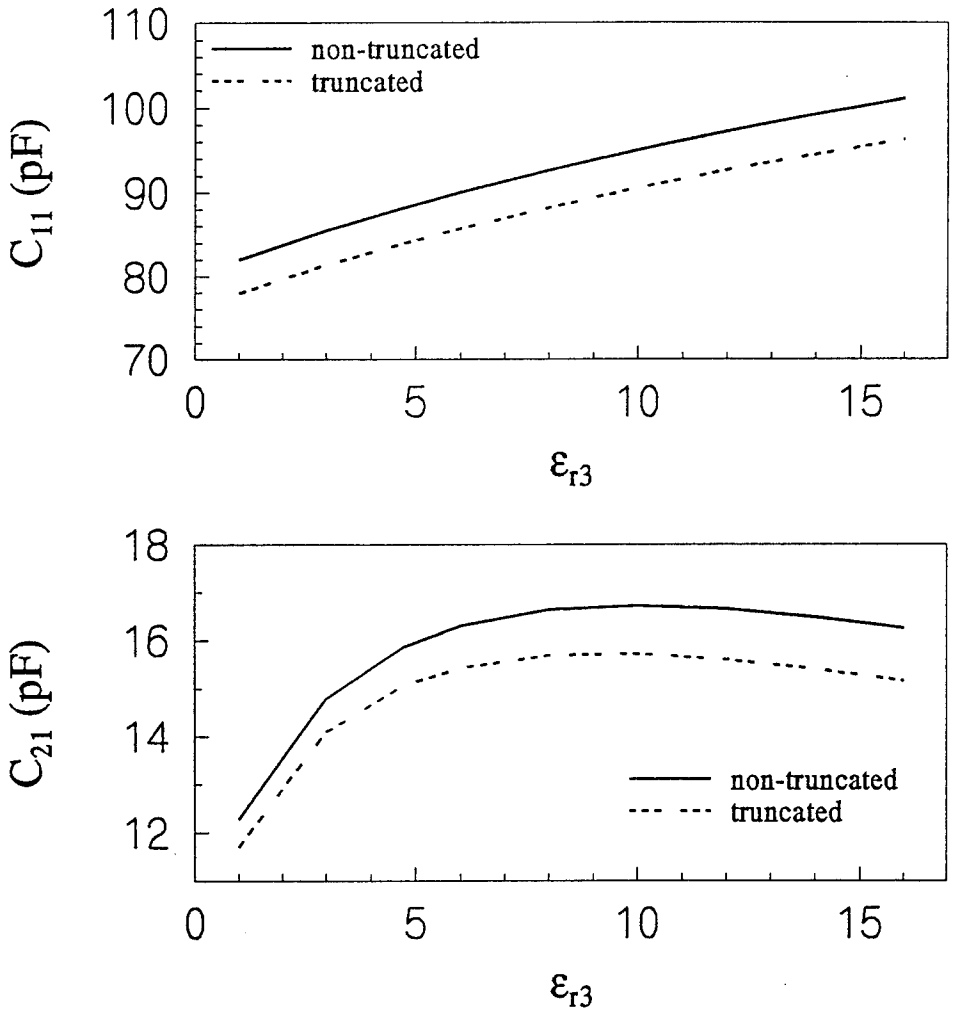

Fig.15a Effect of dielectric notch on capacitances

(h_1=0.2, h_2=0.2, h_3=0.5, t=0.001, δ_w=10°, δ_s=10°, δ_n=6°, ε_{r1}=2.2, ε_{r2}=4.7, α_s=α_o=72°, N_w=10, N_1=4, N_2=1, N_3=3, N_4=4)

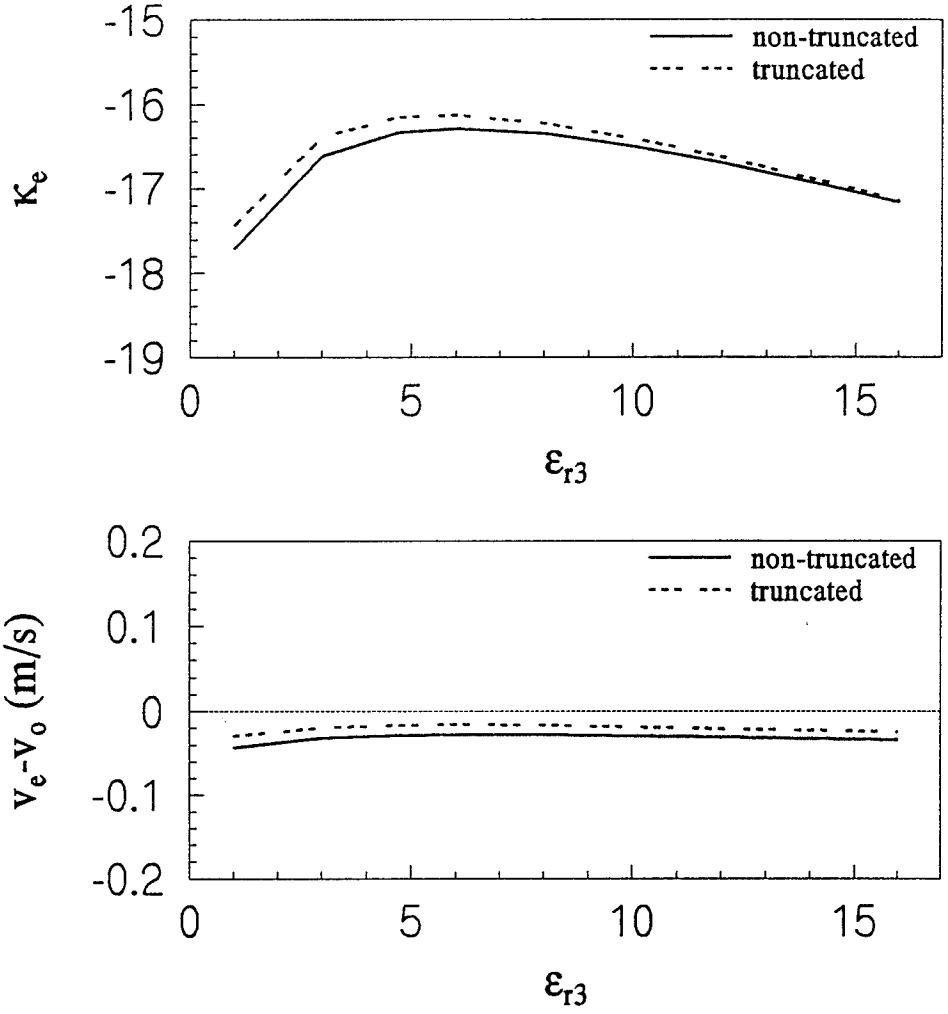

Fig.15b Effect of dielectric notch on coupling and phase velocities

(h_1=0.2, h_2=0.2, h_3=0.5, t=0.001, δ_w=10°, δ_s=10°, δ_n=6°, ε_{r1}=2.2, ε_{r2}=4.7, α_s=α_o=72°, N_w=10, N_1=4, N_2=1, N_3=3, N_4=4)

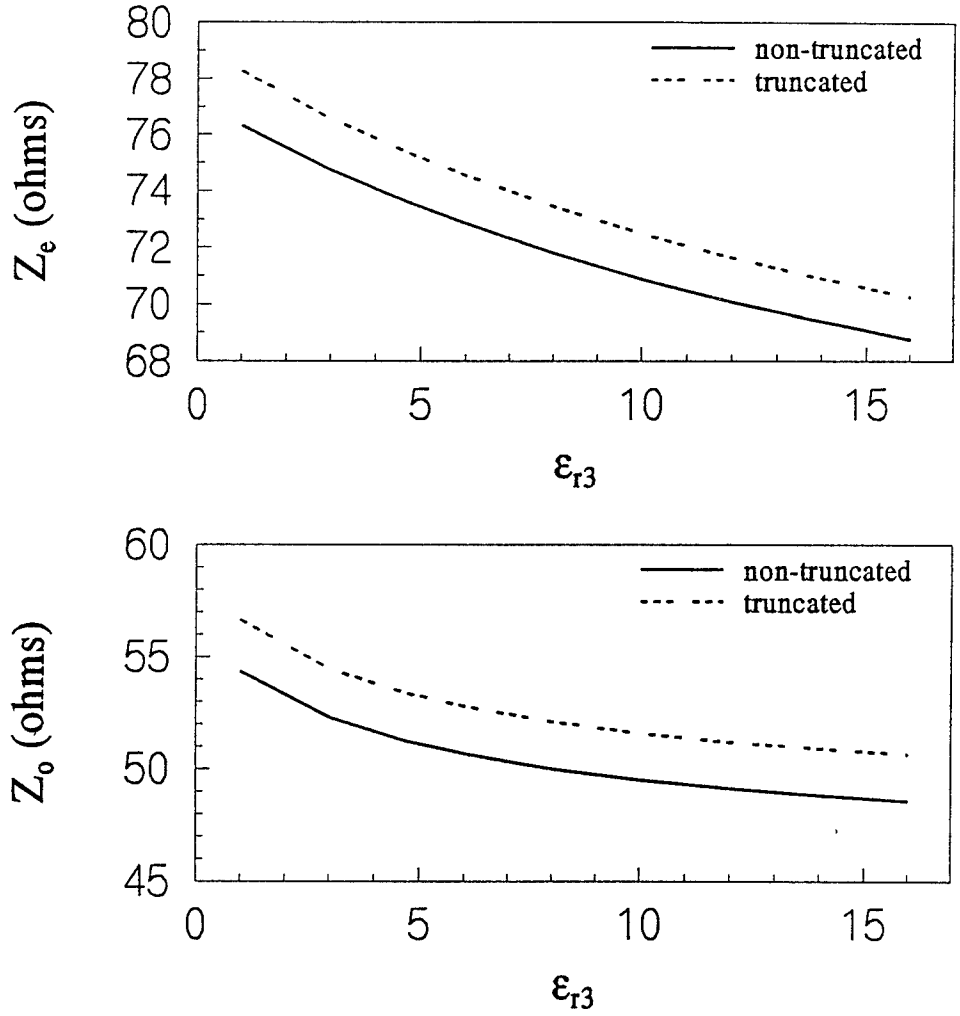

Fig.15c Effect of dielectric notch on impedances

(h_1=0.2, h_2=0.2, h_3=0.5, t=0.001, δ_w=10°, δ_s=10°, δ_n=6°, ε_{r1}=2.2, ε_{r2}=4.7, α_s=α_o=72°, N_w=10, N_1=4, N_2=1, N_3=3, N_4=4)

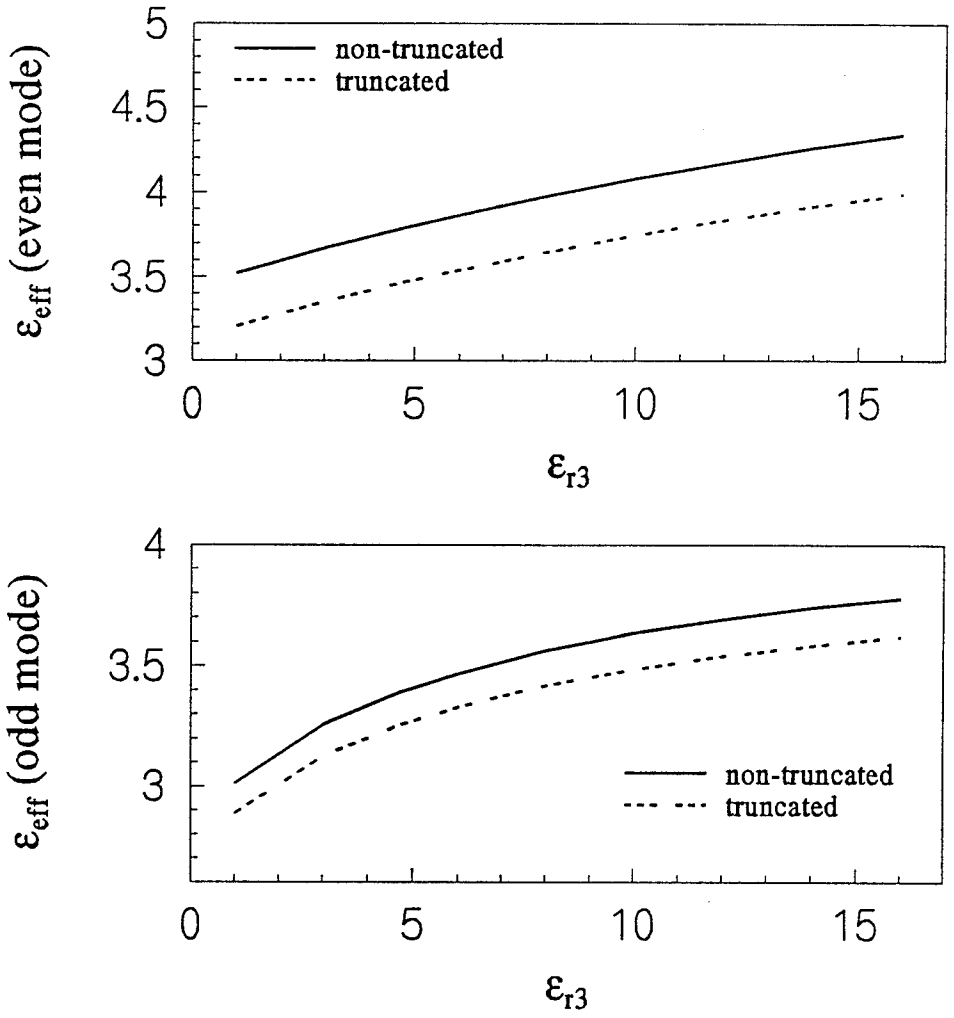

Fig.15d Effect of dielectric notch on effective dielectric constants

(h_1=0.2, h_2=0.2, h_3=0.5, t=0.001, δ_w=10°, δ_s=10°, δ_n=6°, ε_{r1}=2.2, ε_{r2}=4.7, α_s=α_o=72°, N_w=10, N_1=4, N_2=1, N_3=3, N_4=4)

is reduced from 4.7 to 2.2, which means, ϵ_{r2} is now set equal to ϵ_{r1}. Other configuration parameters are the same as used in previous example. Fig.15e shows the self and mutual capacitances (C_{11},C_{21}) versus ϵ_{r3} with ϵ_{r2}=2.2. Compared with the above case, in which ϵ_{r2} is equal to 4.7, both self and mutual capacitances are reduced. As it can be seen, the mutual capacitance (C_{21}) decreases after ϵ_{r3} is approximately 5. Figure.15f demonstrates that the coupling coefficient, k_e, decreases as ϵ_{r3} increases. It is also noted that v_e and v_o are equalized at ϵ_{r3}=5.2 for non-truncated geometry and at ϵ_{r3}=9 for truncated geometry. This figure shows that CMSTL with truncated dielectric can be distortionless with less coupling.

Another case selected for study is the effect of the width of notch on the characteristics of CMSTL. The configuration is the same as the first case in this section, separation between strips, δ_s=10°, but the width of notch, δ_n, is set to 2° and 8°, respectively, and ϵ_{r3} is then varying from 1 to 16. Figure.15g shows the capacitances versus ϵ_{r3}. As can be seen that there is an intersection between the curves in the figure. This occurs when ϵ_{r3}=4.7 (i.e., ϵ_{r3}=ϵ_{r2}), which means that there is no notch in the substrate. At this point, the capacitances should have the same values because the geometry is the same. From Fig.15h, it can be seen that the coupling coefficient is further reduced while the notch is wider. This property shows the advantage of using the widest notch possible for the best decoupling between the strips.

4.1.5. Effect of the Width of the Strips

In this investigation, the width of the strips, δ_w, is varied from 2° to 20° with a fixed spacing between the strips. Other configuration parameters selected are such that h_1=0.2, h_2=0.2, h_3=0.5, t=0.001, δ_s=10°, δ_n=6°, ϵ_{r1}=2.2, ϵ_{r2}=4.7, ϵ_{r3}=9.6, and the angles, α_s, α_o,

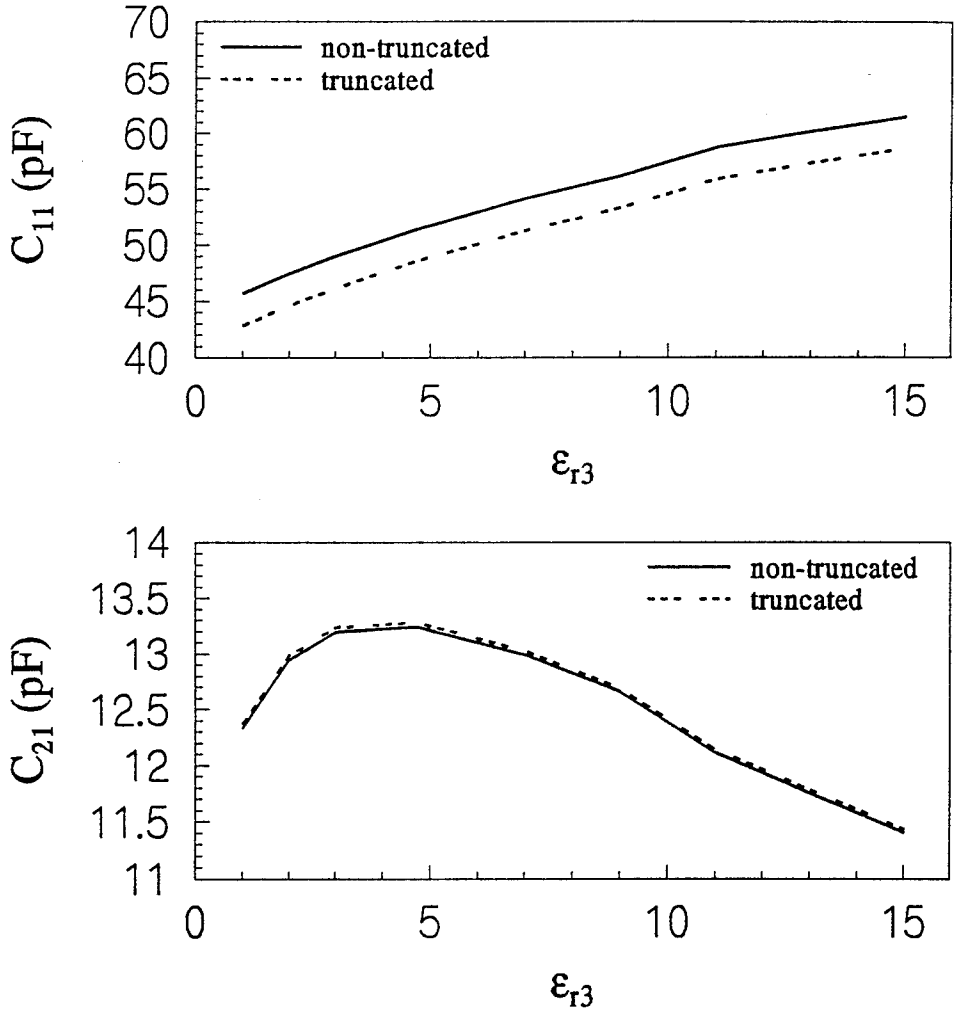

Fig.15e Effect of dielectric notch on capacitances

(h_1=0.2, h_2=0.2, h_3=0.5, t=0.001, δ_w=10°, δ_s=10°, δ_n=6°, ε_{r1}=2.2, ε_{r2}=2.2, α_s=α_o=72°, N_w=10, N_1=4, N_2=1, N_3=3, N_4=4)

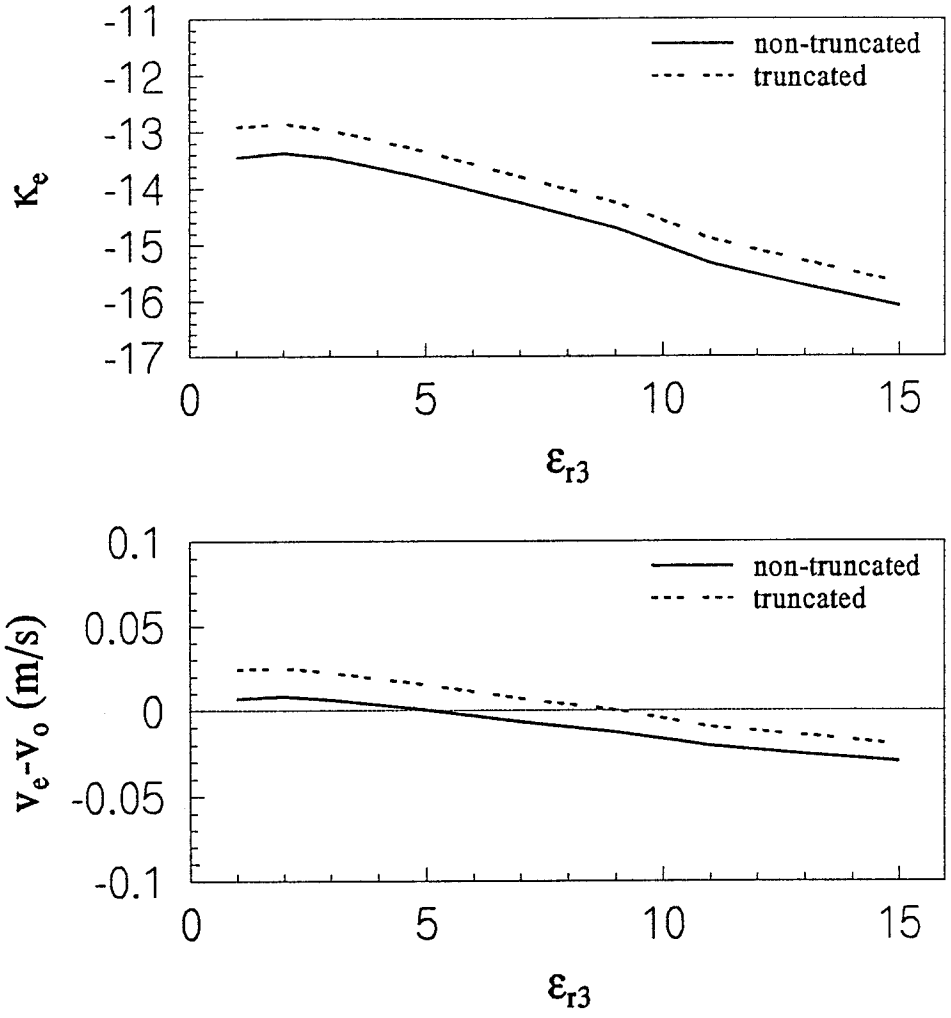

Fig.15f Effect of dielectric notch on coupling and phase velocities

(h_1=0.2, h_2=0.2, h_3=0.5, t=0.001, δ_w=10°, δ_s=10°, δ_n=6°, ε_{r1}=2.2, ε_{r2}=2.2, α_s=α_o=72°, N_w=10, N_1=4, N_2=1, N_3=3, N_4=4)

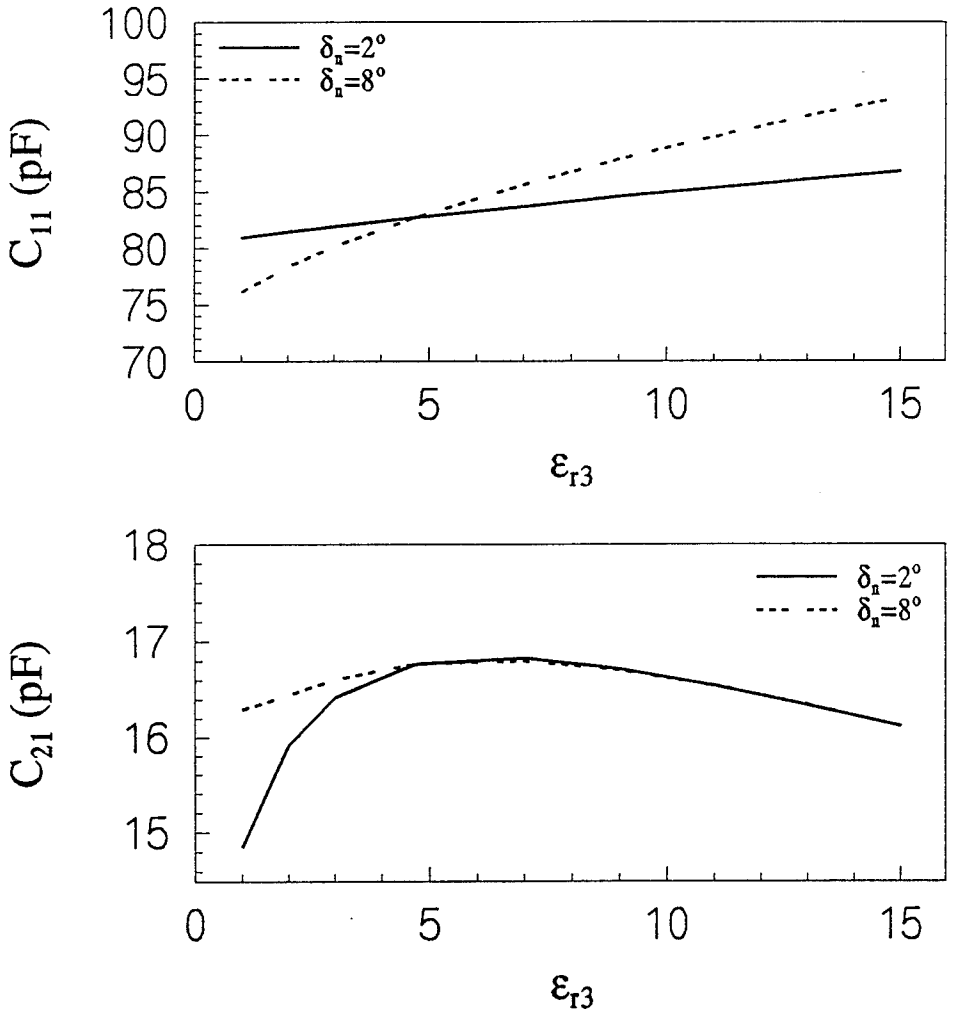

Fig.15g Effect of dielectric notch on capacitances for truncated CMSTL

(h_1=0.2, h_2=0.2, h_3=0.5, t=0.001, δ_w=10°, δ_s=10°, ε_{r1}=2.2, ε_{r2}=4.7, α_s=72°, N_w=10, N_1=4, N_2=1, N_3=3, N_4=4)

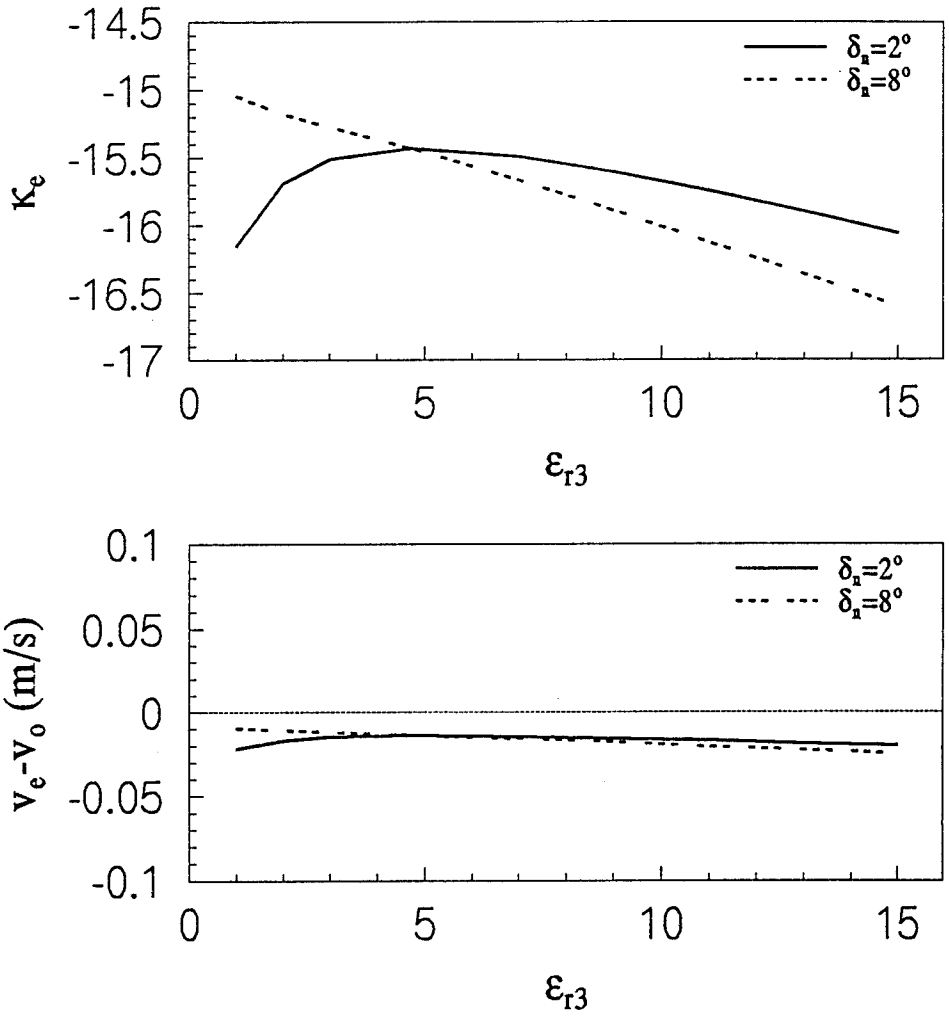

Fig.15h Effect of dielectric notch on coupling and phase velocities for truncated CMSTL

(h_1=0.2, h_2=0.2, h_3=0.5, t=0.001, δ_w=10°, δ_s=10°, ε_{r1}=2.2, ε_{r2}=4.7, α_s=α_o=72°, N_w=10, N_1=4, N_2=1, N_3=3, N_4=4)

are set equal to 65°. Figure.16a shows the effects of changing the width of the two strips on the capacitances versus δ_w. As can be seen in the figure, the self-capacitance increases as the width of strips get wider. However, the mutual-capacitance does not show a significant increase, thus, coupling coefficient is reduced as the strips have larger width, as shown in Fig.16b. From the same figure, one notices that, v_e-v_o, is very close to zero, which means, for this case, that the distortion on the transmission line is almost eliminated. It is also noted that the use of truncated geometry does not show significant changes on the values of the characteristic parameters of the transmission line.

Another case is investigated to test the influences of the dielectric constant of overlay on the characteristics of the CMSTL. For this case, a truncated geometry is used, the size of truncation, defined by α_s and α_o, and all other configuration parameters are the same as in the above case, but ϵ_{r1} is now set 2.2 and 1.0, respectively. Figures.16c to 16d show the influences of different ϵ_{r1} on the characteristic parameter of the CMSTL. As can be seen in Figs.16c and 16d, removing dielectric material from overlay, the mutual capacitance and coupling are further reduced. Figure.16d also shows that the difference, v_e-v_o, is not closer to zero if an air-dielectric overlay is used, which means that the use of an air-dielectric material for the overlay does not show better distortionless control on the line, as compared with the use of a dielectric overlay.

4.1.6. Effect of the Spacing between Strips

The effect of the spacing between the strips on the characteristic parameters of the transmission line is now studied. The width of the strips, δ_w is set to 10°. Other configuration parameters selected are such that h_1=0.2, h_2=0.2, h_3=0.5, t=0.001, δ_n=6°, ϵ_{r1}=2.2, ϵ_{r2}=4.7,

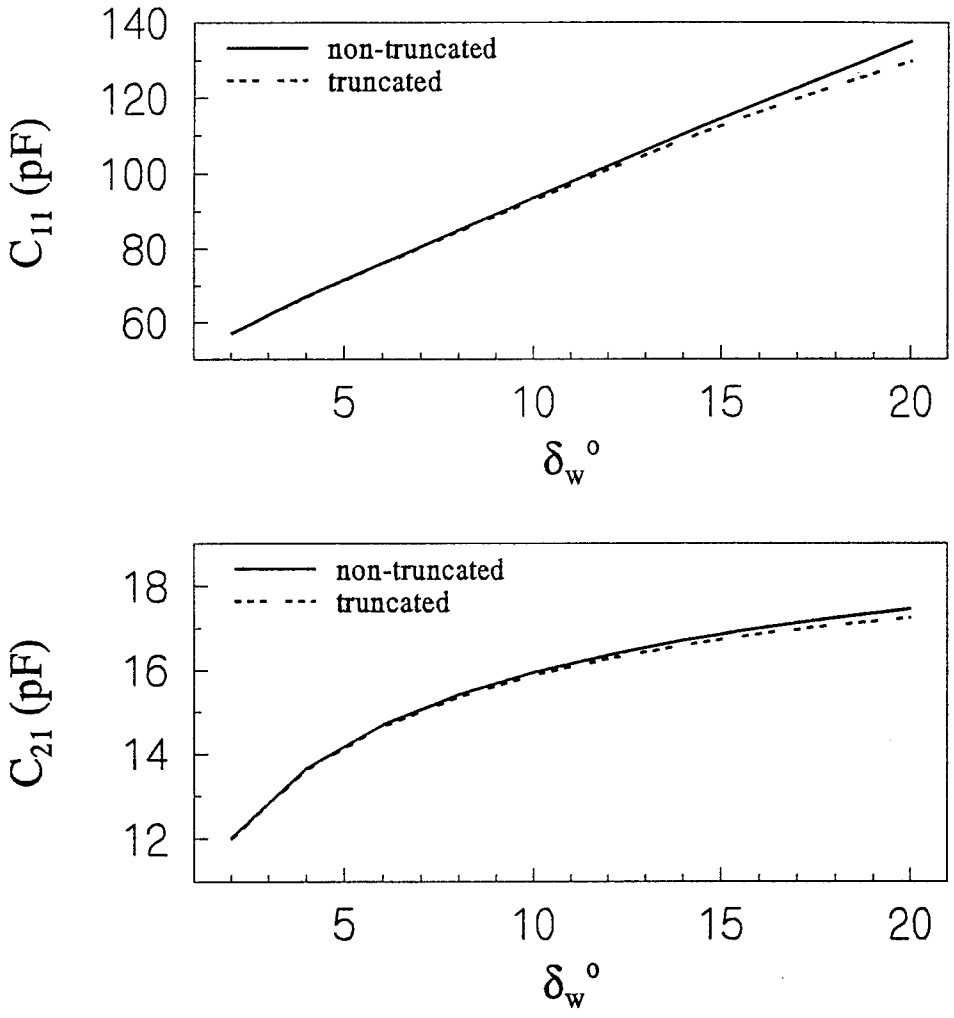

Fig.16a Effect of width of strips on capacitances

(h_1=0.2, h_2=0.2, h_3=0.5, t=0.001, δ_s=10°, δ_n=6°, ε_{r1}=2.2, ε_{r2}=4.7, ε_{r3}=9.6, α_s=α_o=65°, N_1=4, N_2=1, N_3=3, N_4=4)

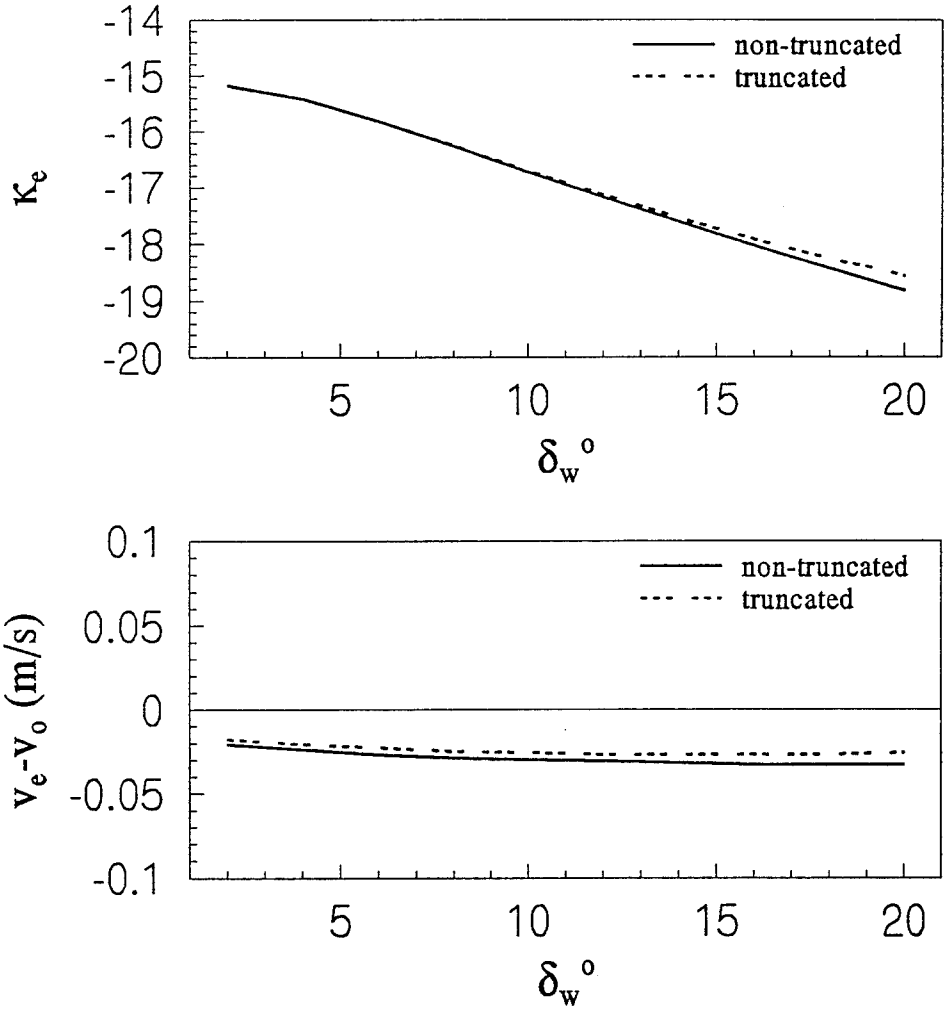

Fig.16b Effect of width of strips on coupling and phase velocities

(h_1=0.2, h_2=0.2, h_3=0.5, t=0.001, δ_s=10°, δ_n=6°, ε_{r1}=2.2, ε_{r2}=4.7, ε_{r3}=9.6, α_s=α_o=65°, N_1=4, N_2=1, N_3=3, N_4=4)

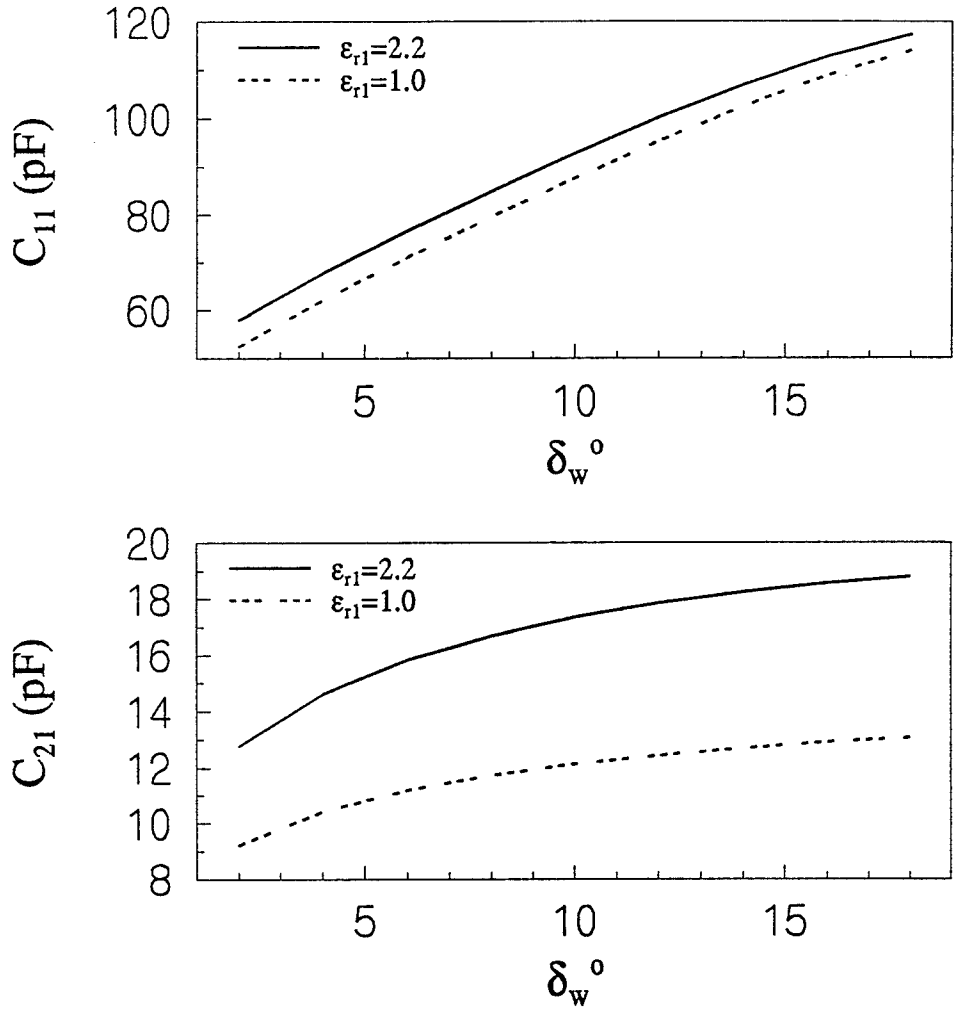

Fig.16c Effect of width of strips on capacitances for truncated CMSTL

(h_1=0.2, h_2=0.1, h_3=0.2, t=0.001, δ_s=10°, δ_n=6°, ε_{r2}=4.7, ε_{r3}=9.6, α_s=65°, N_1=4, N_2=1, N_3=3, N_4=4)

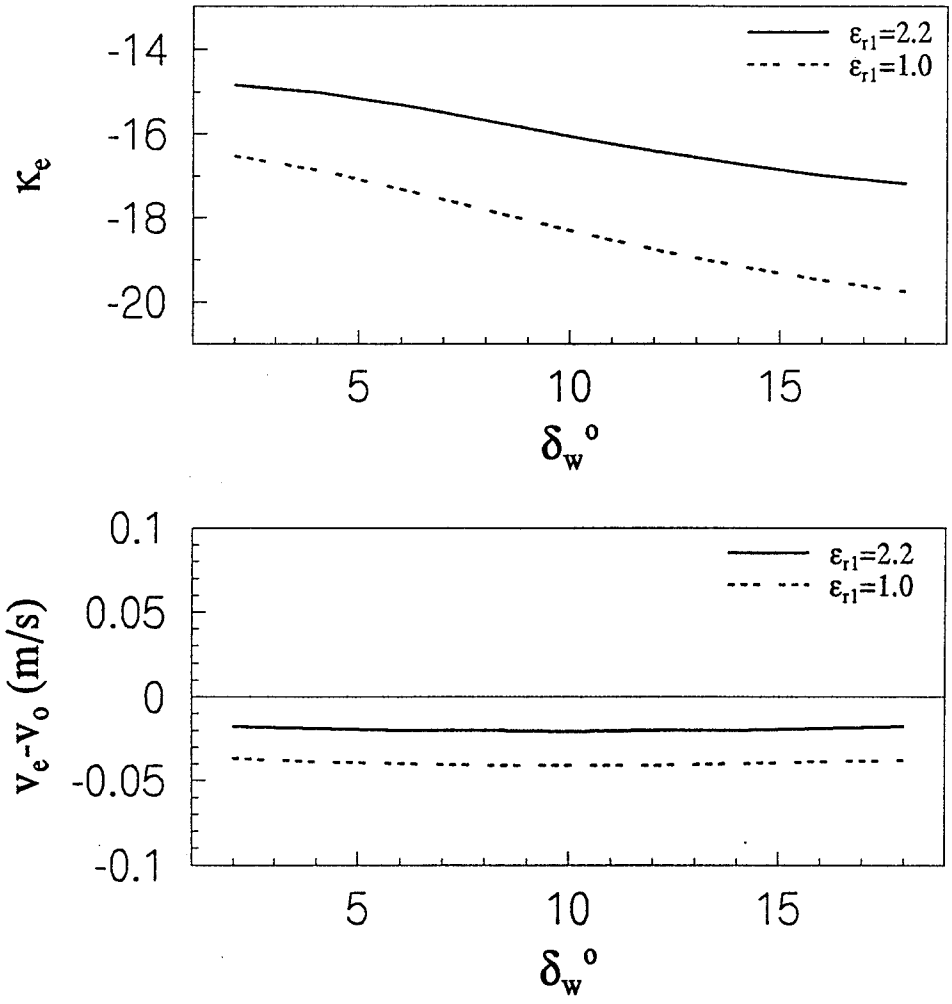

Fig.16d Effect of width of strips on coupling and phase velocities for truncated CMSTL

(h_1=0.2, h_2=0.1, h_3=0.2, t=0.001, δ_s=10°, δ_n=6°, ε_{r2}=4.7, ε_{r3}=9.6, α_s=65°, N_1=4, N_2=1, N_3=3, N_4=4)

ϵ_{r3}=9.6, and the angles, α_s, α_o are set to 67°. The spacing between strips, δ_s, is then varied from 10° to 28°. Figure.17a shows the influences of varying the spacing between strips on the capacitances. It is found that the mutual capacitances decrease with δ_s for both the truncated and the non-truncated geometries. From Fig.17b, it is clear that the coupling coefficient, k_e, decreases as the separation distance increases. Another important behavior is that the difference between even and odd normalized phase velocities is very close to zero with increased spacing between strips, thus, the distortion on the line is further controlled.

Another analysis is made to study the effects of spacing between the strips with an air-dielectric notch in substrate. All configuration parameters are the same as in previous case, the dielectric constant of the notch, ϵ_{r3}, is now set to 1. The same test is then repeated as in Fig.17a. As shown in Fig.17c, both the self and mutual capacitances are reduced, compared with Fig.17a in which a dielectric notch was used. As it can be seen in Fig.17d, however, the coupling coefficient does not show significant changes for the use of an air-dielectric notch. After study all these figures, it is noted that the use of different dielectric constants for the notch does not have much effect on the characteristics of the transmission line, as the separation distance is increased.

4.1.7. Effect of the Heights of the Substrate and the Overlay

The heights of the substrate and overlay are very important parameters to the characteristics of the transmission line. Usually, the heights of the substrate and overlay should be selected carefully in order to obtain the best decoupling and equalize the even and odd phase velocities. For this purpose, the effect of the substrate height is first studied. The configuration

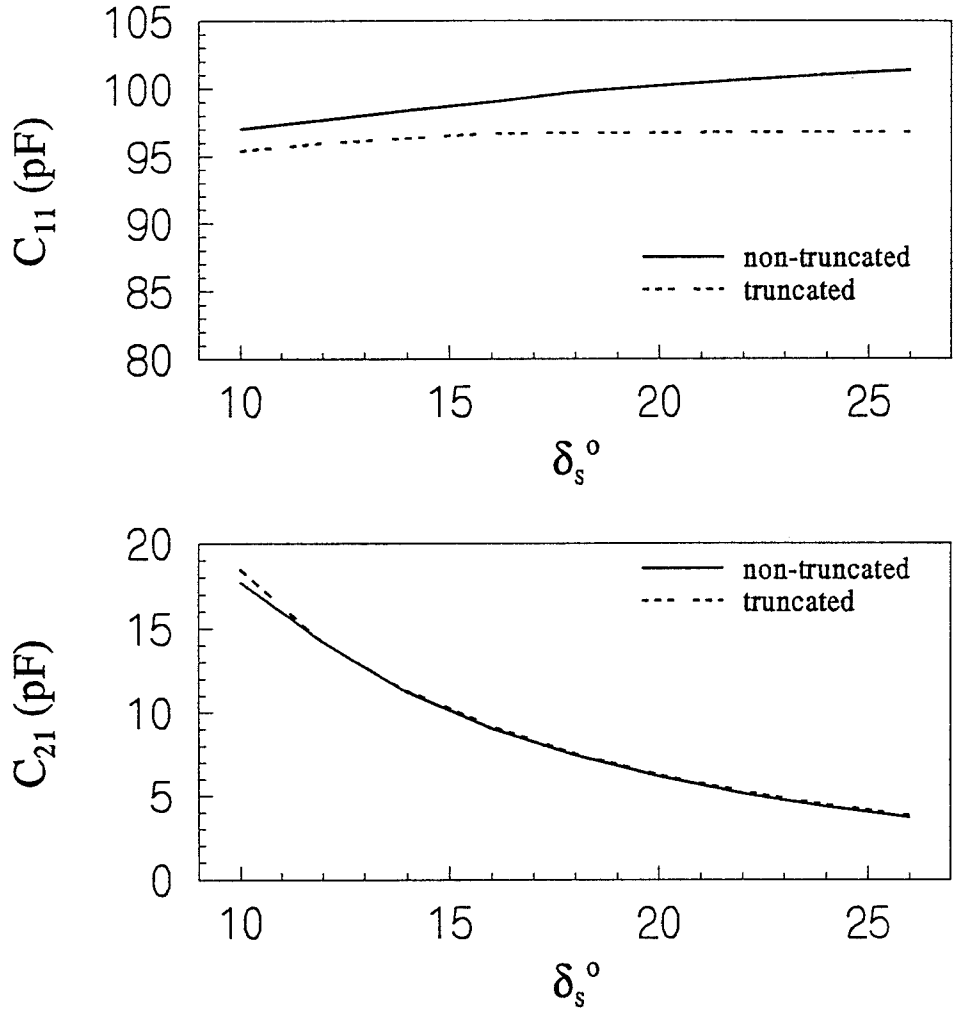

Fig.17a Effect of spacing between strips on capacitances

(h_1=0.2, h_2=0.2, h_3=0.5, t=0.001, δ_w=10°, δ_n=6°, ε_{r1}=2.2, ε_{r2}=4.7, ε_{r3}=9.6, α_s=67°, N_w=10, N_1=4, N_2=1, N_3=3, N_4=5)

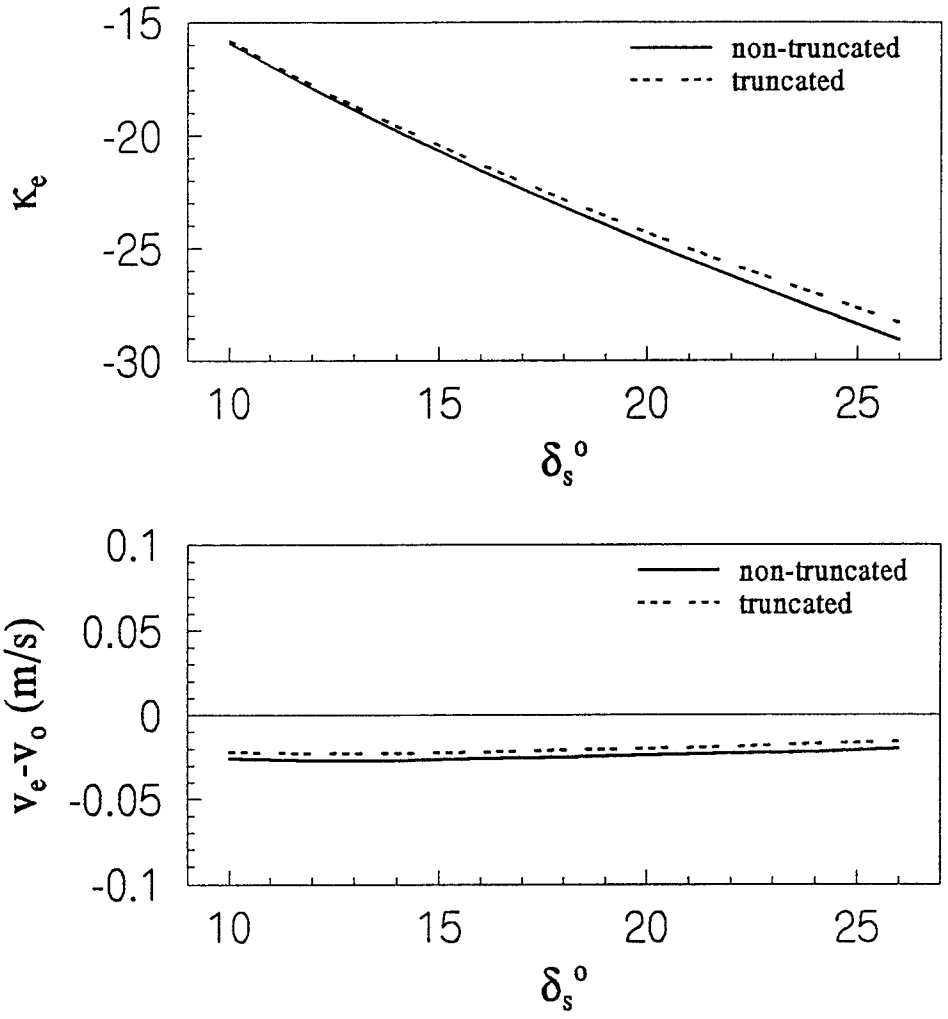

Fig.17b Effect of spacing between strips on coupling and phase velocities

(h_1=0.2, h_2=0.2, h_3=0.5, t=0.001, δ_w=10°, δ_n=6°, ε_{r1}=2.2, ε_{r2}=4.7, ε_{r3}=9.6, α_s=67°, N_w=10, N_1=4, N_2=1, N_3=3, N_4=5)

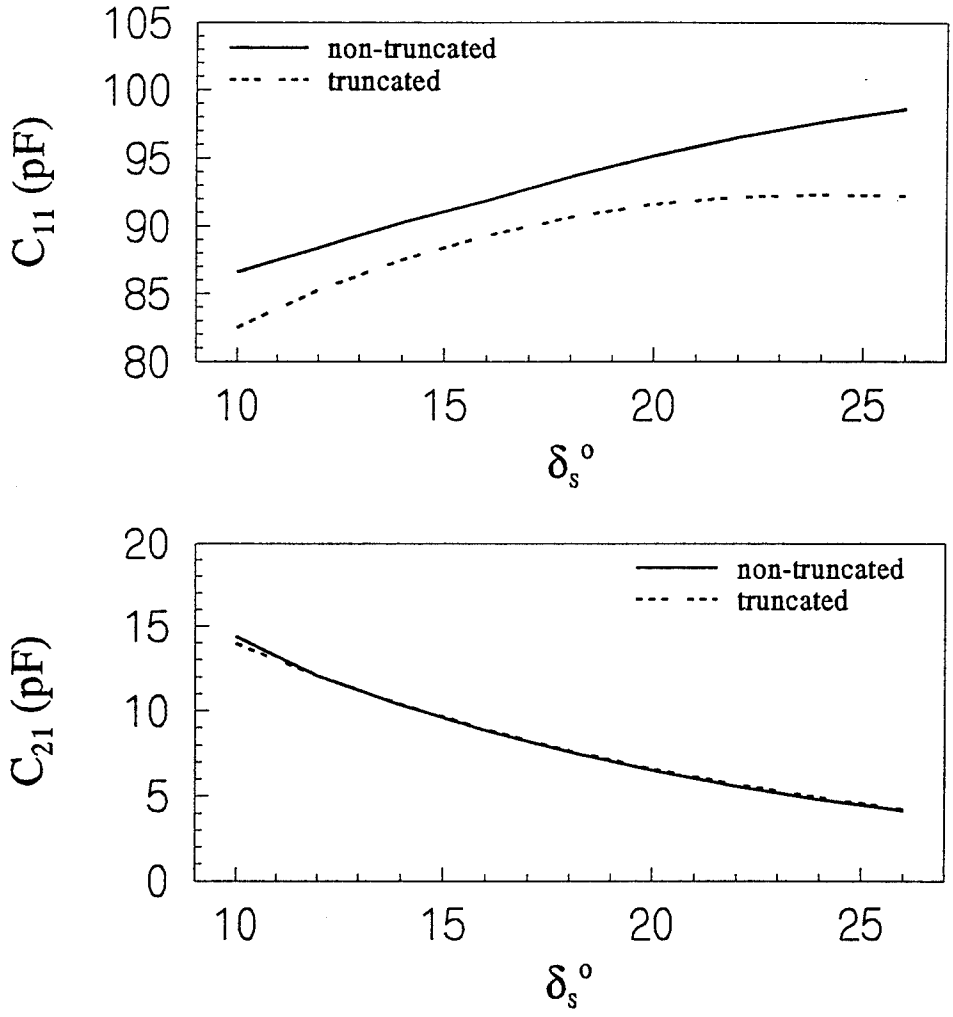

Fig.17c Effect of spacing between strips on capacitances

(h_1=0.2, h_2=0.2, h_3=0.5, t=0.001, δ_w=10°, δ_n=6°, ε_{r1}=2.2, ε_{r2}=4.7, ε_{r3}=1.0, α_s=67°, N_w=10, N_1=4, N_2=1, N_3=3, N_4=5)

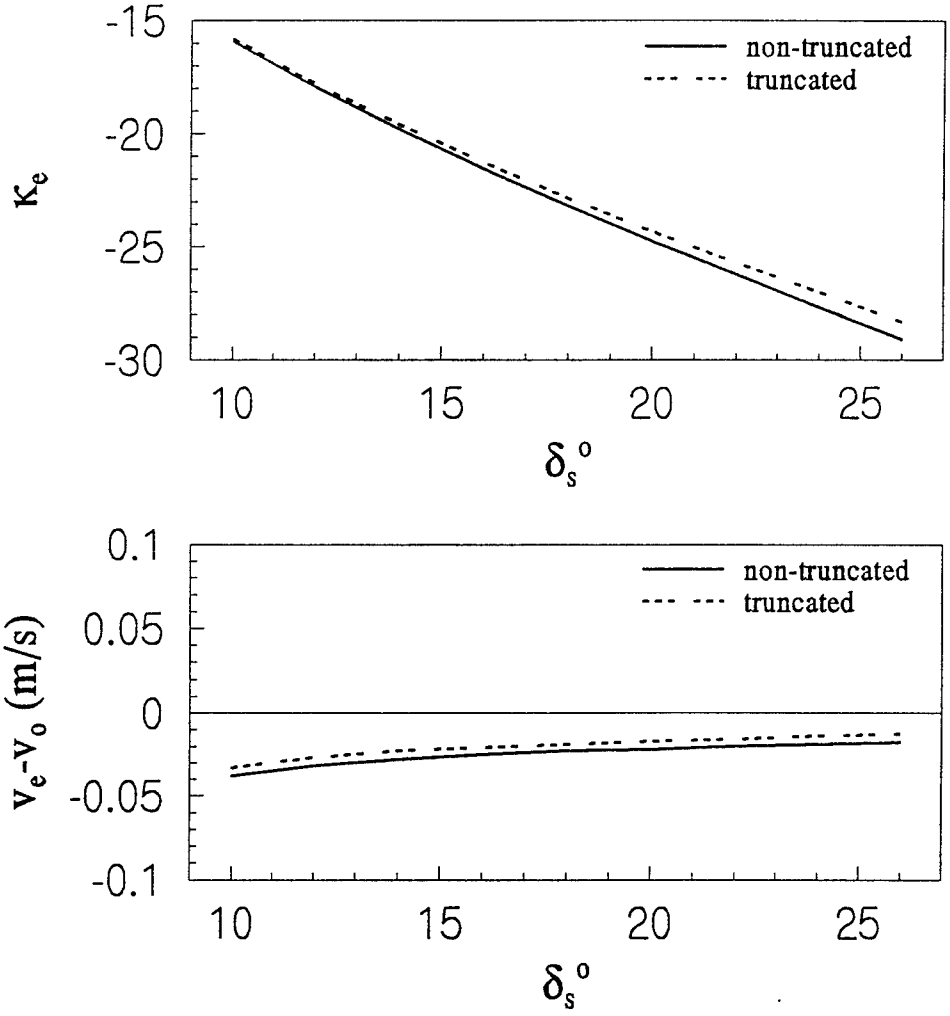

Fig.17d Effect of spacing between strips on coupling and phase velocities

(h_1=0.2, h_2=0.2, h_3=0.5, t=0.001, δ_w=10°, δ_n=6°, ε_{r1}=2.2, ε_{r2}=4.7, ε_{r3}=1.0, α_s=67°, N_w=10, N_1=4, N_2=1, N_3=3, N_4=5)

selected for this case, is such that h_2=0.2, h_3=0.5, t=0.001, δ_s=10°, δ_w=10°, δ_n=6°, ϵ_{r1}=2.2, ϵ_{r2}=4.7, ϵ_{r3}=9.6, and $\alpha_s=\alpha_o$=72°. The height of the substrate, h_1, is then varied from 0.1 to 0.9. Figure.18a shows that the self capacitance decreases and mutual capacitance increases, as h_1 increases, for both truncated and non-truncated structures. With the use of truncated structure, v_e and v_o are equalized when h_1 is approximately 0.3, and the use of non-truncated structure does not exhibits this property, as shown in Fig.18b. Note that the coupling is increased with varied h_1, which means, for the best decoupling, height of the substrate should be kept as smaller as possible. For the same analysis with ϵ_{r1}=4.7 and ϵ_{r2}=2.2, Fig.18d clearly shows that the coupling is further increased, v_e and v_o can not be equalized at any height of the substrate. Hence, in order to reduce the coupling between the strips, the dielectric constant of the overlay should be smaller than that of the substrate.

With the same configuration parameters, the effect of the height of overlay is studied. In this case, h_1 is fixed at 0.2, and the height of the overlay, h_2, is then varied from 0.1 to 0.9. It is clearly seen from Figs.19a and 19b, that different heights of the overlay do not affect much on those characteristic parameters of the transmission line, for this specific case with ϵ_{r1}=2.2, ϵ_{r2}=4.7 and ϵ_{r3}=9.6. For another analysis with ϵ_{r1}=4.7, ϵ_{r2}=2.2 and ϵ_{r3}=9.6, Fig.19c shows that the self capacitance is reduced significantly, however, the mutual capacitance does not show much variations, thus the coupling is further increased, as shown in Fig.19d. From these figures, the same conclusion can be made as in previous case, that is, smaller dielectric constant of the overlay should be used for the best decoupling between the strips.

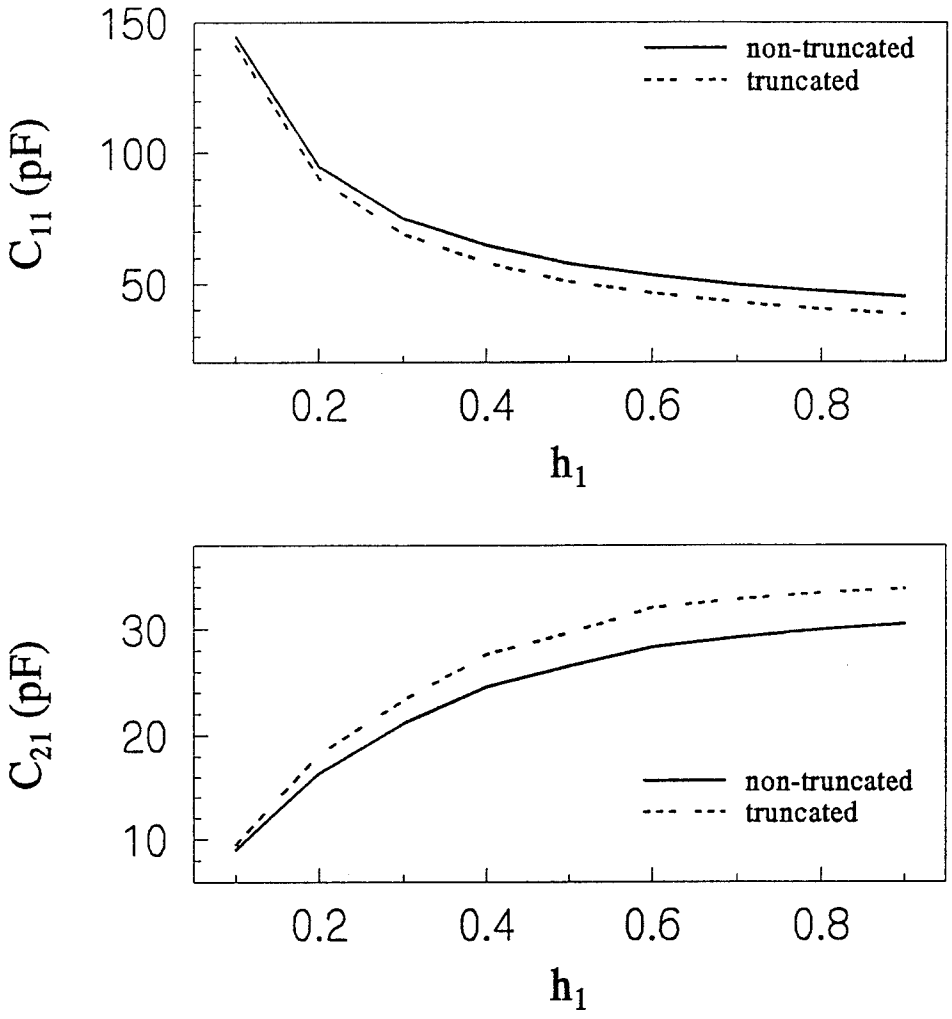

Fig.18a Effect of thickness of substrate on capacitances

(h_2=0.2, h_3=0.5, t=0.001, δ_w=10°, δ_s=10°, δ_n=6°, ε_{r1}=2.2, ε_{r2}=4.7, ε_{r3}=9.6, α_s=72°, N_w=10, N_1=4, N_2=1, N_3=3, N_4=5)

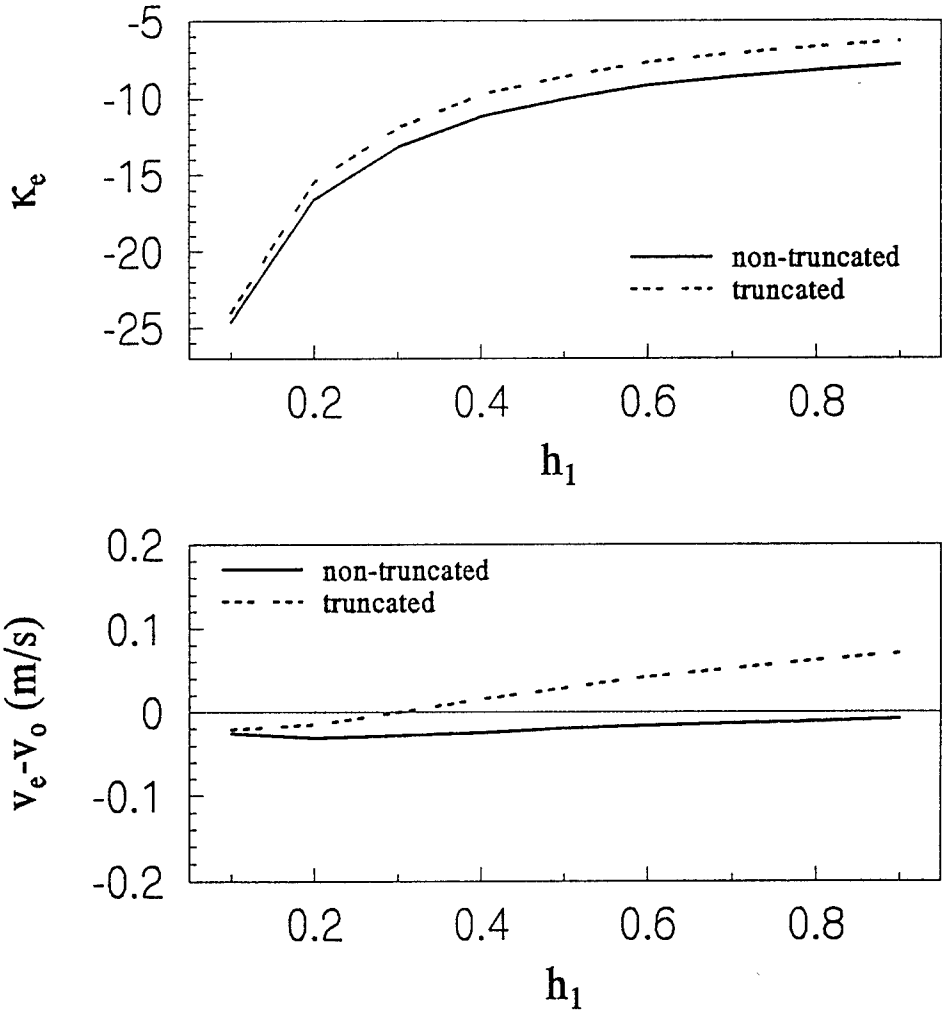

Fig.18b Effect of thickness of substrate on coupling and phase velocities

(h_2=0.2, h_3=0.5, t=0.001, δ_w=10°, δ_s=10°, δ_n=6°, ε_{r1}=2.2, ε_{r2}=4.7, ε_{r3}=9.6, α_s=72°, N_w=10, N_1=4, N_2=1, N_3=3, N_4=5)

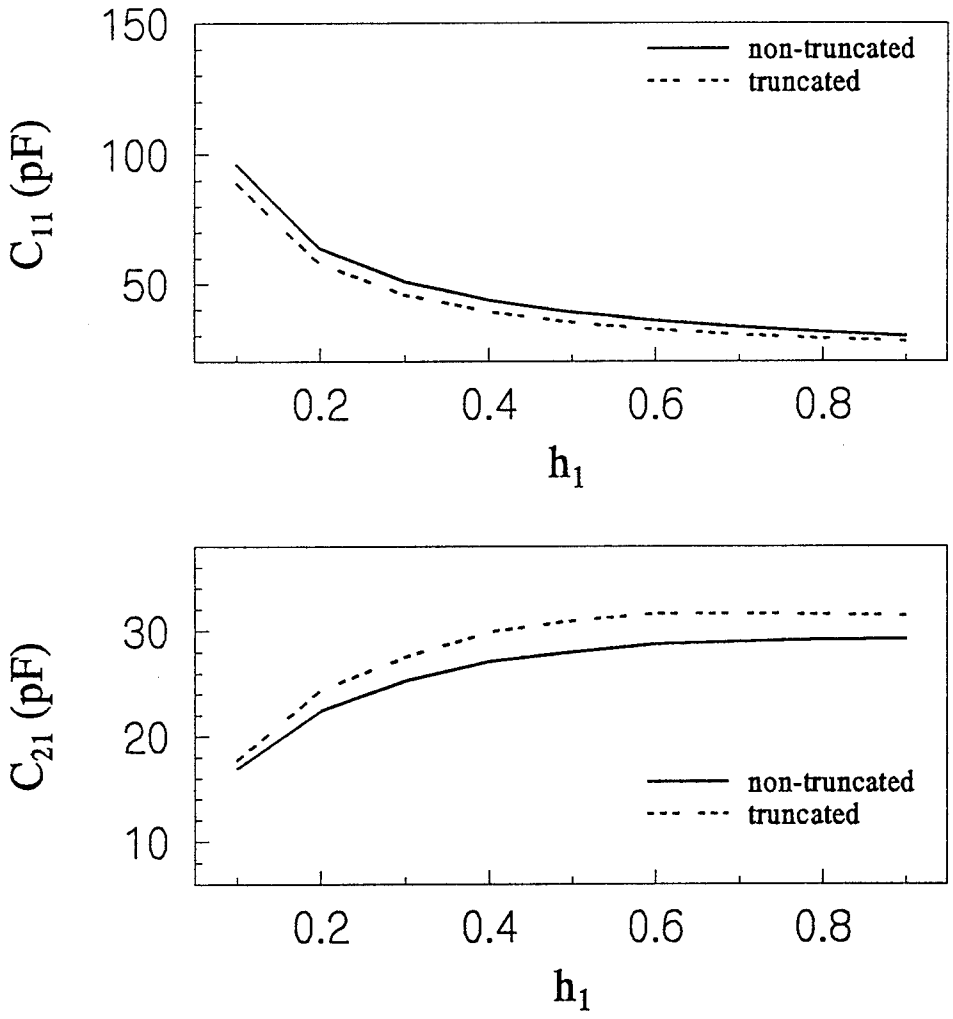

Fig.18c Effect of thickness of substrate on capacitances

(h_2=0.2, h_3=0.5, t=0.001, δ_w=10°, δ_s=10°, δ_n=6°, ε_{r1}=4.7, ε_{r2}=2.2, ε_{r3}=9.6, α_s=72°, N_w=10, N_1=4, N_2=1, N_3=3, N_4=5)

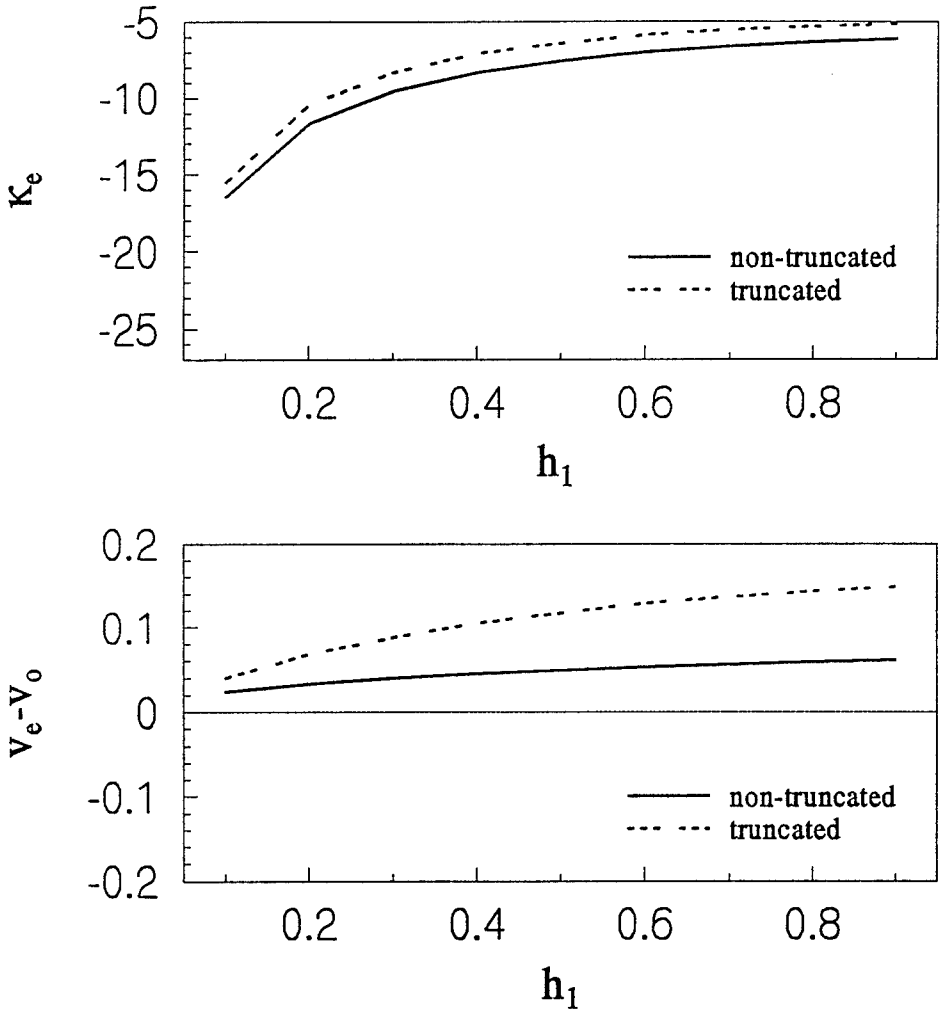

Fig.18d Effect of thickness of substrate on coupling and phase velocities

(h_2=0.2, h_3=0.5, t=0.001, δ_w=10°, δ_s=10°, δ_n=6°, ε_{r1}=4.7, ε_{r2}=2.2, ε_{r3}=9.6, α_s=72°, N_w=10, N_1=4, N_2=1, N_3=3, N_4=5)

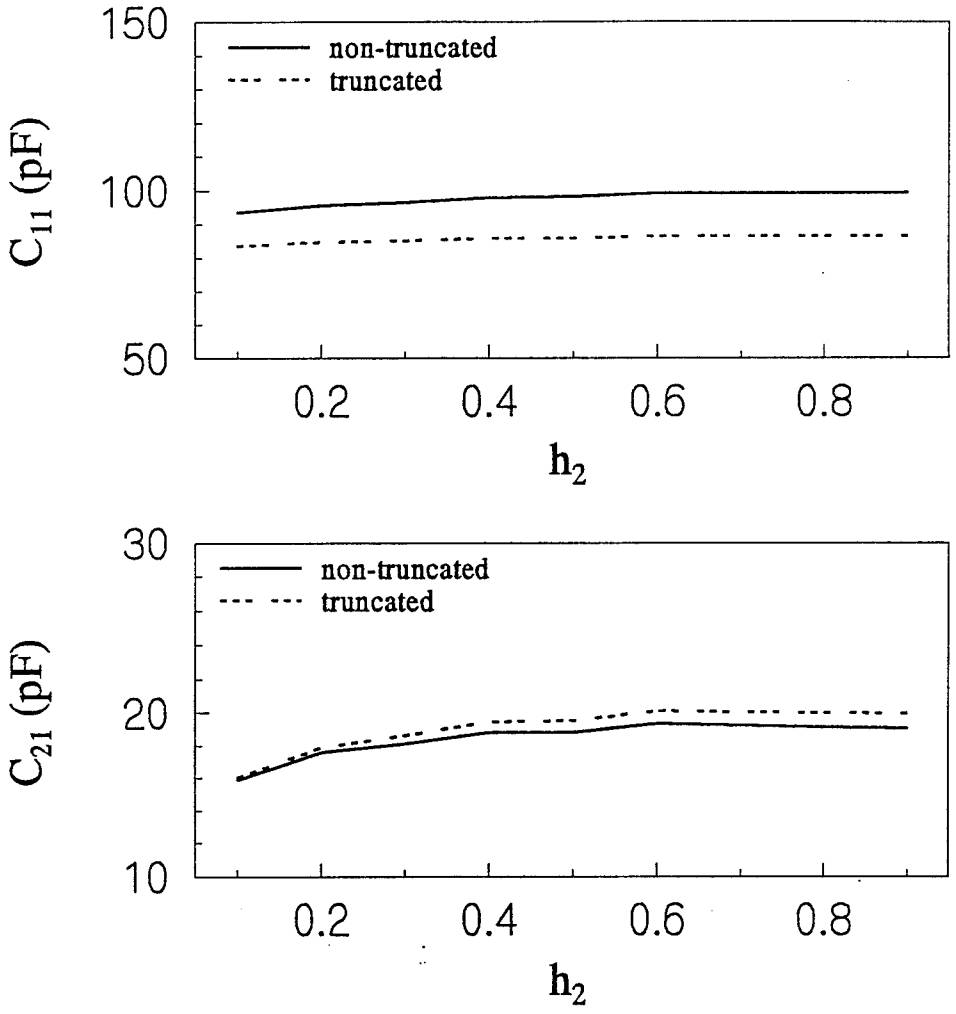

Fig.19a Effect of thickness of overlay on capacitances

(h_1=0.2, h_3=0.5, t=0.001, δ_w=10°, δ_s=10°, δ_n=6°, ε_{r1}=2.2, ε_{r2}=4.7, ε_{r3}=9.6, α_s=72°, N_w=10, N_1=4, N_2=1, N_3=3, N_4=5)

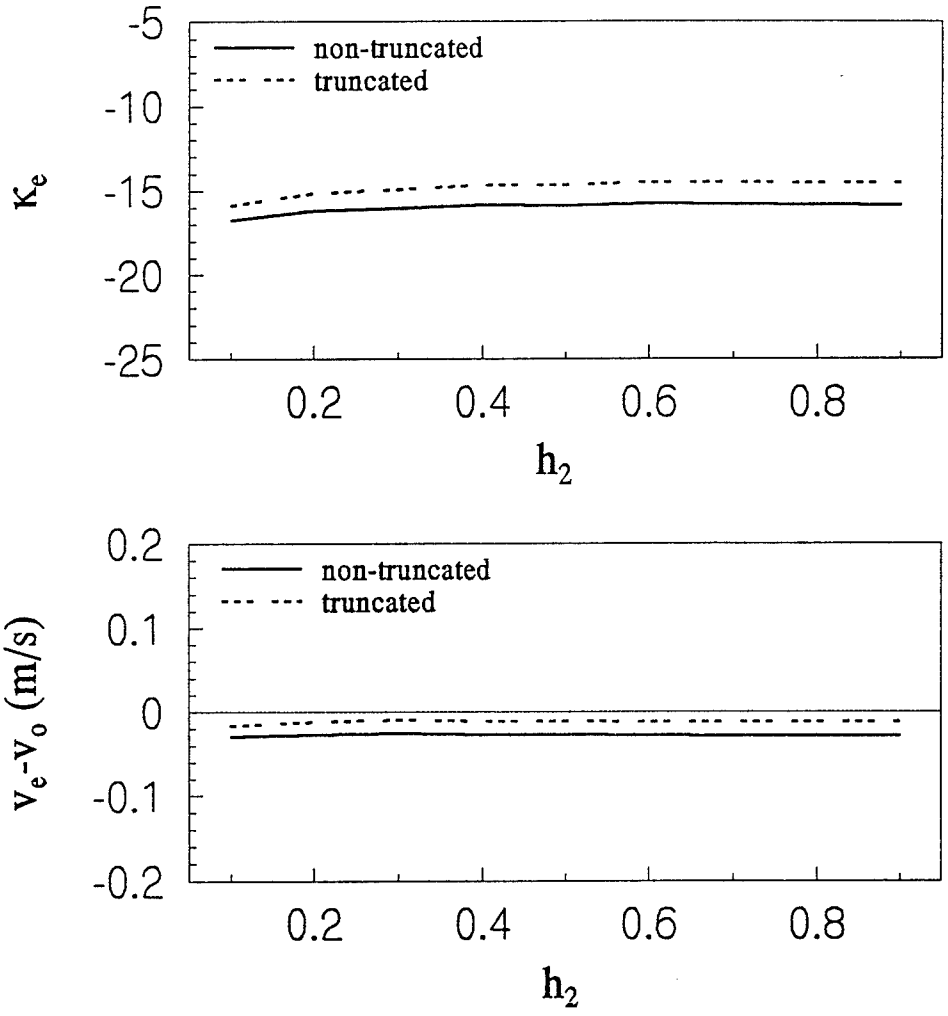

Fig.19b Effect of thickness of overlay on coupling and phase velocities

(h_1=0.2, h_3=0.5, t=0.001, δ_w=10°, δ_s=10°, δ_n=6°, ε_{r1}=2.2, ε_{r2}=4.7, ε_{r3}=9.6, α_s=72°, N_w=10, N_1=4, N_2=1, N_3=3, N_4=5)

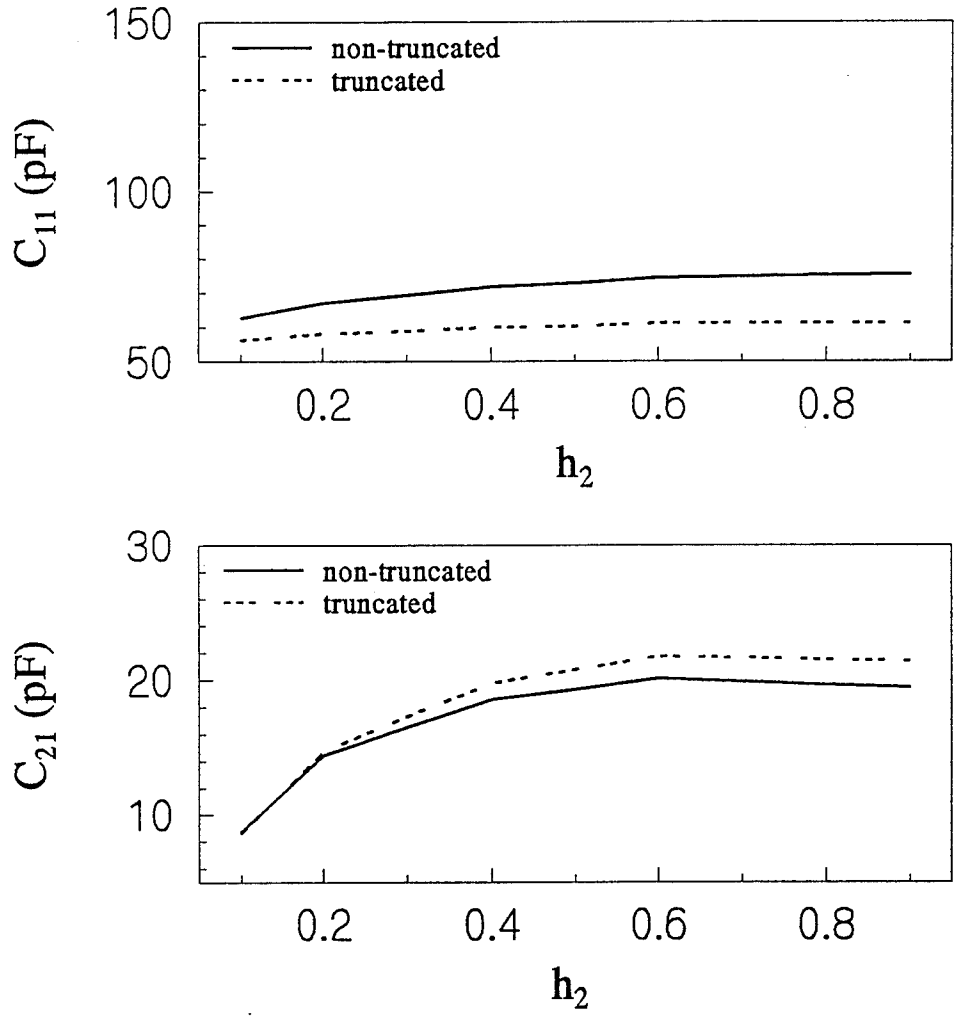

Fig.19c Effect of thickness of overlay on capacitances

(h_2=0.2, h_3=0.5, t=0.001, δ_w=10°, δ_s=10°, δ_n=6°, ε_{r1}=4.7, ε_{r2}=2.2, ε_{r3}=9.6, α_s=α_o=72°, N_w=10, N_1=4, N_2=1, N_3=3, N_4=5)

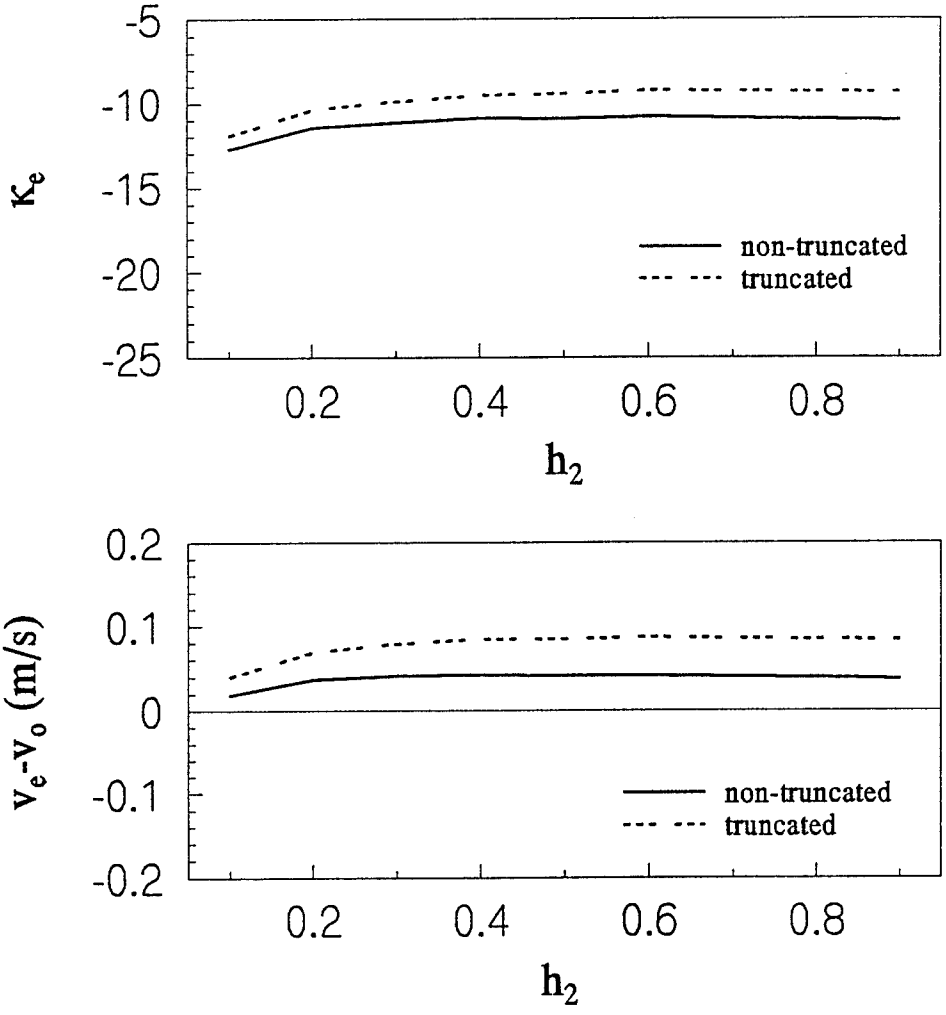

Fig.19d Effect of thickness of overlay on coupling and phase velocities

(h_1=0.2, h_3=0.5, t=0.001, δ_w=10°, δ_s=10°, δ_n=6°, ε_{r1}=4.7, ε_{r2}=2.2, ε_{r3}=9.6, α_s=72°, N_w=10, N_1=4, N_2=1, N_3=3, N_4=5)

4.2 Performance of Transmission Line without a Dielectric Notch

In this section, the characteristics of the CMSTL without a dielectric notch are analyzed. To remove the dielectric notch from the substrate, the dielectric constant in the notch, ϵ_{r3}, and the dielectric constant in the substrate, ϵ_{r2}, are set to be equal to each other ($\epsilon_{r3}=\epsilon_{r2}$). The numerical results for several examples are discussed in the following subsections.

4.2.1 Effect of the Dielectric Constant

The effect of the dielectric constant in overlay is first investigated. The configuration selected is such that $h_1=0.2$, $h_2=0.2$, $h_3=0.5$, $t=0.001$, $\delta_w=10°$, $\delta_s=10°$, the dielectric constants of substrate and notch, ϵ_{r2}, ϵ_{r3} are both set to 4.7, and the dielectric constant of the superstrate (overlay), ϵ_{r1}, is varied from 1 to 16. Figs.20a and 20b show the characteristic parameters versus ϵ_{r1}. As shown in Fig.20a, the mutual capacitances are directly proportional to ϵ_{r1}, for both truncated and non-truncated structures, but self capacitance with the truncated structure did not show significant variations, compared with the use of non-truncated structure. In Fig.20b, it is noted that the coupling coefficient increases as the dielectric constant of the overlay is increased. It is also noted from the same figure that the even and odd mode normalized phase velocities are equalized at approximately $\epsilon_{r1}=5$ for non-truncated structure, and at $\epsilon_{r1}=3.5$ for truncated structure. It is clear that the smaller value of dielectric constant of the overlay should be used to minimize the mutual coupling between the strip lines.

Another analysis is made to study the effect of dielectric constant of the substrate. The same configuration is used for this case, but the dielectric constant of overlay, ϵ_{r1}, is now set to 2.2, ϵ_{r2} and ϵ_{r3} are both varied from 1 to 16. Figure.21a shows that the self and mutual

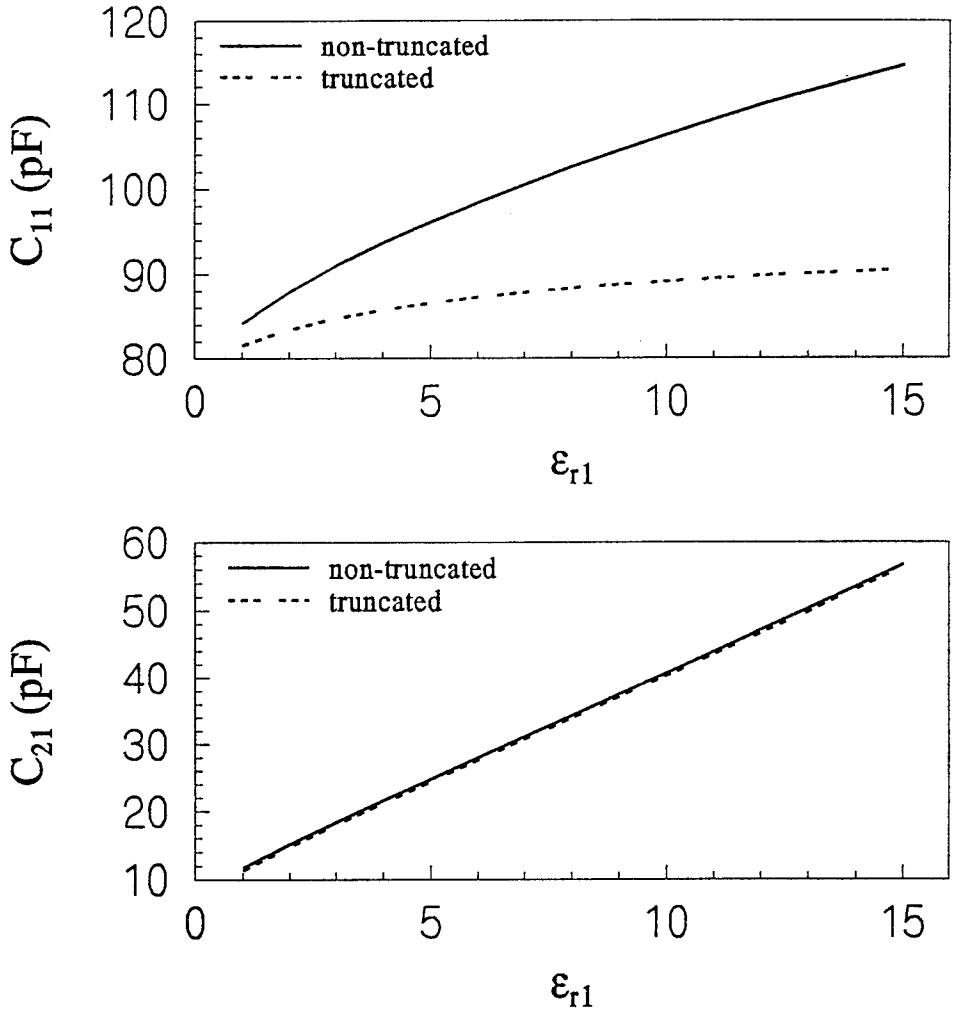

Fig.20a Effect of dielectric overlay on capacitances for no notch geometry

(h_1=0.2, h_2=0.2, h_3=0.5, t=0.001, δ_w=10°, δ_s=10°, δ_n=6°, ε_{r2}=ε_{r3}=4.7, α_s=72°, N_w=10, N_1=4, N_2=1, N_3=3, N_4=5)

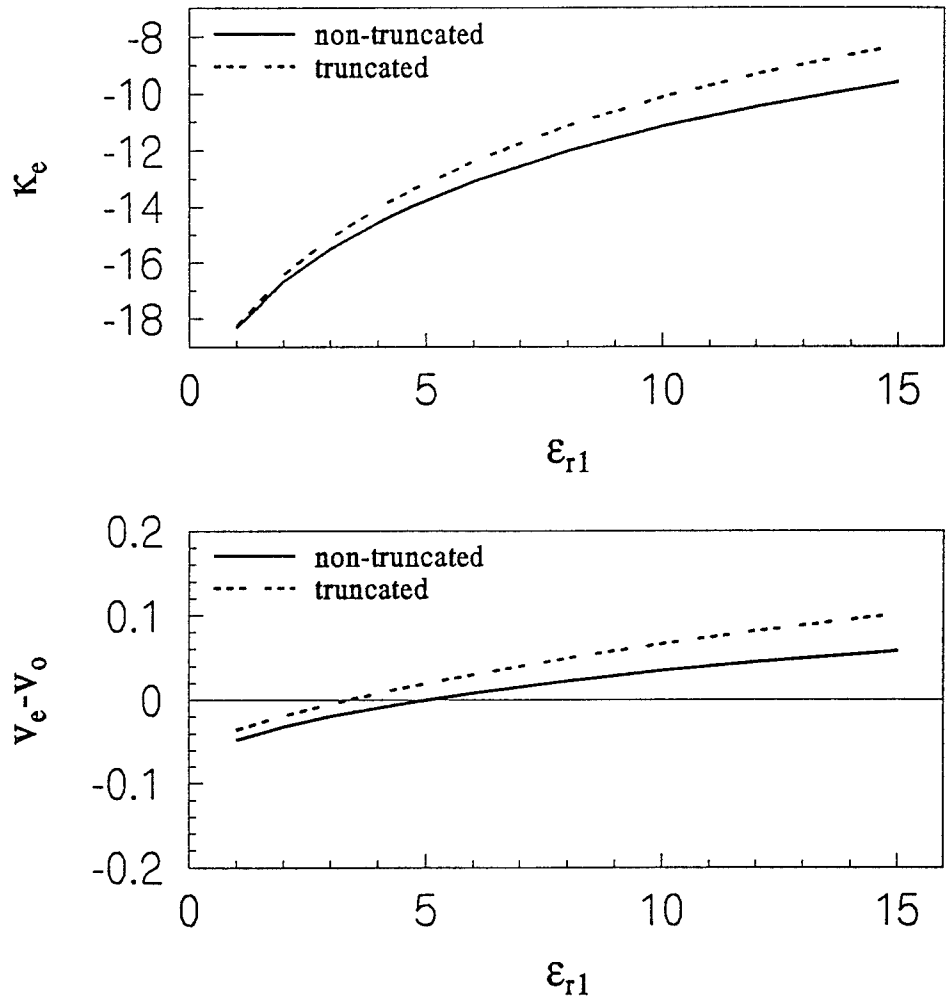

Fig.20b Effect of dielectric overlay on coupling and phase velocities for no notch geometry

(h_1=0.2, h_2=0.2, h_3=0.5, t=0.001, δ_w=10°, δ_s=10°, δ_n=6°, ε_{r2}=ε_{r3}=4.7, α_s=72°, N_w=10, N_1=4, N_2=1, N_3=3, N_4=5)

capacitances are both linearly increasing with ϵ_{r2} and ϵ_{r3}. From Fig.21b, it is found that the coupling coefficient decreases as ϵ_{r2} and ϵ_{r3} increase. In this case, however, the normalized v_e and v_o are equalized at approximately $\epsilon_{r2}=\epsilon_{r3}=2.2$ for non-truncated structure, and at $\epsilon_{r2}=\epsilon_{r3}=3.2$ for the truncated structure.

4.2.2 Effect of the Spacing between Strips

The effect of the spacing between strips is now studied. The configuration selected in this case is such that $h_1=0.2$, $h_2=0.2$, $h_3=0.5$, $\delta_w=10°$, the dielectric constants of substrate and the notch, ϵ_{r2} and ϵ_{r3}, are both set to 4.7, the dielectric constant of the superstrate, ϵ_{r1}, is equal to 2.2, δ_s is then varied from 6° to 24°. In this investigation, strips with thickness are used to study their effects on the characteristic parameters of the transmission line. Figure.22a shows the self capacitance increases and mutual capacitance decreases while the separation distance between the strips increases. It can be easily seen that the use of thick strips increases both self and mutual capacitances, compared with the use of thin strips. It is also noted in Fig.22b that the coupling coefficient decreases with increased spacing between strips. All these figures clearly show that the use of thin strips leads to less coupling and distortion relative to thick strips.

4.3 Effect of the Structure Parameters

In this research project, a truncated structure of the cylindrical strip transmission line has been used in many numerical analysis. There are two major purposes to apply the truncated dielectric to CMSTL, one is for controlling the coupling between the lines and elimination of distortion. The other is to save dielectric materials if the use of the truncated geometry provides

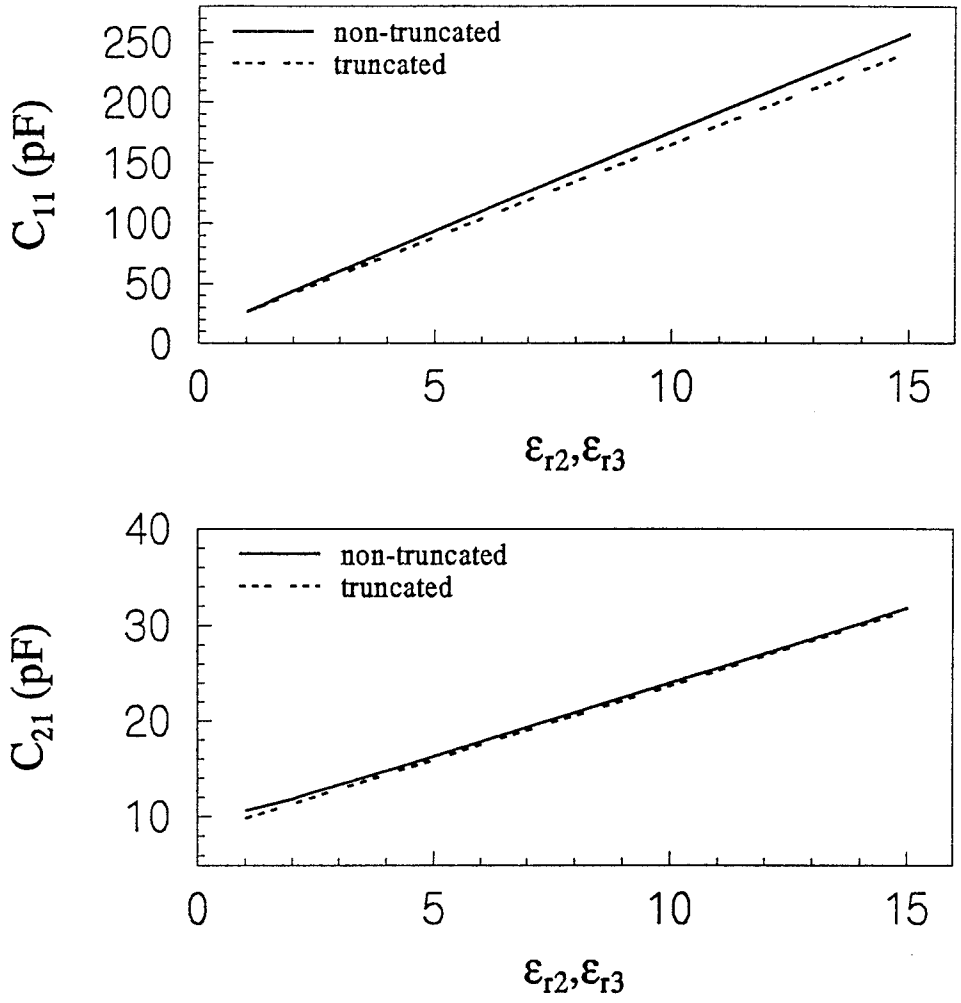

Fig.21a Effect of dielectric substrate on capacitances for no notch geometry

(h_1=0.2, h_2=0.2, h_3=0.5, t=0.001, δ_w=10°, δ_s=10°, δ_n=6°, ε_{r1}=2.2, α_s=72°, N_w=10, N_1=4, N_2=1, N_3=3, N_4=5)

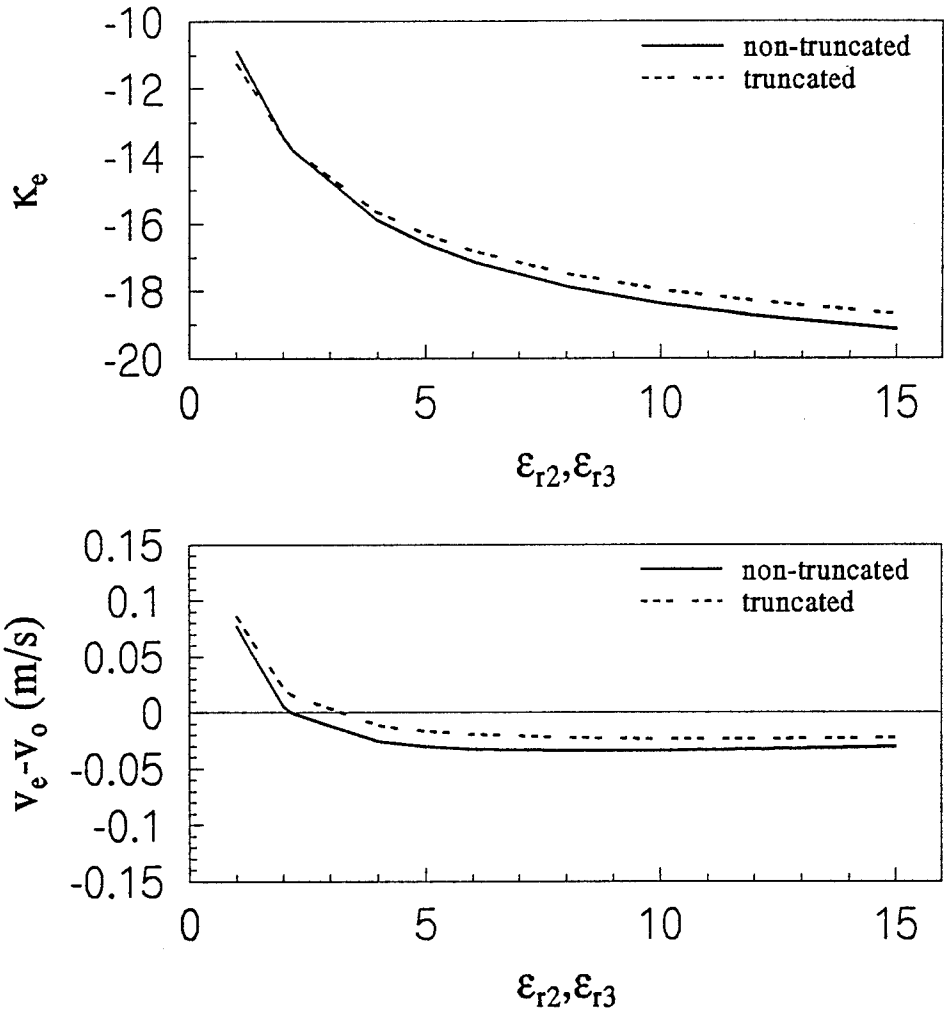

Fig.21b Effect of dielectric substrate on coupling and phase velocities for no notch geometry

(h_1=0.2, h_2=0.2, h_3=0.5, t=0.001, δ_w=10°, δ_s=10°, δ_n=6°, ε_{r1}=2.2, α_s=72°, N_w=10, N_1=4, N_2=1, N_3=3, N_4=5)

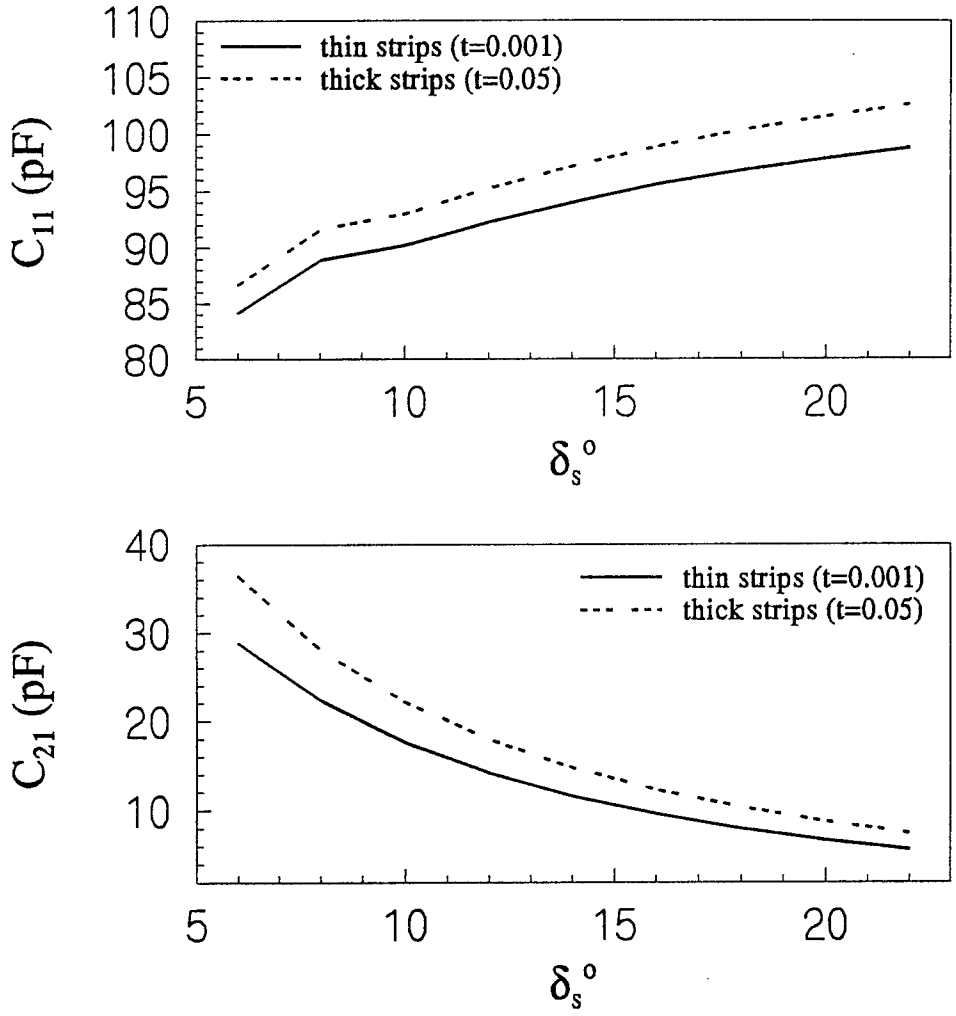

Fig.22a Effect of spacing between strips on capacitances for use of no notch and non-truncated CMSTL

(h_1=0.2, h_2=0.2, h_3=0.5, δ_w=10°, δ_n=4°, ε_{r1}=2.2, ε_{r2}=ε_{r3}=4.7)

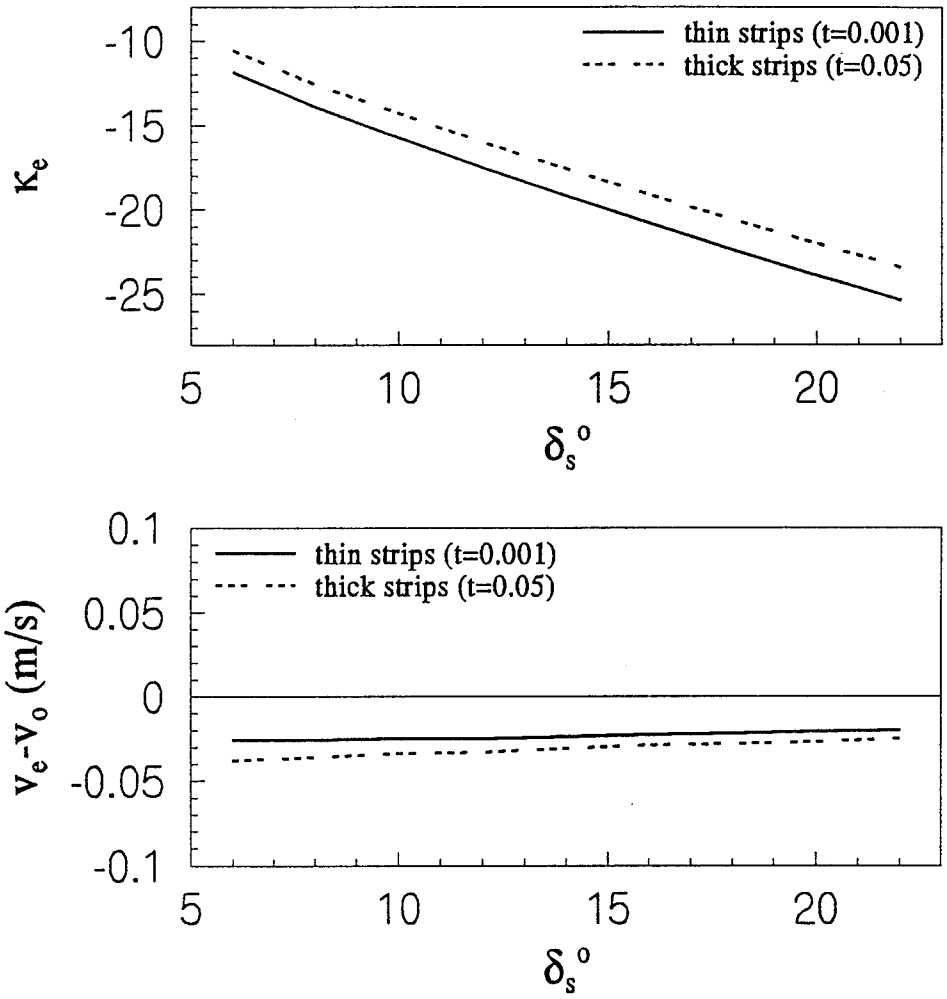

Fig.22b Effect of spacing between strips on coupling and phase velocities for use of no notch and non-truncated CMSTL

(h_1=0.2, h_2=0.2, h_3=0.5, δ_w=10°, δ_n=4°, ε_{r1}=2.2, ε_{r2}=ε_{r3}=4.7)

the same characteristics as the non-truncated CMSTL. Since the size of truncation affects the characteristics of the transmission line, the effect of some structure parameters such as the size of truncation and the thickness of the strips are discussed in the following sections.

4.3.1 Effect of the Size of Truncation

A case is selected to study the effect of the size of the truncated dielectrics. The configuration selected is such that h_1=0.2, h_2=0.2, h_3=0.5, t=0.001, δ_w=10°, δ_s=10°, δ_n=6°, ϵ_{r1}=1.0, and ϵ_{r2}=4.7. The angles, α_s and α_o, are both varied from 0° to 72° with different ϵ_{r3}. It is very clear, from Figs.23a and 23b, that all characteristic parameters are almost constant for all values of α_s and α_o which are less than 40°, for this specific case.

Another case is generated to determine which size of the truncation should be used for the same solution obtained by the use of non-truncated structure. The configuration parameters are h_1=0.2, h_2=0.2, h_3=0.5, t=0.001, δ_w=10°, δ_s=10°, δ_n=6°, ϵ_{r1}=2.2, and ϵ_{r3}=9.6. The dielectric constant, ϵ_{r3}, is then varied from 1 to 10 with different α_s and α_o. It is important to note that use of different size of truncation can control the point where the distortionless on the line occurs. It is clearly noted from Figs.24a and 24b, that the larger the size of the truncation is, the closer the results would be, compared with non-truncated structure. For this case, it is very clear in these figures, that a truncated structure can be used with α_s and α_o are approximately equal to 10°, to produce the same characteristics of a non-truncated CMSTL.

4.3.2 Effect of the Thickness of the Strips

In order to investigate the effect of the thickness of the strips on the characteristic

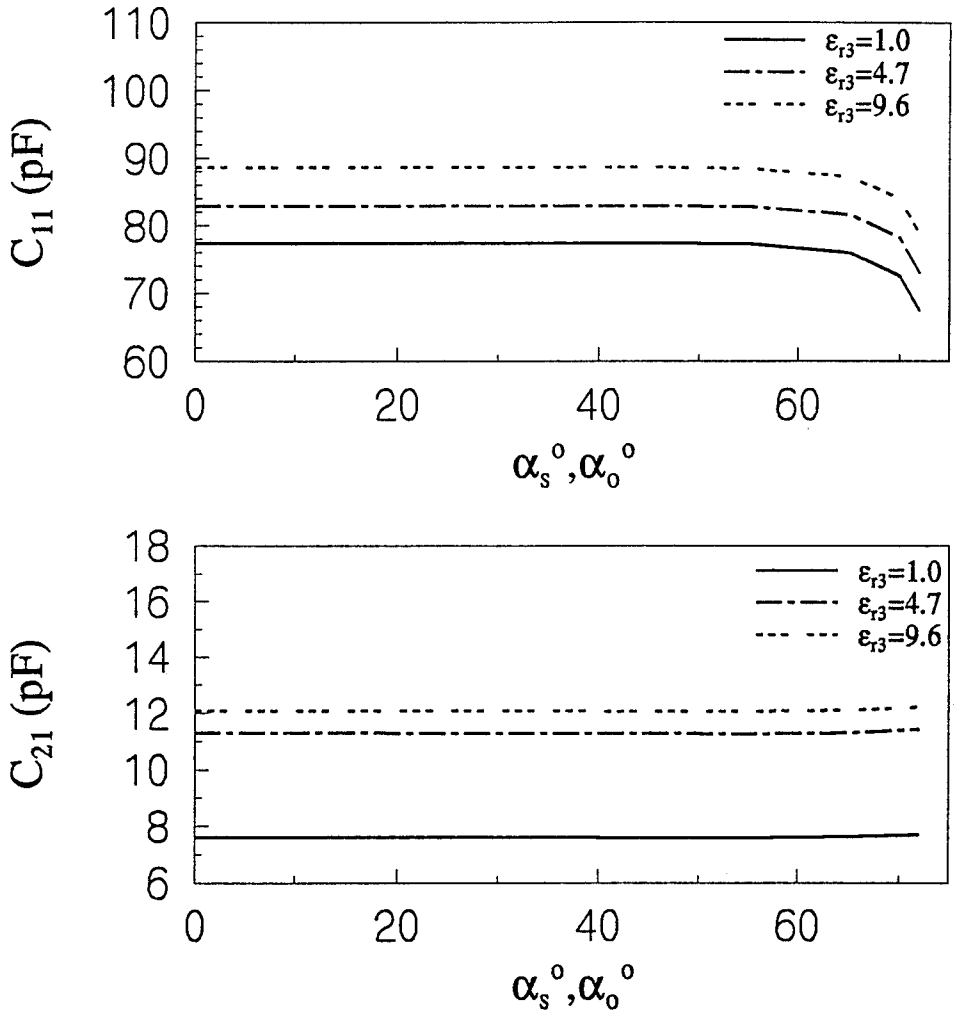

Fig.23a Effect of truncated CMSTL on capacitances

(h_1=0.2, h_2=0.1, h_3=0.5, t=0.001, δ_w=10°, δ_s=10°, δ_n=6°, ε_{r1}=1.0, ε_{r2}=4.7, N_w=10, N_1=4, N_2=1, N_3=3, N_4=5)

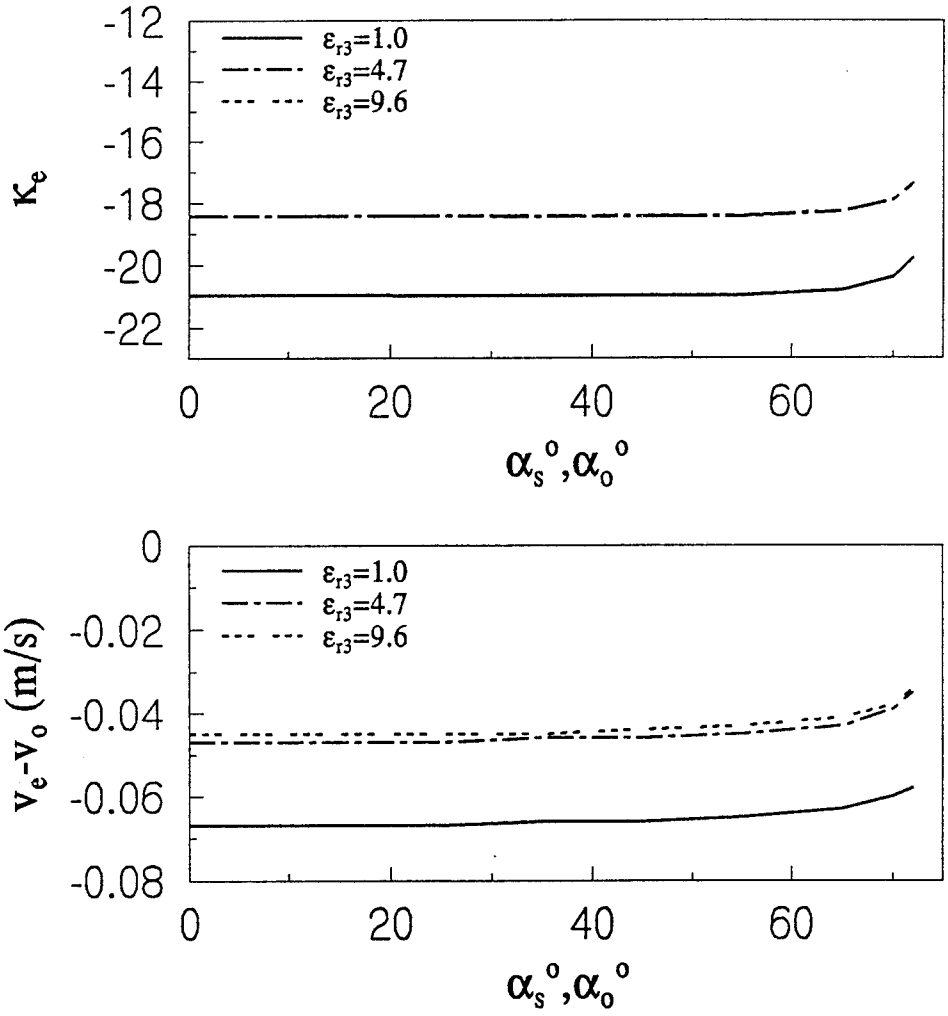

Fig.23b Effect of truncated CMSTL on coupling and phase velocities

(h_1=0.2, h_2=0.1, h_3=0.5, t=0.001, δ_w=10°, δ_s=10°, δ_{ll}=6°, ε_{r1}=1.0, ε_{r2}=4.7, N_w=10, N_1=4, N_2=1, N_3=3, N_4=5)

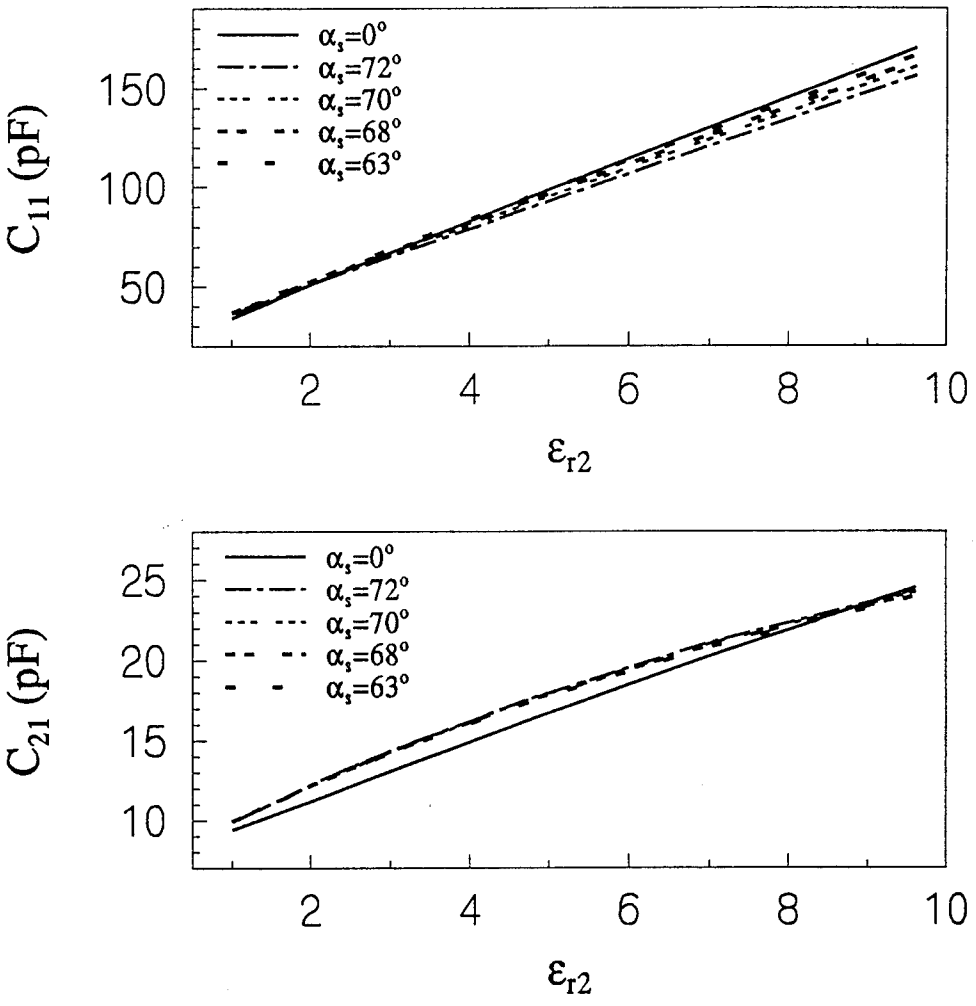

Fig.24a Effect of dielectric substrate on capacitances for use of different truncation

(h_1=0.2, h_2=0.2, h_3=0.5, t=0.001, δ_w=10°, δ_s=10°, δ_n=6°, ε_{r1}=2.2, ε_{r3}=9.6, N_w=10, N_1=4, N_2=1, N_3=3, N_4=5)

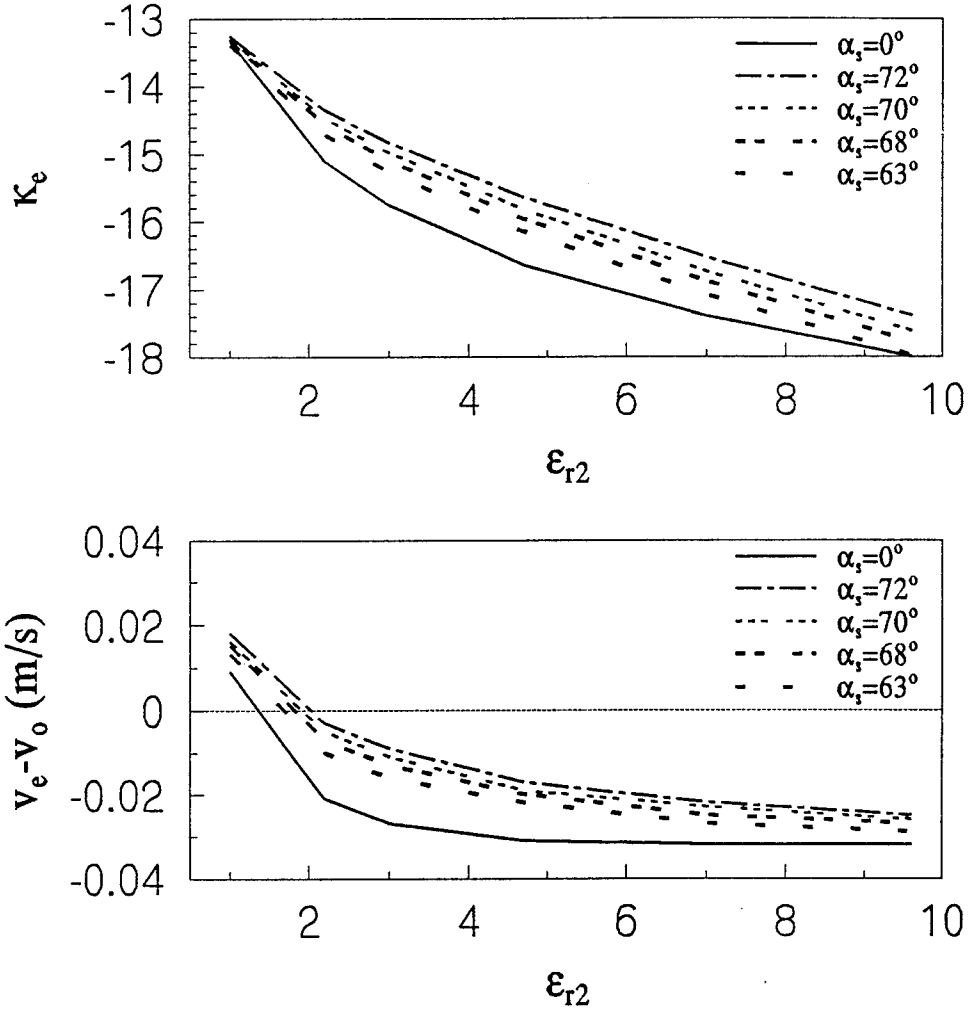

Fig.24b Effect of dielectric substrate on coupling and phase velocities for use of different truncation

(h_1=0.2, h_2=0.2, h_3=0.5, t=0.001, δ_w=10°, δ_s=10°, δ_n=6°, ε_{r1}=2.2, ε_{r3}=9.6, N_w=10, N_1=4, N_2=1, N_3=3, N_4=5)

parameters of the transmission line, a structure is selected such that h_1=0.2, h_2=0.2, h_3=0.5, δ_s=10°, δ_w=10°, δ_n=6°, ϵ_{r1}=1.0 and ϵ_{r2}=4.7, and the angles, α_s and α_o, are set to 10°. The thickness of the strips, t, is then varied from 0.001 to 0.28 with different ϵ_{r3}. The linear behavior can be observed in Fig.25a, where both self and mutual capacitances are increased, as the thickness of the strips is increased. Figure.25b shows that the coupling and the distortion increase with t. It is clearly noted that thin strips should be used for reducing coupling and distortion.

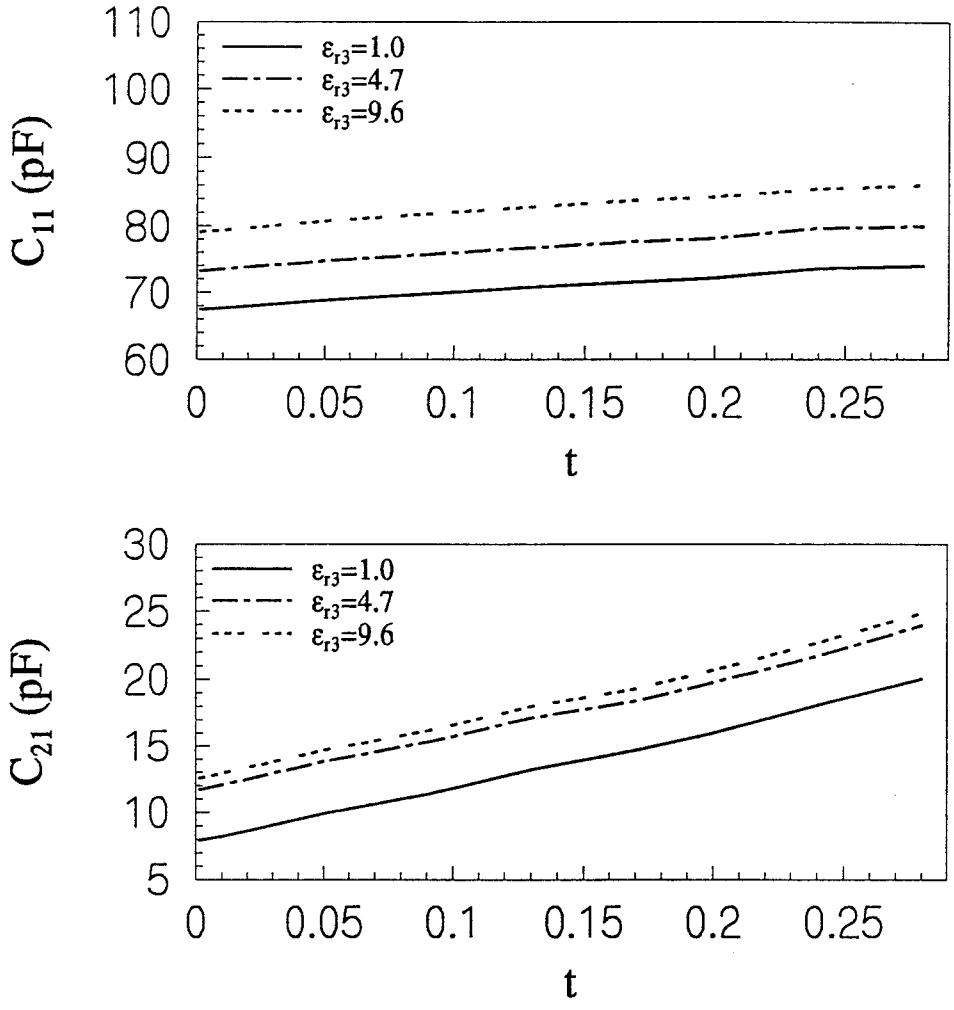

Fig.25a Effect of thickness of strips on capacitances for truncated CMSTL

(h_1=0.2, h_2=0.3, h_3=0.5, δ_w=10°, δ_s=10°, δ_n=6°, ε_{r1}=1.0, ε_{r2}=4.7, α_s=α_o=72°, N_w=10, N_1=4, N_2=1, N_3=3, N_4=5)

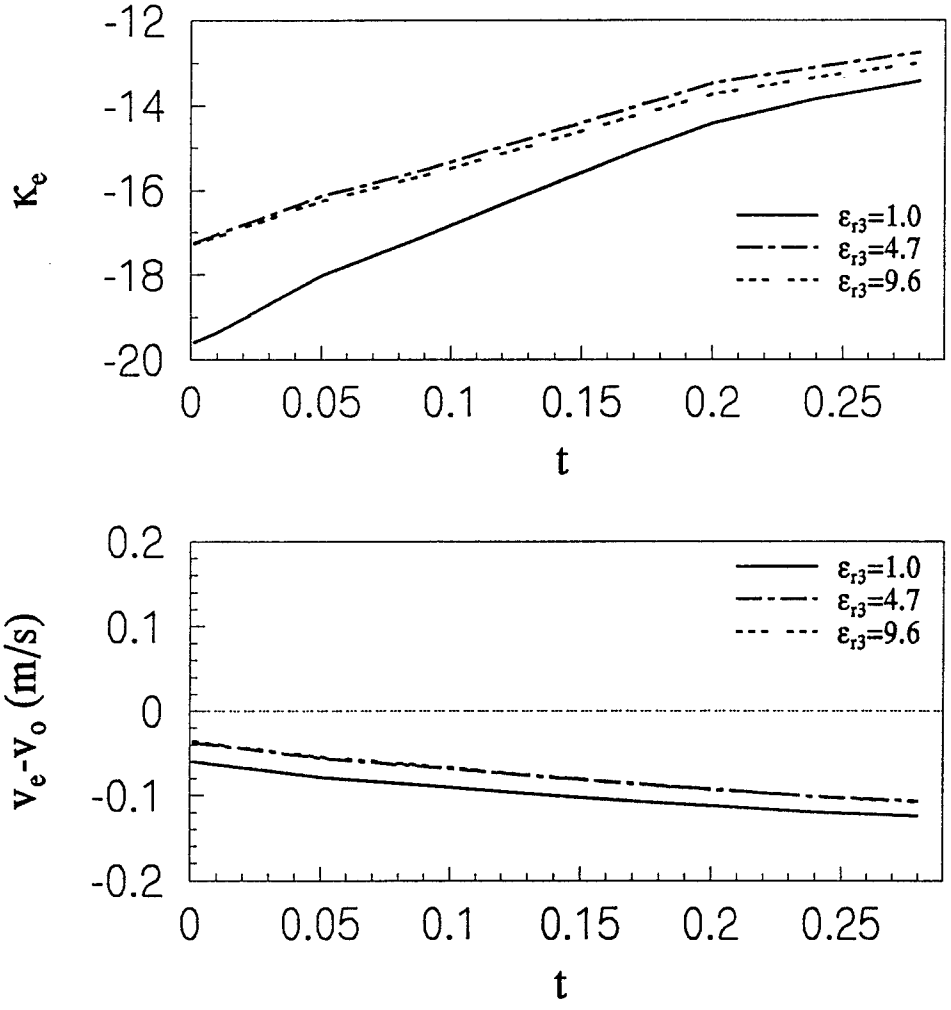

Fig.25b Effect of thickness of strips on coupling and phase velocities for truncated CMSTL

(h_1=0.2, h_2=0.3, h_3=0.5, δ_w=10°, δ_s=10°, δ_n=6°, ε_{r1}=1.0, ε_{r2}=4.7, α_s=72°, N_w=10, N_1=4, N_2=1, N_3=3, N_4=5)

V. SUMMARY AND CONCLUSIONS

A finite difference formulation for the analysis of the characteristics of a two-conducting strips cylindrical transmission line with a dielectric notch between the strips is presented. The dielectric materials are assumed to be lossless, isotopic, and homogeneous, while the thickness of the conducting strips are not necessarily assumed to be zero. Microstrip lines with full and truncated dielectric materials are used in the numerical analysis. The decoupling and distortion control between such two-conductor strip transmission line are investigated.

It has been shown here that the coupling between strip lines can be minimized by altering the dielectric constant of the notch material and use of proper truncation of the substrate material. A distortionless line is achieved when these parameters are selected properly. The truncation of the dielectric substrate and overlay provides a way to achieve zero distortion. With proper dielectric materials in different regions, it is found that the width of the strips should be as wide as possible and the thickness should be kept as thin as possible for the best decoupling and distortion control. The results also show that using dielectric overlay increases the coupling, but may reduce the distortion with proper values for the permittivity in the overlay. It is also found that transmission lines with truncated dielectric materials provides the same results obtained with non-truncated geometry.

VII. REFERENCES

[1] K. K. Joshi and B. N. Das, " Analysis of elliptic and cylindrical striplines using Laplace's equation," *IEEE Trans. Microwave Theory Tech.*, vol. MTT-28, pp. 381-386, May 1980.

[2] C. H. Chan and R. Mittra, " Analysis of a class of cylindrical multiconductor transmission lines using an iterative approach," *IEEE Trans. Microwave Theory Tech.*, vol. MTT-35, pp. 415-423, April 1987.

[3] A. Nakatani and N. G. Alexopoulos, "Coupled microstrip lines on a cylindrical substrate," *IEEE Trans. Microwave Theory Tech.*, Vol. MTT-35, pp. 1392-1398, December 1987.

[4] C. J. Reddy and M. D. Deshpande, " Analysis of cylindrical stripline with multilayer dielectrics," *IEEE Trans. Microwave Theory Tech.*, vol. MTT-34, pp. 701-706, June 1986.

[5] N. G. Alexopoulos, " Cylindrical substrate microstrip line characterization," *IEEE Trans. Microwave Theory Tech.*, vol. MTT-35, pp. 843-849, September 1987.

[6] R. F. Harrington and K. Pontoppidan, " Applications of numerical methods in electromagnetic field," *Proc. Inst. Elec. Eng., pp.* 316-321, Oct. 1970.

[7] K. K. Joshi and B. N. Das, " Characteristic impedance of elliptic cylindrical strips and microstrip lines filled with layered substrate," *Proc. Inst. Elec. Eng.*, Pt. H, vol. 127, pp. 245-250, June 1983.

[8] D. Kajfez," Quasi-TEM modes on coupled transmission lines with asymmetric Conductors," *Electrotechnical Review,* vol. 44, no. 1, pp. 1-9, 1977.

[9] D. Kajfez, *Notes on Microwave Circuits.* Oxford, Mississippi: Kajfez Consulting, 1986, vol. 2, Chapter 7.

[10] A. Khebir, A. B. Kouki, and R. Mittra, " Absorbing boundary condition for quasi-TEM analysis of microwave transmission lines via the finite element method," *J. Electromagnetic Waves Appl.,* vol. 4, no. 2, 1990.

[11] J. J. Dongama, C.B. Maler, J.B. Bunch, and G.W. Stewart, *Linpack User's Guide.*

[12] W. R. Smythe, *Static and Dynamic Electricity.* New York, Hemisphere Publishing Company, pp. 63-64, 1989.

[13] C. E. Smith and R. S. Chang," Microstrip transmission line with finite-width dielectric," *IEEE Trans. Microwave Theory Tech.,* vol. MTT-28, no. 2, pp. 90-94, February 1980.

[14] A. Z. Elsherbeni, C. E. Smith, B. Moumneh, H. Golestanian, and S. He," Crosstalk reduction in integrated circuits and microwave/millimeter wave interconnections," *Final Report, the Army Research Office,* Technical Report No. 93-1, Department of Electrical Engineering, University of Mississippi, January 1993.

[15] N. G. Alexopoulos and A. Nakatani, "Cylindrical substrate microstrip line characterization," *IEEE Trans. Microwave Theory Tech.,* vol. MTT-35, pp. 843-849, Sept. 1987.

[16] S. He, A. Z. Elsherbeni, and C.E. Smith," Decoupling between two conductor microstrip transmission line," *IEEE Trans. Microwave Theory Tech.,* vol. MTT-41, no. 1, pp. 53-61, January 1993.

[17] A. Z. Elsherbeni, B. Moumneh, C. E. Smith," Characteristics of two-conductor microstrip transmission lines embedded in a ground plane using the finite difference technique," *Technical Report*, No. 93-3, Department of Electrical Engineering, University of Mississippi, July 1993.

[18] A. Z. Elsherbeni, C.E. Smith, H. Golestanian, and S. He," Quasi-TEM characteristics of a two-conductor multi layer microstrip transmission line with dielectric overlay and a notch between the strips," *J. Electromagnetic Waves Appl.*, vol. 7, no. 6, pp. 769-789, 1993.

[19] A. Z. Elsherbeni, B. Moumneh, S. A. Hutchens, and C. E. Smith," Quasi-static analysis of a coupled microstrip transmission line embedded in a ground plane using finite difference method," *Proc. North America Radio Science Meeting (URSI)*, Ann Arbor, MI, p. 16, July 1993.

[20] J. K. Gilb and C. A. Balanis," Pulse distortion on multilayer coupled microstrip Lines," *IEEE Trans. Microwave Theory Tech.*, vol. MTT-37, no. 10, pp. 1620-1627, October 1989.

[21] R. K. Hoffmann, *Handbook of Microwave Integrated Circuits*. Norwood: Artech House, 1987, Chapter 9.

[22] A. Z. Elsherbeni, B. Moumneh, C. E. Smith, and H. Golestanian," Coupling between two-conductor multi-Layer shielded microstrip transmission line", *Proc. of IEEE Southeastern Symposium on System Theory*, Tuscaloosa, AL, pp. 6-10, March 1993.

[23] S. B. Cohn," Shielded coupled-strip transmission line," *IRE Trans. Microwave Theory Tech.*, pp. 29-38, October 1955.

[24] C. Wei, et. al., " Multiconductor transmission lines in multilayered dielectric media," *IEEE Trans. Microwave Theory Tech.*, vol. MTT-32, pp. 439-449, April 1984.